Saffman-Taylor Fingers in Deformed Hele-Shaw Cells

Thesis by

Donal A. Gallagher

In Partial Fulfillment of the Requirements

for the Degree of

Doctor of Philosophy

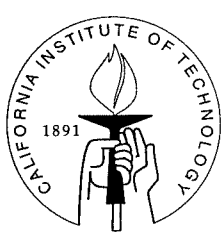

California Institute of Technology

Pasadena, California

1999

(Submitted December 16, 1998)

To Stephanie

Acknowledgements

I would like to extend my thanks to my advisor, Prof. P. G. Saffman, who suggested this work and guided this thesis to its completion. I am grateful to the other members of the thesis defence committee, Prof. G. B. Whitham, Prof. D. I. Meiron and Prof. D. I. Pullin. I would also like to acknowledge the contributions of Prof. D. Meiron to Chapter 2 and Prof. S. Tanveer to Chapter 3.

Many thanks are due to Dr. John Pelesko and Dr. David Hill for reading this thesis; their suggestions left it better for having done so. I would also like to thank all the graduate students of the Applied Mathematics department at Caltech, in particular Dr. David Hill, James Gleeson, Peter Park, Dr. Anatoly Baumstein and Dr. Kayvan Ardalan for many helpful discussions. Thanks are also due to Sheila Shull for making my stay at Caltech so pleasant.

Over the years at Caltech I have met many fine people and I would like to acknowledge their friendship which enriched my stay: Laurence Fumagalli, Kevin Konty, Arsalan Farooq, Voyle Coleman, Drs. Des Patterson, Adam Kent, Elizabeth Nagy, Jim Spotila, John Pezaris, Sergio Turteltaub, Bob Nichols, Misha Rudnev, John Pelesko, Patrick Guidotti and all the members of the Caltech Rugby Club.

I owe the deepest debt of gratitude to my parents for their guidance and support, as well as to my sister Aoife and brothers Barry and Niall.

Finally, to my wife Stephanie, thank you for sharing these years with me.

Abstract

Viscous fingering occurs when an essentially inviscid fluid is used to displace a viscous fluid in a porous medium or a Hele-Shaw cell. Long finger-shaped protrusions of the non-viscous fluid are found to advance into the viscous fluid. The importance of viscous fingering was first realised when attempts were made to retrieve oil from underground reservoirs by water injection.

When one displaces oil in a Hele-Shaw cell of width a with air, an initially plane interface between the two fluids becomes unstable. This interface eventually develops into a finger shaped protrusion of width λa moving at constant speed. Experimentally, in the presence of *small* surface tension at the air-oil interface the constant λ is found to be near $1/2$. An exact solution of the model equations was found by Saffman and Taylor in the absence of surface tension.

Until now the fingering problem has only been studied in Hele-Shaw of constant gap corresponding to a porous medium with constant permeability. In order to understand the effect of non-homogenous permeability we look at the problem of fingering in a Hele-Shaw cell of varying gap. We consider variations in the direction perpendicular to the motion of the finger allowing steady fingers to exist.

We extend previous work on the constant gap case to show how the presence of surface tension interacts with variations in the gap to change the solution structure in a non-trivial way. For example values of λ less than a half are possible. It is even found that solutions cease to exist for small surface tension in some cases. We solve the problem using both numerical methods based on conformal mapping and analytical methods involving asymptotics beyond all orders.

Contents

List of Figures

Chapter 1 Introduction

1.1 Introduction

The fingering problem in a Hele-Shaw cell has a long and interesting history. The development of a theoretical understanding of the problem has led to advances in singular perturbation theory and numerical methods. Not least among the reasons for studying two phase flow in a Hele-Shaw cell is its similarity to two phase flow in a porous medium. The displacement of crude oil by water in porous rock and the attendant instability of an initially plane interface as well as the subsequent formation of fingers is a problem of considerable practical importance in oil recovery engineering. The formation of fingers in a Hele-Shaw cell is also one of the classical examples of pattern formation in physical systems.

A Hele-Shaw cell is an apparatus consisting of two glass plates, separated by a small distance, filled with one or more fluids. For the purposes of this study when we refer to a Hele-Shaw cell we mean an apparatus with rectangular plan view, much longer in one direction than the other. An initially plane interface between oil with viscosity μ and essentially inviscid air moving at constant speed U is unstable when the direction of motion is towards the oil. Surface tension, T, on the oil air interface tends to suppress the instability of short wavelength perturbations. In experiments, after a period of competition between growing perturbations, a long, repeatable, finger-shaped protrusion of air moving at constant speed develops. The problem is to determine the shape and speed of the finger as a function of the cell geometry and the physical constants of the fluids.

The formation of the finger was discovered by Saffman and Taylor [1] in a now classical paper. Experimentally, the fraction of the width of the cell that the finger occupied was found to be a unique function of the capillary number ($Ca = \mu U/T$) and tended to one half as Ca became large. By contrast, Saffman and Taylor derived

an exact solution to the model equations describing the motion of a finger of *any* width in a cell of constant gap with zero surface tension. They could find no physical reason for the selection of a finger width close to one half the total cell width although they felt that surface tension must be crucial. There the problem lay for almost two decades until the discovery by several groups simultaneously [13], [14], [15], that surface tension selects an enumerable infinity of solutions from the Saffman-Taylor one parameter family of solutions. Only one of the enumerable infinity of solutions was found to be linearly stable. The selection mechanism involves the use of asymptotics beyond all orders, a relatively new and still developing branch of singular perturbation theory. Numerical approaches to finding steady solutions and determining their stability involve non-trivial accuracy issues, and inevitably fail in the limit of small surface tension, a most singular limit for this problem. Analytical techniques are necessary to determine the behaviour for small surface tension.

To date studies have been limited to Hele-Shaw cells of constant gap. In this thesis we examine fingers in a Hele-Shaw cell of varying gap, analogous to non-homogeneous permeability in a porous medium. We look at the problem numerically for finite amplitude variations in gap and surface tension. We then proceed to study the problem analytically for small gap variation and surface tension. Both approaches give results that are in good agreement in their ranges of validity. We find new and qualitatively different behaviour from the constant gap case that may explain some observed phenomena.

Finger patterns are the end result of the instability of a plane interface in a cell of constant gap. The plane interface is no longer a steady solution in a cell of varying gap. We present the analogous solution and find that gap variations have a non-trivial effect on bifurcations to finite amplitude steady solutions.

In the remainder of this Chapter we review the equations of motion and boundary conditions for a viscous fluid in a Hele-Shaw cell or a porous medium. An analogy is drawn between the two. Chapter 2 is concerned with a numerical approach to calculating steady fingers. An analytic solution valid for small surface tension and small gap variation is presented in Chapter 3. In Chapter 4 we present results for

finite interfaces in a cell of varying gap.

1.2 Equations of Motion

The equations of motion are somewhat different from the usual equations of fluid motion so we review them in this Section for completeness. We will consider the equations both in a Hele-Shaw cell of varying gap and in a porous medium of varying permeability and porosity. An analogy between the two will be drawn.

1.2.1 Hele-Shaw Cell

As mentioned in the introduction a Hele-Shaw cell is an apparatus consisting of two rigid plates separated by a small gap. We will consider a cell of rectangular plan view, infinite in extent in one direction (see Figure 1.1.) We introduce rectangular Cartesian coordinates as indicated. Later we will consider a gap which varies only in the lateral (y) direction allowing the possibility of steady solutions with motion in the longitudinal (x) direction caused by a moving interface. The equations will be formulated without this restriction. Thus we will define the upper and lower plates respectively by

$$z = h_2(x, y), \qquad z = h_1(x, y), \tag{1.1}$$

(see Figure 1.2.)

We will now consider the simplifying approximations that this geometry allows us to make to the Navier-Stokes equations. We start with the usual Navier-Stokes equations for an incompressible fluid

$$\rho\left(\frac{\partial \mathbf{u}}{\partial t} + \mathbf{u}.\nabla\mathbf{u}\right) = -\nabla p + \mu\nabla^2\mathbf{u}, \tag{1.2}$$

$$\nabla \cdot \mathbf{u} = 0. \tag{1.3}$$

We now assume that the dominant balance of forces in a Hele-Shaw cell is between

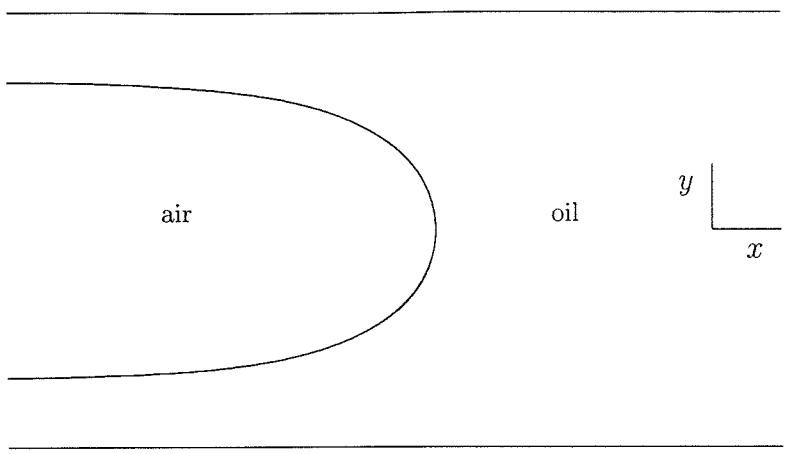

Figure 1.1: Hele-Shaw Cell with finger.

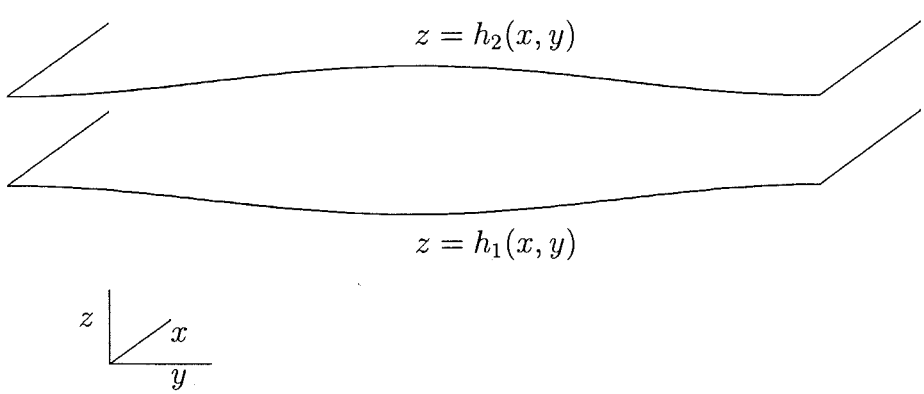

Figure 1.2: Gap between plates of cell.

the viscous forces and the pressure gradients giving us

$$\frac{\partial p}{\partial x} = \mu \nabla^2 u, \tag{1.4}$$

$$\frac{\partial p}{\partial y} = \mu \nabla^2 v, \tag{1.5}$$

$$\frac{\partial p}{\partial z} = \mu \nabla^2 w, \tag{1.6}$$

along with the incompressibility condition

$$\frac{\partial u}{\partial x} + \frac{\partial v}{\partial y} + \frac{\partial w}{\partial z} = 0. \tag{1.7}$$

We make two assumptions: *i*) that the gap is a slowly varying function of x and y and hence w is negligible, *ii*) that z gradients of u and v are much larger than gradients in the other directions. Thus we further approximate the momentum equations by

$$\frac{\partial p}{\partial x} = \mu \frac{\partial^2 u}{\partial z^2}, \tag{1.8}$$

$$\frac{\partial p}{\partial y} = \mu \frac{\partial^2 v}{\partial z^2}, \tag{1.9}$$

$$\frac{\partial p}{\partial z} = 0, \tag{1.10}$$

along with the incompressibility condition

$$\frac{\partial u}{\partial x} + \frac{\partial v}{\partial y} = 0. \tag{1.11}$$

The z momentum equation (1.10) implies that the pressure is a function of x and y alone allowing us to integrate (1.8) and (1.9) twice with respect to z. On applying the no-slip boundary condition on the top and bottom plates we find

$$u = \frac{1}{2\mu}(z - h_1)(z - h_2)\frac{\partial p}{\partial x}, \tag{1.12}$$

$$v = \frac{1}{2\mu}(z - h_1)(z - h_2)\frac{\partial p}{\partial y}. \tag{1.13}$$

We can now define gap averaged velocities by integrating the velocities across the gap and dividing by the distance. We denote the averaged velocities with a bar

$$\overline{u}(x,y) = \frac{1}{(h_2-h_1)}\int_{h_1}^{h_2} u(x,y,z)dz, \tag{1.14}$$

$$\overline{v}(x,y) = \frac{1}{(h_2-h_1)}\int_{h_1}^{h_2} v(x,y,z)dz. \tag{1.15}$$

Instead of strict continuity (1.11) we impose continuity in the average sense, that is the flux through any curve drawn in the xy plane is zero. Written in terms of the averaged velocity this gives

$$\int_C (h_2-h_1)\overline{\mathbf{u}}\cdot\mathbf{n}ds = 0, \tag{1.16}$$

where C is any closed curve inside the fluid domain. An application of the divergence theorem gives us

$$\boldsymbol{\nabla}\cdot\left((h_2-h_1)\overline{\mathbf{u}}\right) = 0. \tag{1.17}$$

From the definition (1.14)-(1.15) of the averaged velocities, on substitution for the velocities from (1.12) and (1.13), we find

$$\overline{\mathbf{u}} = -\frac{(h_2-h_1)^2}{12\mu}\boldsymbol{\nabla}p. \tag{1.18}$$

This, substituted into the averaged continuity equation (1.17), gives us the equation for the pressure

$$\boldsymbol{\nabla}\cdot\left((h_2-h_1)^3\boldsymbol{\nabla}p\right) = 0. \tag{1.19}$$

Since only the difference, h_2-h_1, appears we define a gap function $h(x,y)$ as follows

$$h(x,y) = (h_2-h_1). \tag{1.20}$$

The pressure equation (1.19) is the fundamental equation with the averaged velocities derived from p through (1.18).

1.2.2 Porous Medium

The basic equations describing the motion of a fluid through a porous medium are due to D'Arcy and may be written as

$$\mathbf{q} = -\frac{k}{\mu}\nabla p, \tag{1.21}$$

where $\mathbf{q}$ is the flux of fluid per unit area, k is the permeability of the medium, μ the viscosity of the fluid and p is the pressure in the fluid. The local velocity with which a fluid element moves is related to the flux through

$$\mathcal{P}\mathbf{u} = \mathbf{q}, \tag{1.22}$$

where $\mathcal{P}$ is the porosity of the medium (the porosity of a medium is unity minus the fraction of an infinitesimal volume occupied by voids.) Incompressibility applied to the flux implies

$$\nabla \cdot \mathbf{q} = 0. \tag{1.23}$$

1.2.3 Boundary Conditions

At any interface, free or fixed, in either a Hele-Shaw cell or a porous medium we have the usual kinematic boundary condition. The normal velocity of the fluid should be equal to the velocity of the interface normal to itself, that is,

$$\mathbf{u} \cdot \mathbf{n} = \frac{d\mathbf{x}}{dt} \cdot \mathbf{n}, \tag{1.24}$$

where $\mathbf{x}$ is the position vector of a point on the boundary, $\mathbf{n}$ is the normal to the interface and $\mathbf{u}$ the velocity of the fluid on the interface.

In addition to the kinematic condition we have a dynamic condition which prescribes a jump in pressure at any free boundary. In the case of a Hele-Shaw cell the pressure jump is due to surface tension acting on the interface between two fluids.

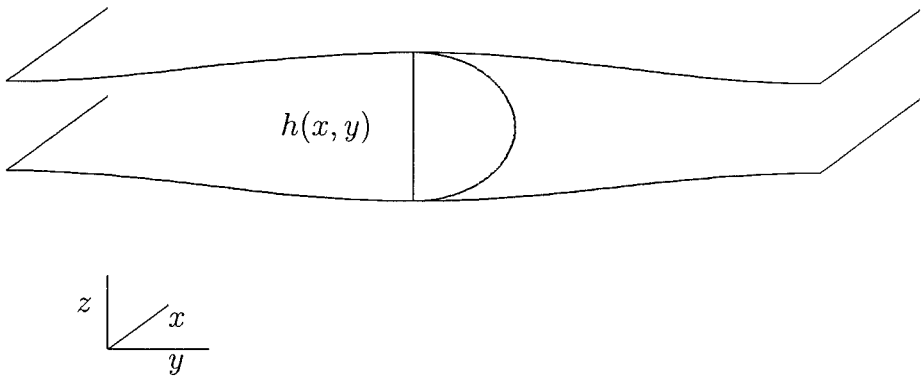

Figure 1.3: Meniscus in transverse direction.

We impose the boundary condition that

$$\Delta p = T(\frac{1}{R_1} + \frac{1}{R_2}), \tag{1.25}$$

where T is the surface tension at the interface and R_1 and R_2 are the principle radii of curvature. We will assume that the interface has radius of curvature R_1 in the xy plane. We will call the curvature in this plane the lateral curvature and denote it by κ. We call the curvature induced by the separation of the plates the transverse curvature. We will further assume that, since the gap width is small, the meniscus is roughly semicircular in the transverse direction with radius $h(x, y)/2$, where $h(x, y)$ is the gap function (see Figure 1.3.) Thus we get

$$\Delta p = T(\kappa + \frac{2}{h(x, y)}). \tag{1.26}$$

This boundary condition is sometimes known in the literature as the McLean-Saffman boundary condition. It is a simplification which ignores the complexities of the local flow near the interface and any wetting film effects. Other boundary conditions have been proposed and are discussed in a review article by Saffman [2].

In the case of two dimensional flow in a porous medium the boundary condition which is frequently used is

$$\Delta p = T\kappa, \tag{1.27}$$

where κ is the curvature of the interface in the xy plane and T is an effective surface tension derived from the properties of the porous medium and the viscous fluid. This is the same as Hele-Shaw cell boundary condition without the term for transverse curvature.

A general boundary condition for both a porous medium and a Hele-Shaw cell can thus be written as

$$\Delta p = T(\kappa + \frac{2\beta}{h(x,y)}), \tag{1.28}$$

where $\beta = 0, 1$ and is included to facilitate our discussion later.

1.2.4 The Analogy with Hele-Shaw Cell Flow

It is clear the equations of motion in a porous medium are the same as those in a Hele-Shaw cell with gap function $h(x,y)$ if the following conditions hold:

- The permeability is related to the porosity through

$$\left(\frac{\mathcal{P}}{12}\right)^3 = k. \tag{1.29}$$

  If this is true then we can make the identification $k = h^3(x,y)$.

- The pressure jump at a free boundary is the same, i.e., $\beta = 0$.

By looking at both $\beta = 0$ and $\beta = 1$ we can study flow in a Hele-Shaw cell of non-constant gap and flow in a porous medium with non-homogeneous permeability and porosity.

Chapter 2 Numerical Selection of Fingers

2.1 Introduction

The study of viscous fingering in Hele-Shaw cells was undertaken by Saffman and Taylor [1]. They conducted experiments in a long Hele-Shaw cell of width a and found that steady finger shaped interfaces could propagate at constant speed. For small dimensionless surface tension it was established that the width of the finger was approximately one half the width of the cell. An exact solution of the equations of motion in the absence of surface tension for a cell of constant gap was found. The exact solution contained a free parameter λ, the width of the finger as a fraction of the total width. No physical reason for the selection of the $\lambda = 1/2$ finger for small surface tension was found. McLean and Saffman [3], [4] studied the problem using numerical methods and found an isolated solution for each value of surface tension and further found that the width of this finger went to $\lambda = 1/2$ for small surface tension. The finger shapes were in excellent agreement with the experiments of Saffman and Taylor for small surface tension. Romero [20] and Vanden-Broeck [21] found that the McLean solution was not unique and that there were at least four branches of solutions in the presence of surface tension. All the branches tend to $\lambda = 1/2$ in the limit of small surface tension. Only the first branch found by McLean is linearly stable in the limit of small surface tension [5], [6], [7]. Vanden-Broeck conjectured that there was an enumerable infinity of solutions branches, all with widths tending to one half.

Subsequent authors have conducted numerical studies on fingering problems in different geometries and with altered boundary conditions. Ben Amar [8] studied fingering in sector geometry in a Hele-Shaw cell and found that solution branches

merged in pairs in the presence of surface tension. Levine and Tu [19] studied the fingering problem in a radially symmetric porous tube and also found branch merger for small surface tension. Dorsey and Martin [17] and Combescot [18] studied anisotropic surface tension in channel geometry and found that values of λ less than a half were possible.

The problem has also been studied experimentally. In a study by Couder et al. [9] a bubble was introduced at the tip of the finger inducing large curvature. It was found that the width of the fingers could be made considerably less than a half in this way. Zocchi et al. [10] found similar results when high local curvature was introduced on the finger boundary through a thin wire along the length of the cell. In a series of careful experiments in a standard Hele-Shaw cell of constant gap, Tabeling et al. [11] found that the stable finger could occupy less than half the width of the cell for very small surface tension. They say the following: "When a finger is moving in a Hele-Shaw cell the normal velocity varies along the interface, and therefore one expects the film thickness to be non-uniform behind the interface, which means the that the finger moves in a channel of variable gap. Intuitively, one feels that the physical problem may be strongly affected by this phenomenon, and this has been studied by Park and Homsy (1984)." In fact, Park and Homsy [12] developed an asymptotic expression in surface tension for a modified boundary condition to be applied at the interface.

In this Chapter we consider the problem of fingering in a Hele-Shaw cell whose gap varies in the direction perpendicular to the direction of propagation of the finger, in our notation $h(x, y) = h(y)$. We choose a particular perturbation to the gap which is a cosine shaped bulge or contraction, symmetric about the cell centreline. We find that, in the presence of surface tension, even small perturbations to the gap (a few percent) cause solution branches to merge when the plates contract along the cell centreline. In the case where the plates bulge apart, widths less than a half are found.

We solve the problem using a numerical method based on a conformal map. We simplify the computational domain by seeking an unknown conformal map that maps the fluid filled domain outside the finger to the unit strip in the complex plane. We formulate the free boundary problem in the next Section and find an expression for the

asymptotic shape of the tails of the finger and the pressure in the tails. In Section 2.3 we find a conformal map that gives us fingers with the correct asymptotic shape in the tails and some unknown coefficients describing the shape elsewhere. We describe how we solve for the pressure in the new simplified domain and how we satisfy the pressure boundary condition on the finger while simultaneously solving for the conformal map and hence the interface shape. We present the results in Section 2.4.

2.2 Formulation

We formulate the problem of finding steady finger-like interfaces moving at constant speed in a way that is convenient. We work in a frame of reference fixed with respect to the apparatus in which the finger is moving at speed U (see Figure 2.1.) The finger is assumed to be filled with an inviscid fluid at constant pressure, $p = const.$, whose dynamics is neglected. To solve the problem we seek the pressure, p, in the region filled by the viscous fluid and an interface, Γ. The pressure satisfies the elliptic equation

$$\nabla \cdot (h^3 \nabla p) = 0. \tag{2.1}$$

The pressure at the interface is due solely to the influence of surface tension and thus the dynamic boundary condition is

$$p|_\Gamma = T(\kappa - \frac{2\beta}{h(y)}). \tag{2.2}$$

On the free interface the kinematic condition (1.24) is

$$\frac{-h^2(y)}{12\mu} \left.\frac{\partial p}{\partial n}\right|_\Gamma = U n_1, \tag{2.3}$$

The flux conditions on the walls and at infinity are

$$\frac{\partial p}{\partial y} = 0, \qquad y = \pm a, \tag{2.4}$$

$$p \sim cx, \qquad x \to \infty, \; -a < y < a \tag{2.5}$$

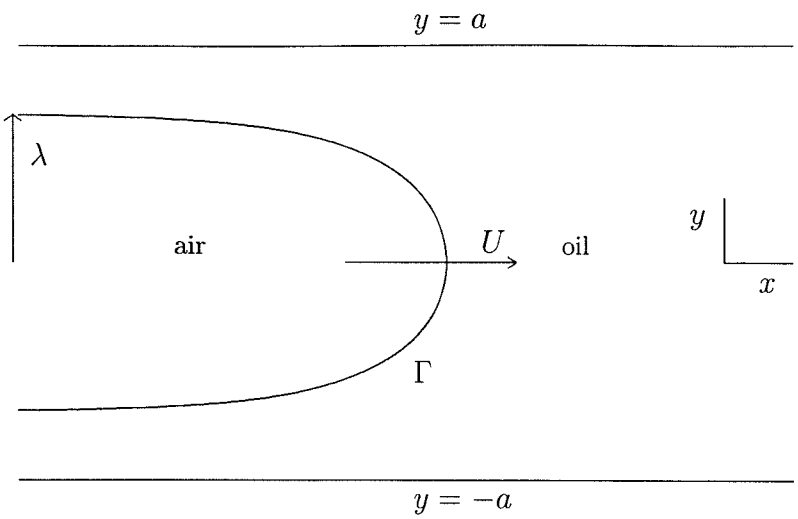

Figure 2.1: Finger moving at constant speed.

$$p \sim \frac{-2T\beta}{h(\lambda)}, \qquad x \to -\infty,\ \lambda a < |y| < a. \tag{2.6}$$

In the dynamic condition the parameter β takes on value 0 or 1 and is there to facilitate the discussion later on. In these boundary conditions n_1 and c are defined by

$$n_1 = \mathbf{n}.\mathbf{e}_x \tag{2.7}$$

$$c = -12\mu U \frac{\int_{-\lambda a}^{\lambda a} h(y)dy}{\int_{-a}^{a} h^3(y)dy}. \tag{2.8}$$

The constant c is defined in this way so that the flux at positive infinity is compatible with the fluid displaced by the moving finger.

We notice that time does not enter the equations explicitly anywhere and thus if we solve the equations at time $t = 0$ then the solution for all other times is given by the substitution $x \to x - Ut$.

2.2.1 Dimensionless Problem

We define an average gap width b by

$$b = \frac{1}{2a}\int_{-a}^{a} h(y)dy. \tag{2.9}$$

With this definition of b we non-dimensionalise the physical variables by setting

$$\widehat{x} = x/a, \tag{2.10}$$

$$\widehat{y} = y/a, \tag{2.11}$$

$$\widehat{h} = h/b, \tag{2.12}$$

$$\widehat{\kappa} = a\kappa, \tag{2.13}$$

$$\widehat{\overline{\mathbf{u}}} = \overline{\mathbf{u}}/U, \tag{2.14}$$

$$\phi = -\frac{pb^2}{12\mu U a}. \tag{2.15}$$

Dropping the hats for notational convenience, our problem is to find a dimensionless pressure ϕ and an interface Γ such that

$$\boldsymbol{\nabla}\cdot(h^3\boldsymbol{\nabla}\phi) = 0, \tag{2.16}$$

with boundary conditions on Γ

$$\phi|_{\Gamma} = \sigma(-\kappa + \frac{a}{b}\frac{2\beta}{h(y)}), \tag{2.17}$$

$$\left.\frac{\partial\phi}{\partial n}\right|_{\Gamma} = n_1/h^2(y), \tag{2.18}$$

and boundary conditions on the walls and at infinity

$$\frac{\partial\phi}{\partial y} = 0, \qquad y = \pm 1, \tag{2.19}$$

$$\phi \sim cx, \qquad x \to \infty,\ -1 < y < 1, \tag{2.20}$$

$$\phi \sim \frac{a}{b}\frac{2\sigma\beta}{h(\lambda)} \qquad x \to -\infty,\ \lambda < |y| < 1, \tag{2.21}$$

with

$$c = \frac{\int_{-\lambda}^{\lambda} h(y)dy}{\int_{-1}^{1} h^3(y)dy}, \tag{2.22}$$

$$\sigma = \frac{Tb^2}{12\mu U a^2}. \tag{2.23}$$

The parameter σ may be considered as a dimensionless surface-tension or modified capillary number. We note that the aspect ratio, a/b, is a large number, $a/b \simeq 100$ is typical and in light of this the second term on the right hand side of the dynamic boundary condition (2.17) is large and cannot be ignored.

At this point it is as well to notice that the solution, consisting of a pair $[\phi, \Gamma]$, is still a solution under the transformation

$$x \to x + x_0, \tag{2.24}$$

that is the solution is translation invariant. This translation invariance will have implications later and will lead to an additional constraint on the numerical solution.

In the rest of this Chapter we will restrict our attention to functions $h(y)$ that are symmetric about the channel centre-line, $y = 0$, and we will assume that the resulting solution $[p, \Gamma]$ also has the same symmetry. The investigations of Tanveer [16] indicate that there are no asymmetric solutions for finite surface tension in the case of constant gap. Thus we will replace the boundary conditions (2.19) with

$$\frac{\partial \phi}{\partial y} = 0, \qquad y = 0, 1, \tag{2.25}$$

and confine our attention to the domain $0 < y < 1$, $0 < x < \infty$, with the understanding that the solution in the rest of the domain is the image under $y \to -y$.

The solution to the problem for zero surface tension and $h(y) = 1$ was first found by Saffman and Taylor [1] and the interface shape is given by

$$x = \frac{1-\lambda}{\pi} \ln \frac{1}{2}\left(1 + \cos\frac{\pi y}{\lambda}\right), \qquad -\lambda < y < \lambda. \tag{2.26}$$

2.2.2 Asymptotic Interface Shape

While we are unable to find an exact closed form solution for non-zero surface tension and non-constant gap we are able to construct an asymptotic solution to the problem describing the shape of the tails of the finger as $x \to -\infty$. This asymptotic solution will be valuable when constructing an accurate numerical approximation to the solution everywhere.

For convenience we will define the interface as $\Gamma = \{x, y | y = Y(x)\}$. Separation of variables suggests a solution of the form

$$Y(x) \sim \lambda - Ae^{kx} + O(e^{2kx}), \tag{2.27}$$

$$\phi \sim C + De^{kx} g(y;\lambda) + O(e^{2kx}), \tag{2.28}$$

with $k > 0$, where g satisfies the second order ordinary differential equation

$$\frac{d}{dy}\left(h^3(y)\frac{d}{dy}g(y;k)\right) + h^3(y)k^2 g(y;k) = 0, \tag{2.29}$$

with boundary conditions $g(1) = 1$, $g'(1) = 0$. By our choice of boundary conditions ϕ already satisfies the no flux condition at the wall (2.19). We now attempt to satisfy the dynamic and kinematic conditions (2.17) and (2.18) on the free interface. In doing so we use the results

$$\mathbf{n} \sim (-Ake^{2kx}, -1) + O(e^{2kx}), \tag{2.30}$$

$$\frac{\partial \phi}{\partial n} \sim -De^{kx} g'(y;k) + O(e^{2kx}), \tag{2.31}$$

$$\kappa \sim Ak^2 e^{kx} + O(e^{2kx}), \tag{2.32}$$

$$h^{-2}|_\Gamma \sim h^{-2}(\lambda) + 2\frac{h'(\lambda)}{h^2(\lambda)}Ae^{kx} + O(e^{2kx}). \tag{2.33}$$

Equating the constant terms in the dynamic condition (2.17) we get

$$C = \sigma \frac{a}{b}\frac{2\beta}{h(\lambda)}. \tag{2.34}$$

Equating the first order terms in (2.17) and(2.18) we get the system of equations

$$\begin{pmatrix} g(\lambda;k) & -\sigma\left[2\beta\frac{h'(\lambda)}{h^2(\lambda)}\frac{a}{b}+k^2\right] \\ -g'(\lambda;k) & kh^{-2}(\lambda) \end{pmatrix} \begin{pmatrix} D \\ A \end{pmatrix} = \begin{pmatrix} 0 \\ 0 \end{pmatrix}. \tag{2.35}$$

For this homogeneous system to have a solution we require that the determinant vanish identically, or

$$kg(\lambda;k) - \sigma g'(\lambda;k)\left[2\beta h'(\lambda)\frac{a}{b}+k^2h^2(\lambda)\right] = 0. \tag{2.36}$$

This non-linear equation fixes the relationship between λ and k. Given λ one must solve (2.36) for k, the decay rate of the tail. Once (2.36) is satisfied there is a unique relationship between D and A given by

$$D = A\frac{k}{h^2(\lambda)g'(\lambda;k)}. \tag{2.37}$$

We will use both (2.36) and (2.37) in our numerical scheme when we specify the asymptotic behaviour in the tails.

2.3 Numerical Method

2.3.1 Overview

We use a relatively straightforward method based on conformal mapping. While the tools of analytic function theory are not available to us to solve for the pressure, we will still use a conformal map to map the fluid filled domain to the strip $0 \leq \xi < \infty$, $0 \leq \eta \leq 1$. The unknowns of our problem will be the coefficients in a particular representation of the conformal map.

For a given map (not necessarily one corresponding to a steady finger shape) our linear elliptic partial differential equation transforms to another linear elliptic equation with variable coefficients. We have the advantage that the domain is much simplified and remains fixed. We can now solve for the pressure in the mapped domain

using a second order finite difference numerical scheme. We solve for the pressure with boundary conditions (2.18)-(2.20). Having done this, the amount by which the pressure fails to satisfy the dynamic boundary condition (2.17) becomes the function which we wish to make zero. We iterate on the unknown map coefficients, using Newton's method, until all the boundary conditions are satisfied and the conformal map defining the fluid filled domain, hence the steady interface, has converged. In implementing Newton's method we must solve a new PDE to calculate each row of the Jacobian. Since this is a very expensive step it is essential that we have an efficient way of representing the conformal map.

2.3.2 Conformal Map

For the reasons mentioned above it is necessary that we have an efficient way of representing the conformal map that maps the strip $0 \leq \xi < \infty$, $-1 \leq \eta \leq 1$ to a finger-like shape with the correct asymptotic behaviour in the tails. We will further require that the map be symmetric about $\eta = 0$. We use as a starting point the conformal map which gives the solution for zero surface tension found by Saffman and Taylor [1].

First we define some notation. We will use the complex variable $\zeta = \xi + i\eta$ to give the rectangular Cartesian coordinates (ξ, η) of a point in the mapped domain. Similarly we use the complex variable $z = x + iy$ to designate the coordinates of points in the physical domain under the conformal map given by the function $z = z(\zeta)$ which is analytic in the strip. The Saffman-Taylor zero surface tension solution is given by

$$z_{st}(\zeta) = \zeta + \frac{1}{k} \ln \frac{1}{2} \left(1 + \exp(-\pi\zeta)\right), \tag{2.38}$$

$$k = \frac{\pi}{2(1-\lambda)}. \tag{2.39}$$

The interface shape is given by $z = z_{st}(i\eta)$ and the width, λ, is a free parameter taking on any value from zero to one. Figures 2.2 and 2.6 help clarify the image of the boundaries of the strip under the map (2.38). It is possible to determine the shape of the tail that this gives as $x \to -\infty$. To accomplish this we set $\zeta = i(1 - r)$

and examine $r \to 0_+$. After some algebra we find

$$y \sim \lambda - r(1 - \frac{\pi}{2k}) + O(r^2), \tag{2.40}$$

$$x \sim \frac{1}{k} \ln \frac{\pi}{2} r + o(\ln r). \tag{2.41}$$

or

$$Y(x) \sim \lambda - \frac{2\lambda}{\pi} e^{kx}. \tag{2.42}$$

This is superficially of the form we require for the non-zero surface tension non-constant gap case but the decay rate, k, of the tail is given by (2.39) while for our problem we require that the relationship between k and λ be given by (2.36).

The correct tail shape for non-constant gap is given by the image of a curve that approaches $\eta = i$ at an angle $\pi/2 - \theta$ to the imaginary axis. To see this we allow ζ to approach i along a ray such the $\zeta = i + r\exp(-i\theta)$. In this case we find, after some careful algebra, that

$$y \sim (1 - \frac{\theta}{k}) - r\sin\theta(1 - \frac{\pi}{2k}), \tag{2.43}$$

$$x \sim \frac{1}{k} \ln \frac{\pi}{2} r + (1 - \frac{\pi}{2k}) r\cos\theta. \tag{2.44}$$

Now we get the interface

$$Y(x) \sim (1 - \frac{\theta}{k}) - \frac{\pi}{2}\sin\theta(1 - \frac{\pi}{2k}) e^{kx}. \tag{2.45}$$

Thus if we fix λ and find k such that (2.36) is satisfied then we must approach along the ray

$$\theta = k(1 - \lambda), \tag{2.46}$$

in order to get the correct asymptotic behaviour for our problem as $x \to -\infty$.

With this in mind we will create our conformal map by composing the Saffman-Taylor map (2.38) with one that approaches $\zeta = i$ along the ray as described above. To accomplish this we construct a map from the strip to a domain that approaches

$\pm i$ along rays at the correct angle as depicted in figure 2.5. We are now in a position to describe the sequence of maps which will take us from the strip in the ζ plane to our final finger shape in the z plane. First there is a 'small' unknown map $\zeta_1(\zeta)$ which deforms the interface $-i < \zeta < i$. Then we have a composite map $\zeta_4 \circ \zeta_3 \circ \zeta_2$ which has the effect of deforming the image under $\zeta \to \zeta_1$ of $-i < \zeta < i$ into a concave shape approaching $\pm i$ at an angle θ. Finally we use the Saffman-Taylor map (2.38) to get the desired finger shape. The map is given by

$$z(\zeta) = z_{st} \circ \zeta_4 \circ \zeta_3 \circ \zeta_2 \circ \zeta_1(\zeta). \tag{2.47}$$

These maps are described schematically in figures 2.2-2.6. They are given by the formulae

$$\zeta_1(\zeta) = \zeta + \sum_{l=0}^{\infty} u_l \exp(-l\pi\zeta), \tag{2.48}$$

$$\zeta_2(\zeta_1) = i \sinh(\frac{\pi}{2}\zeta_1), \tag{2.49}$$

$$\zeta_3(\zeta_2) = \frac{2\theta}{\pi}\left[\frac{(\zeta_2+1)^{2\theta/\pi} + (\zeta_2-1)^{2\theta/\pi}}{(\zeta_2+1)^{2\theta/\pi} - (\zeta_2-1)^{2\theta/\pi}}\right], \tag{2.50}$$

$$\zeta_4(\zeta_3) = \frac{2}{\pi}\ln\left(-i\frac{\pi}{2\theta}\zeta_3 + \sqrt{1-(\pi\zeta_3/2\theta)^2}\right), \tag{2.51}$$

$$z_{st}(\zeta_4) = \zeta_4 + \frac{1}{k}\ln\frac{1}{2}(1+\exp(-\pi\zeta_4)). \tag{2.52}$$

The coefficients $\{u_n\}$ of ζ_1 are real valued.

At least one constraint on ζ_1 is obvious, i.e. $\zeta_1(i) = i$, which can be expressed as

$$\sum_{l=0}^{\infty}(-1)^l u_l = 0. \tag{2.53}$$

A further constraint relating to translation invariance of the finger will be discussed in Appendix A. For the purpose of calculating the map ζ_1 numerically we truncate the sum (2.48) at some finite value $l = L$. Our task will be to determine the coefficients $\{u_l\}$ and the pressure, $\phi(\xi, \eta)$.

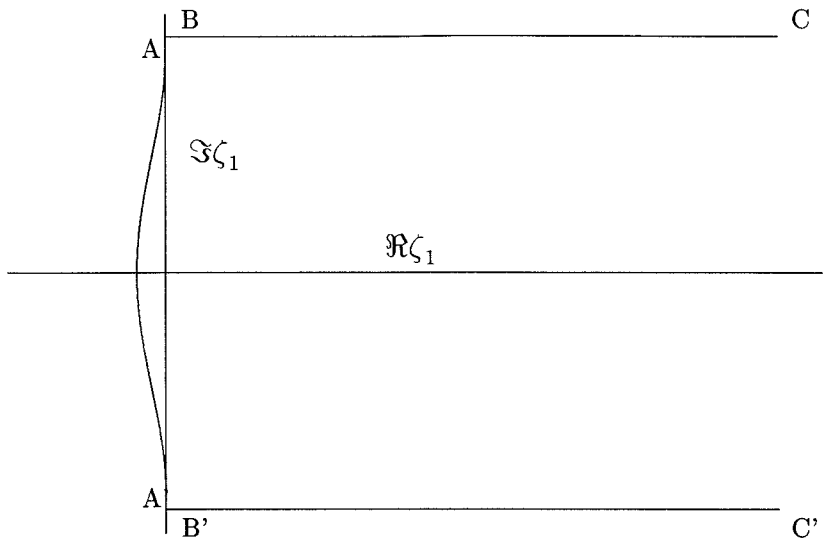

Figure 2.2: The map $\zeta_1(\zeta)$.

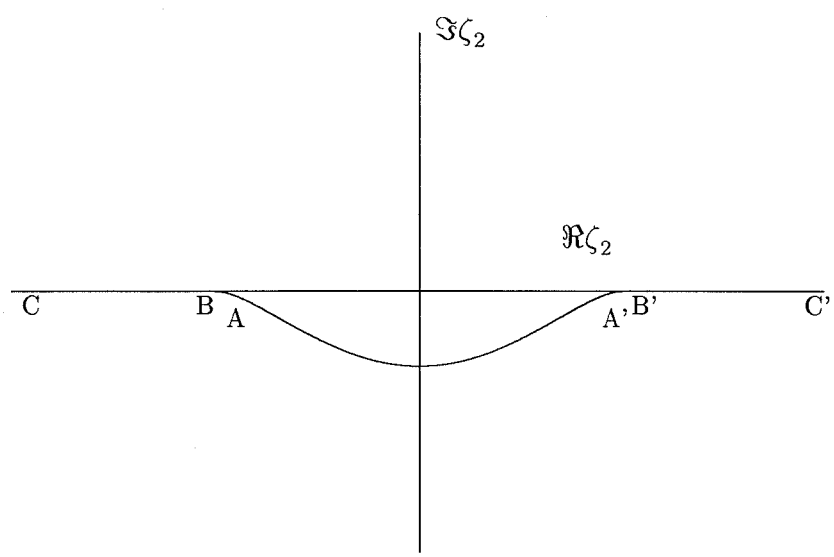

Figure 2.3: The map $\zeta_2 \circ \zeta_1(\zeta)$.

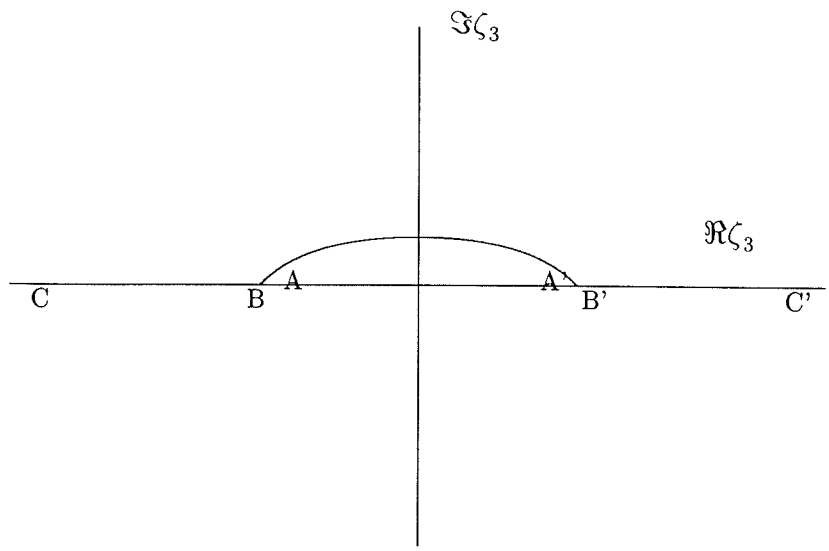

Figure 2.4: The map $\zeta_3 \circ \zeta_2 \circ \zeta_1(\zeta)$.

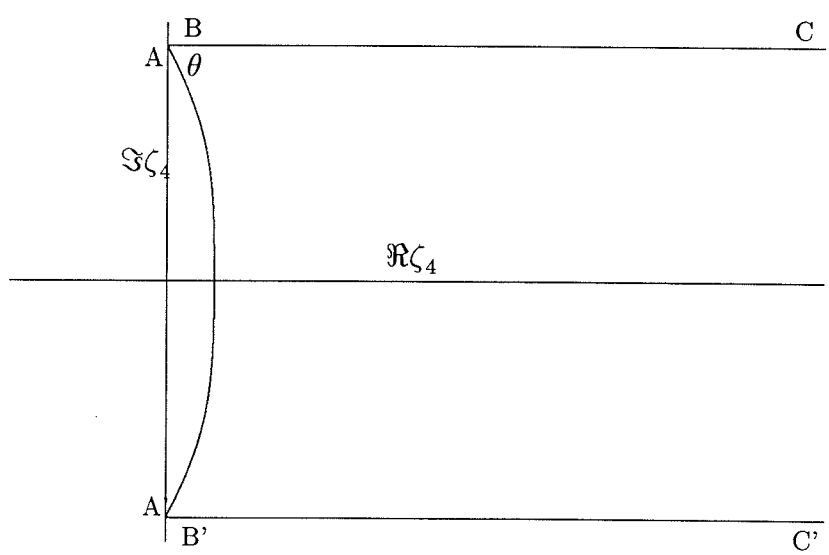

Figure 2.5: The map $\zeta_4 \circ \zeta_3 \circ \zeta_2 \circ \zeta_1(\zeta)$.

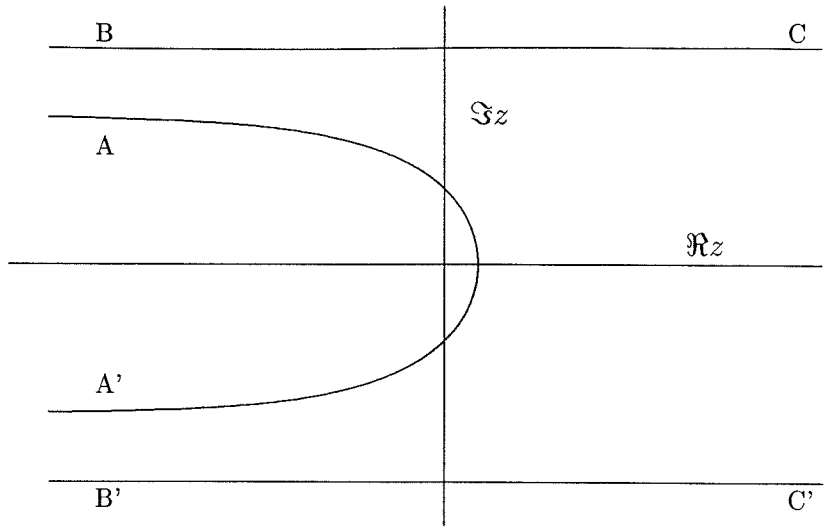

Figure 2.6: The final map $z(\zeta)$.

2.3.3 Equation and Boundary Conditions in the Mapped Domain

We now consider the effect of the inverse map $\zeta = \zeta(z)$ on the equation and boundary conditions. As mentioned before, since we are considering symmetric solutions, we will only consider the inverse image of $y > 0$, that is, $\eta > 0$. It can be shown that the equation for ϕ,

$$\boldsymbol{\nabla} \cdot (h^3(y)\boldsymbol{\nabla}\phi) = 0, \tag{2.54}$$

becomes

$$\nabla^2\phi + \frac{3h'(y)}{h(y)\,|\zeta_z|^2}\left(-\operatorname{Im}\zeta_z\frac{\partial\phi}{\partial\xi} + \operatorname{Re}\zeta_z\frac{\partial\phi}{\partial\eta}\right) = 0, \tag{2.55}$$

on the strip $0 < \eta < 1$, $0 < \xi < \infty$, where $y = \operatorname{Im} z$ and $\zeta_z = 1/z_\zeta$. While (2.55) is not as straightforward as (2.54) , in that the coefficient functions are not as simple, it is still linear.

The mapped boundary conditions are also relatively straightforward. The curvature of the interface, parameterised by $0 < \zeta < i$, is given by the expression

$$\kappa = \left.\frac{\operatorname{Re}(\overline{z_\zeta} z_{\zeta\zeta})}{|z_\zeta|^3}\right|_{\xi=0}. \tag{2.56}$$

Thus the dynamic boundary condition (2.17) becomes

$$\phi|_{\xi=0} = \sigma \left(- \left. \frac{\mathrm{Re}(\overline{z_\zeta} z_{\zeta\zeta})}{|z_\zeta|^3} \right|_{\xi=0} + \frac{a}{b} \frac{2\beta}{h(\mathrm{Im}\, z|_{\xi=0})} \right). \tag{2.57}$$

The kinematic boundary condition, (2.18), is

$$\left. \frac{\partial \phi}{\partial \xi} \right|_{\xi=0} = \frac{1}{h^2(\mathrm{Im}\, z|_{\xi=0})} \mathrm{Re}\, z_\zeta. \tag{2.58}$$

The other flux boundary conditions are

$$\frac{\partial \phi}{\partial \eta} = 0, \qquad \eta = 0, 1, \tag{2.59}$$

$$\phi \sim c\xi, \qquad \xi \to \infty, \tag{2.60}$$

where c is defined by (2.8.)

At this point we note equation (2.55), with boundary conditions (2.58)-(2.60), is sufficient to determine ϕ up to a constant. We have a steady finger shape when we find a map, $z(\zeta)$, such that the pressure boundary condition (2.57) is also satisfied.

2.3.4 Numerical Solution of Equation

In this Section we describe how to construct a numerical approximation to the solution of the pressure equation (2.55) subject to boundary conditions (2.58)-(2.60). In order to work on a finite domain we perform one final map that maps the strip $0 < \eta < 1$, $0 < \xi < \infty$ to the rectangle $0 < \eta < 1$, $0 < q < 1$. We find that a suitable map is given by

$$q = 1 - e^{-\xi}. \tag{2.61}$$

Under this map

$$\frac{\partial}{\partial \xi} = (1 - q) \frac{\partial}{\partial q}. \tag{2.62}$$

The final pressure equation is thus

$$(1-q)^2\frac{\partial^2\phi}{\partial q^2}+\frac{\partial^2\phi}{\partial\eta^2}+(1-q)(w_1(q,\eta)-1)\frac{\partial\phi}{\partial q}+w_2(q,\eta)\frac{\partial\phi}{\partial\eta}=0, \tag{2.63}$$

where

$$w_1(q,\eta) = -\frac{3h'(y(\eta))}{h(y(\eta))\,|\zeta_z|^2}\,\mathrm{Im}\,\zeta_z, \tag{2.64}$$

$$w_2(q,\eta) = \frac{3h'(y(\eta))}{h(y(\eta))\,|\zeta_z|^2}\,\mathrm{Re}\,\zeta_z, \tag{2.65}$$

$$\zeta = -\ln(1-q)+i\eta. \tag{2.66}$$

For later convenience we will define the linear differential operator in (2.63) by

$$\mathfrak{L} := (1-q)^2\frac{\partial^2}{\partial q^2}+\frac{\partial^2}{\partial\eta^2}+(1-q)(w_1(q,\eta)-1)\frac{\partial}{\partial q}+w_2(q,\eta)\frac{\partial}{\partial\eta}. \tag{2.67}$$

The flux boundary conditions (2.58)-(2.60) transform to

$$\frac{\partial\phi}{\partial q} = \frac{1}{h^2(\mathrm{Im}\;z|_{\xi=0})}\,\mathrm{Re}\,z_\zeta, \qquad q=0 \tag{2.68}$$

$$\frac{\partial\phi}{\partial\eta} = 0, \qquad \eta=0,1, \tag{2.69}$$

$$\phi \sim -c\ln(1-q), \qquad q\to 1. \tag{2.70}$$

At this point it is clear from (2.70) that the solution is unbounded as $q\to 1$ (corresponding to $x\to\infty$ in the physical domain) and this singularity must be dealt with if we are to accurately compute the solution. What is not so clear is that, in general, while ϕ is continuous in the corner $q=0,\eta=1$, some of its derivatives are not and this singular behaviour must also be dealt with in order to get an accurate solution. This singularity is discussed in Appendix A.

To deal with these problems we subtract the singular parts from ϕ and attempt to numerically compute the remainder which is better behaved than the original. Thus

for the purposes of our numerical scheme we let

$$\phi = \widetilde{\phi} + \phi_{asym} + \phi_{\infty}. \tag{2.71}$$

where ϕ_{∞} is the part that is singular as $q \to 1$, and ϕ_{asym} is the part that is singular in the corner. Thus we numerically solve for $\widetilde{\phi}$, satisfying the inhomogeneous elliptic equation

$$\mathfrak{L}\widetilde{\phi} = -\mathfrak{L}\phi_{asym} - \mathfrak{L}\phi_{\infty}, \tag{2.72}$$

with appropriately modified boundary conditions. It is clear from (2.70) that we should take ϕ_{∞} as

$$\phi_{\infty} = -c\ln(1-q). \tag{2.73}$$

We leave the determination of ϕ_{asym} to Appendix A.

In order to solve the inhomogeneous equation (2.72) we use a uniform square grid with $(N+1)^2$ grid points $q_i = i/N$, $\eta_j = j/N$, $i,j = 0..N$. We discretise using second order accurate finite differences on a five point stencil. Because of the problems associated with $q \to 1$ and the corner $q = 0$, $\eta = 1$, we solve the PDE on the interior of the domain $i,j = 1..N-1$ and thus use second order accurate one-sided difference formulae to impose the Neumann boundary conditions on $q = 0$, and $\eta = 0, 1$. Because the solution to the problem with Neumann boundary conditions on all four sides is only determined up to a constant, we impose the Dirichlet condition on $q = 1$ that

$$\phi - \phi_{\infty} = 0. \tag{2.74}$$

We then add a suitable constant to ensure $\widetilde{\phi}$ has the correct value in the corner $q = 0$, $\eta = 1$, corresponding to the pressure at infinity in the tails.

Values of the map $z(\zeta)$, and its derivatives, are computed using Fortran code generated by the symbolic manipulator Maple. Values of the function $g(y;k)$ required for ϕ_{asym} are calculated using an Adams-Bashford-Moulton solver from the SLATEC library.

The details described above give us a well posed, well conditioned matrix problem

for the discrete approximation, $\widetilde{\phi}_{ij}$ $i,j = 1..N-1$, which we solve using the A.D.I. method with suitably chosen convergence parameters.

Having solved for $\widetilde{\phi}_{ij}$ on the interior of the domain we use the second order one-sided difference formula

$$\widetilde{\phi}_{0,j} = \left[4\widetilde{\phi}_{1,j} - \widetilde{\phi}_{2,j} - 2\Delta q \left. \frac{\partial \widetilde{\phi}}{\partial q} \right|_{q=0} \right] /3 + O(\Delta q^2), \tag{2.75}$$

to reconstruct $\widetilde{\phi}_{0,j}$ $j = 1..N-1$. We then compute the approximation the full solution on the interface

$$\phi_{0,j} = \phi_{asym}(0, j\Delta\eta) + \phi_{\infty}(0, j\Delta\eta) + \widetilde{\phi}_{0,j}, \ j = 1..N-1. \tag{2.76}$$

We recall that from Appendix A that we require

$$\phi(0,\eta) \sim C(1-\eta)^{4\theta/\pi}, \ \eta \to 1, \tag{2.77}$$

and we use this information to determine a suitable constant to subtract from $\widetilde{\phi}_{i,j}$ so that this is true to second order in $\Delta\eta$. Finally we determine $\phi_{0,0}$ such that

$$\left. \frac{\partial \phi}{\partial \eta} \right|_{0,0} = 0 + O(\Delta\eta^2). \tag{2.78}$$

Having done this we have constructed a second order accurate approximation to $\phi(0,\eta)$ at points η_i, $i = 0..N$ given $\partial\phi/\partial\eta|_{q=0}$.

2.3.5 Satisfying the Pressure Boundary Condition

We have described above how, given a conformal map $z(\zeta)$, it is possible to calculate a second order accurate approximation to the pressure ϕ satisfying

$$\left. \frac{\partial \phi}{\partial n} \right|_{\Gamma} = n_1/h^2(y), \tag{2.79}$$

$$\frac{\partial \phi}{\partial y} = 0, \qquad y = 0, 1, \tag{2.80}$$

$$\phi \sim cx, \qquad x \to \infty. \tag{2.81}$$

It remains to find the particular conformal map, and hence interface shape, such that the pressure boundary condition

$$\phi|_\Gamma = \sigma\left(-\kappa + \frac{a}{b}\frac{2\beta}{h(y)}\right) \tag{2.82}$$

is satisfied. In order to accomplish this task we use Newton's method.

We evaluate the pressure boundary condition, (2.82), at the M discrete points

$$\zeta_m = i\eta_m,$$

$\eta_m = m/M$, $m = 0..M-1$. Thus we get M equations

$$\phi|_{\zeta_m} - \sigma\left(-\kappa_m + \frac{a}{b}\frac{2\beta}{h(y_m)}\right) = 0, \tag{2.83}$$

which we wish to satisfy, where

$$\kappa_m = \left.\frac{\mathrm{Re}(\overline{z_\zeta} z_{\zeta\zeta})}{|z_\zeta|^3}\right|_{\zeta_m}, \tag{2.84}$$

$$y_m = \mathrm{Im}\, z(\zeta_m). \tag{2.85}$$

We have two further constraints on the conformal map which come from $\zeta_1(i) = i$ and translation invariance and they are

$$\sum_{l=0}^{L}(-1)^l u_l = 0, \tag{2.86}$$

$$\sum_{l=0}^{L} l^2(-1)^l u_l = 0. \tag{2.87}$$

Note that there are $L+1$ coefficients u_l.

In the case of zero surface tension ($\sigma = 0$) and constant gap we know that there is a continuous family of solutions parameterised by λ [1]. Thus for zero surface

tension we set $L = M + 1$ and we have $M + 2$ equations for the $M + 2$ unknowns u_l, $l = 0..M + 1$ of the form

$$\mathbf{F}(\mathbf{x}) = 0, \ \mathbf{x} = (u_l). \tag{2.88}$$

For non-zero surface tension ($\sigma \neq 0$) we know that, when $h = const.$, there exists a discrete infinity of solutions at isolated values of λ [4], [20], [21]. We do not expect a varying gap to change this situation. For non-zero surface tension λ is thus an unknown and we find that if we set $L = M$, we get $M + 2$ equations for $M + 2$ unknowns u_l , $l = 0..M$ and λ of the form

$$\mathbf{F}(\mathbf{x}) = 0, \ \mathbf{x} = (u_l, \lambda). \tag{2.89}$$

Further that this set of equations results in a non-singular Jacobian.

We implement Newtons method, that is, given an initial guess $\mathbf{x}^0$ we iterate using the formula

$$\mathbf{x}^{n+1} = \mathbf{x}^n - \frac{\partial \mathbf{F}}{\partial \mathbf{x}}^{-1} \mathbf{F}(\mathbf{x}^n). \tag{2.90}$$

We calculate $\partial \mathbf{F}/\partial \mathbf{x}$ numerically using the usual second order accurate centered difference formula

$$\frac{\partial F_i}{\partial x_j} = \frac{F_i(x_l + \Delta x_l) - F_i(x_l - \Delta x_l)}{2\Delta x_l} + O(\Delta x_l^2). \tag{2.91}$$

Each time one of the u_l is varied we recompute the map and solve a new PDE. When λ is varied it is necessary to compute the new value of k satisfying (2.36) and thus find the new value of the angle θ and then recompute the map and solve the PDE.

The accuracy with which we can compute $\partial F_i/\partial u_l$ depends on the accuracy of the PDE solver. It is found that we have sufficient accuracy when the number of grid points on a side for the PDE solver is twice the number of unknowns describing the conformal map, or in terms of the notation we have been using, $N = 2M$.

The Newton method is considered converged when $\max |F_i| < 10^{-8}$ and this usually occurred in two or three iterations.

2.4 Results

Clearly there is an infinite choice of gap variation functions, $h(y)$, from which to choose. We pick the specific function

$$h(y) = 1 + \varepsilon \cos \pi(y + 1), \tag{2.92}$$

for three reasons. First, when epsilon equals zero we recover the constant gap case considered by other authors for comparison of our results. Second, we are able to solve the problem analytically for small surface tension and epsilon and we wish to compare the results. Lastly it is a reasonable, generic perturbation that could describe elastic buckling of the plates in a Hele-Shaw cell under pressure or suction.

All of the results presented in this section have be calculated with $M = 16$ and $N = 32$, that is a grid with 32 mesh points on a side. Doubling M and N was found to only affect the fourth significant figure of λ and $M = 16$ was considered sufficient.

For zero surface tension we find that it is possible to compute a solution given any width, λ, and that for small ε the solution is close to the Saffman-Taylor solution. Thus for $\varepsilon \neq 0$ the solution structure is similar to the constant gap case, a one parameter family of solutions parameterised by the width, λ. These results confirm the finding in Chapter 3 that gap variation is a regular perturbation for zero surface tension. We show one of these solutions compared to the Saffman-Taylor solution of the same width in Figure 2.7.

For non-zero surface tension the situation is rather different. There are two effects to be considered, the lateral curvature alone ($\beta = 0$) and the combination of lateral and transverse curvature ($\beta = 1$). We find that the lateral curvature is a singular perturbation in that it selects solutions at discrete values of λ from the continuum of zero surface tension solutions. The addition of transverse curvature term considerably modifies the solutions since it is larger in numerical value than the lateral curvature term. We recall that $\beta = 0$ corresponds to porous media flow and $\beta = 1$ corresponds to Hele-Shaw cell flow.

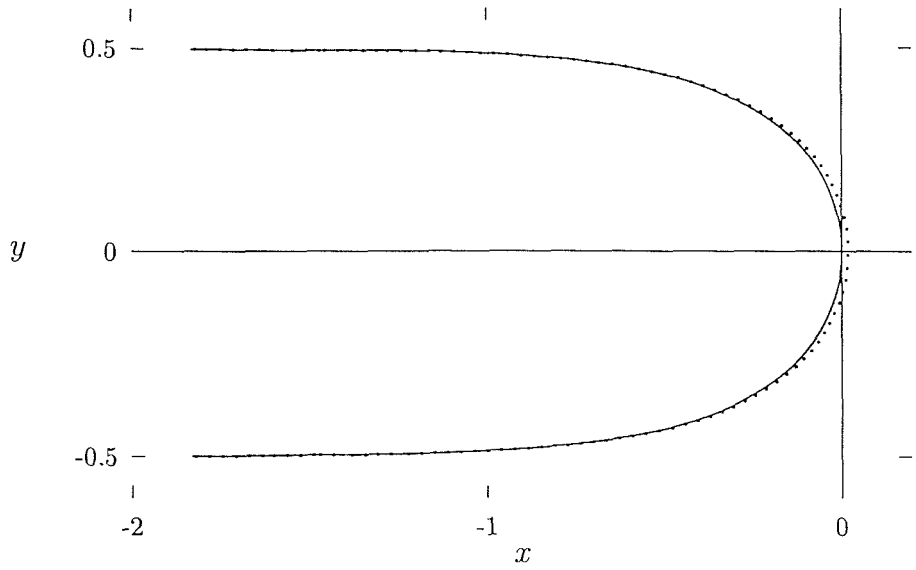

Figure 2.7: Interface shape with zero surface tension, $\lambda = 1/2$. (-) $\varepsilon = 0$, (..) $\varepsilon = 0.01$.

2.4.1 Effect of Lateral Curvature

In this case we only consider the change in pressure on the interface due to curvature in the lateral direction, that is we satisfy the boundary condition

$$\phi|_\Gamma = -\sigma\kappa. \tag{2.93}$$

This corresponds to the porous medium boundary condition. Variations in gap now only affect the flow through the equation for pressure but are still found to have a non-trivial effect on the solution.

When $\varepsilon = 0$ it is relatively straightforward to find the first few solution branches found by previous authors [4], [20], [21]. There is an enumerable infinity of solution branches and on each branch of solutions λ is greater than a half with all the branches tending to $\lambda = 1/2$ like $\lambda - 1/2 = \delta_n \sigma^{2/3}$. We are able to reproduce these results and the curves of λ versus σ for the first four branches are presented in Figure 2.8. It becomes difficult to follow any solution branch below $\sigma \simeq 1 \times 10^{-4}$ as the Jacobian matrix of the system of equations becomes ill-conditioned.

For ε non-zero we find two distinct types of behaviour depending on the sign of ε. We note that ε greater than zero corresponds to plates that are closer together along

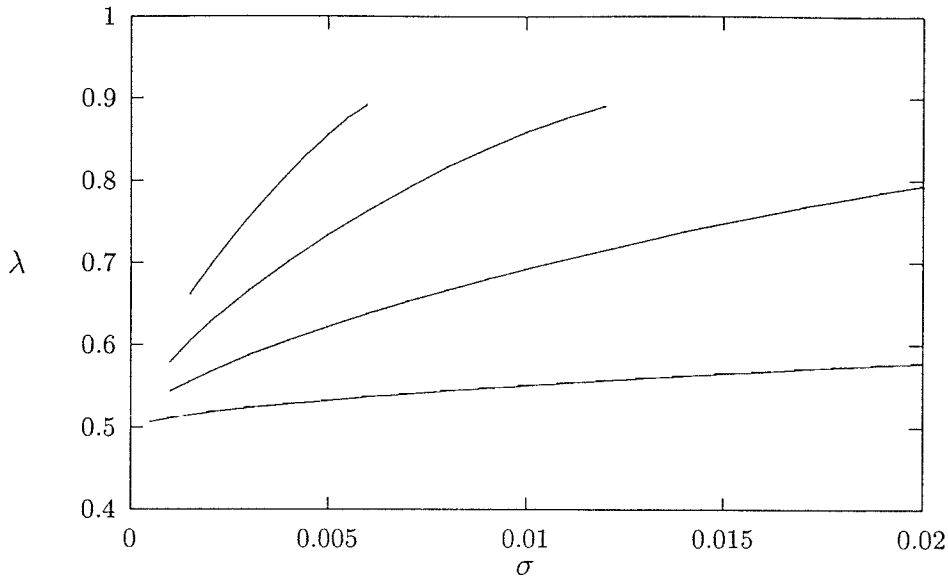

Figure 2.8: Width as a function of σ with $\varepsilon = 0$; first four branches.

the channel centreline than at the walls while ε less than zero corresponds to a bulge along the centreline. We plot the gap variations in Figure 2.9 for future reference.

When ε is greater than zero we find that the solution branches merge in pairs at finite values of surface tension leading to a qualitatively different solution structure from that for a cell of constant gap. For each positive ε the branches merge at some value of λ greater than a half. We find merger for the first four branches but we immediately suspect that the situation is the same for higher branches and the analytic results confirm this. It is again difficult to follow the solutions for small values of surface tension due to the ill conditioning mentioned above. This merger has been seen before in different physical situations, viscous fingering in radially symmetric porous tubes [19] and Hele-Shaw cell flow in sector geometry [18] but in those cases there were large differences in formulation from channel flow whilst the perturbations required to find the same merging scenario here are small. We present curves for three different values of $\varepsilon > 0$ in Figures 2.10, 2.11 and 2.12. Even for the largest value of ε presented here ($\varepsilon = 0.05$) the total variation in gap across the cell is only 10%.

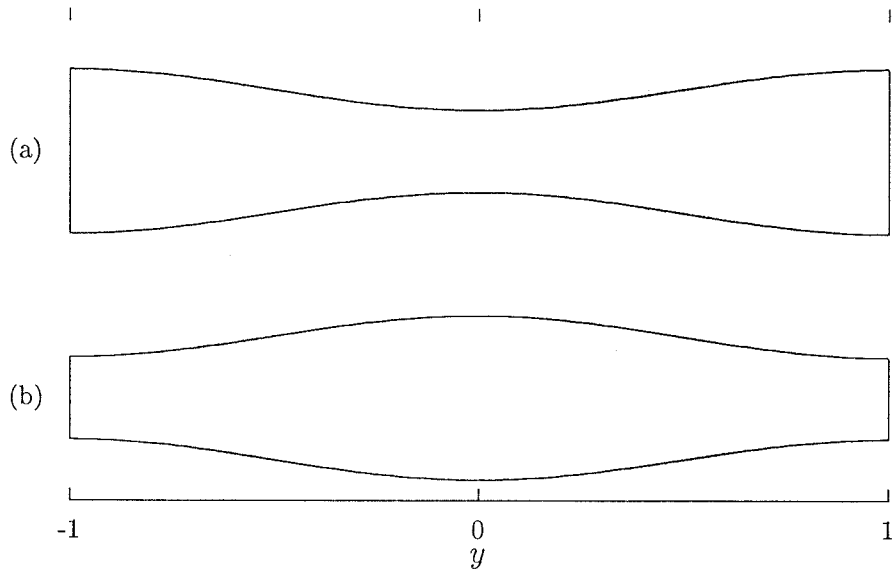

Figure 2.9: Gap variations in lateral direction, (a) $\varepsilon > 0$, (b) $\varepsilon < 0$.

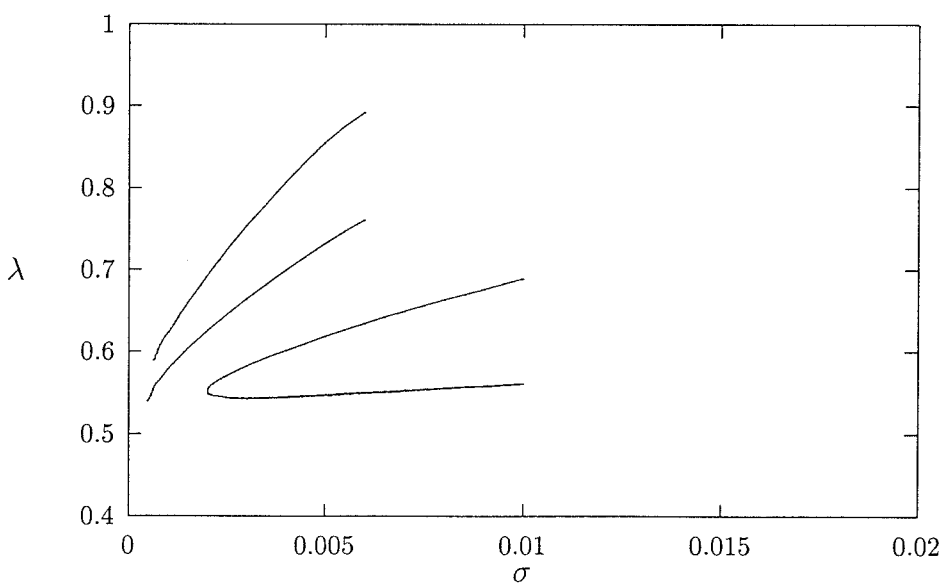

Figure 2.10: Width as a function of σ with $\varepsilon = 0.005$.

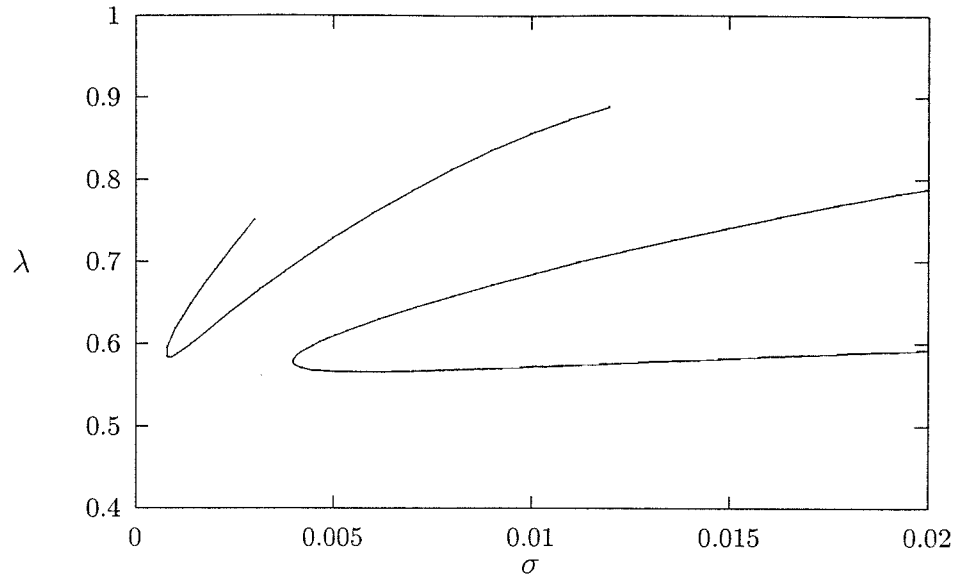

Figure 2.11: Width as a function of σ with $\varepsilon = 0.01$.

When ε is less than zero we find a different scenario. For small negative values of ε the solution branches drop below $\lambda = 1/2$ but become hard to follow before any merging occurs. For larger magnitudes of ε the curves attain values of λ considerably less than a half and seem to merge for very small finite surface tension. This is in itself an interesting result as widths less than a half have only been found previously only by introducing anisotropy into the surface tension [17] or by placing a bubble at the tip of the finger to induce high curvature there [9]. The results are presented in Figures 2.13, 2.14 and 2.15 for different values of ε less than zero. The analytic results are less clear in this case. While values of λ less than a half are predicted the question of branch merger in the small ε, small σ limit remains open.

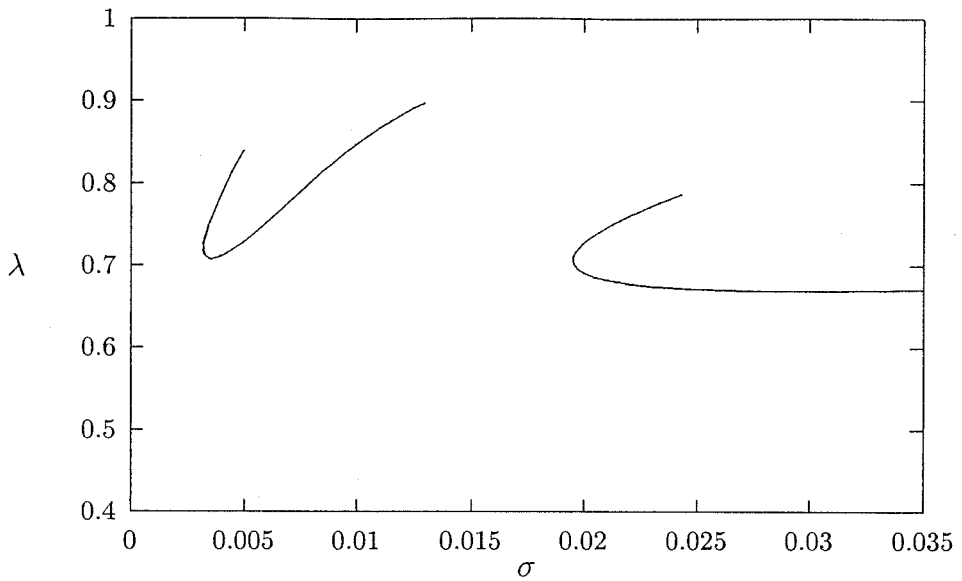

Figure 2.12: Width as a function of σ with $\varepsilon = 0.05$.

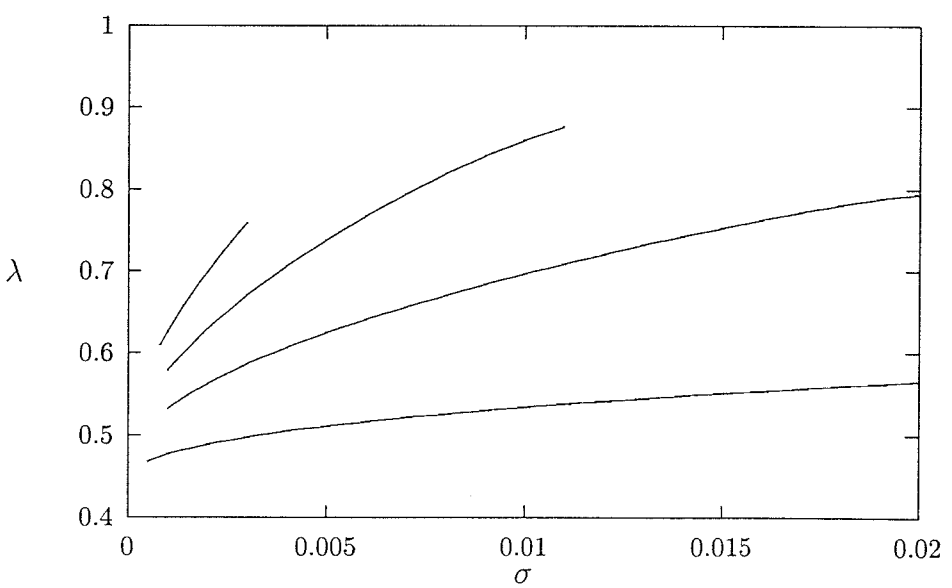

Figure 2.13: Width as a function of σ with $\varepsilon = -0.01$.

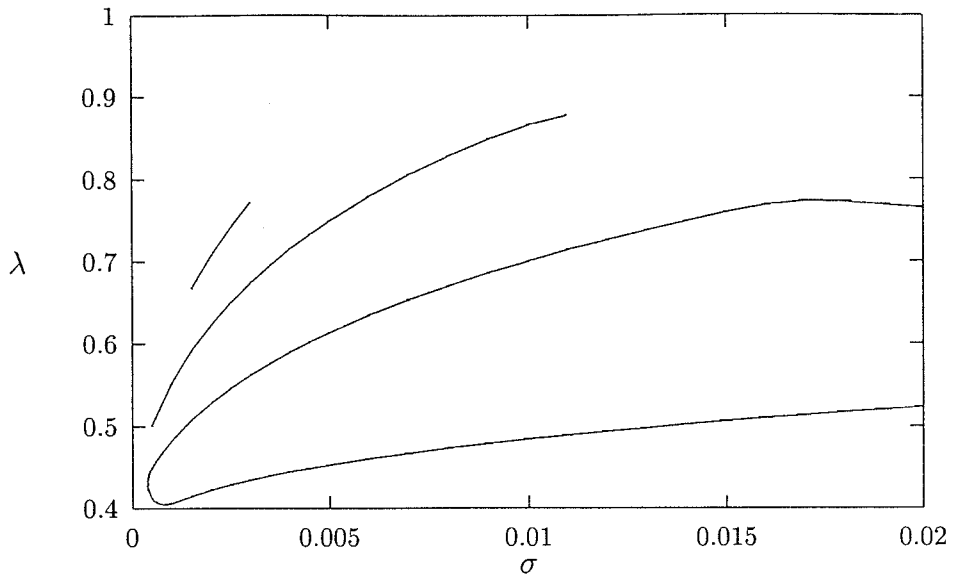

Figure 2.14: Width as a function of σ with $\varepsilon = -0.05$.

2.4.2 Additional Effect of Transverse Curvature

In this Section we present results for the combined effects of lateral and transverse curvature. That is we impose the boundary condition

$$\phi|_\Gamma = \sigma\left(-\kappa + \frac{a}{b}\frac{2}{h(y)}\right), \tag{2.94}$$

corresponding to the boundary condition for Hele-Shaw cell flow. We must choose an aspect ratio, a/b, and for the results presented here we choose $a/b = 100$ which is the correct order for many experimental apparatuses. We find that the singular results of the last Section are enhanced but the qualitative structure is unchanged, at least for small ε. In the Figures here we present the first two solution branches.

For epsilon greater than zero the solutions again merge in pairs. The results for $\varepsilon = 5 \times 10^{-3}$ and $\varepsilon = 9 \times 10^{-3}$ are shown in Figures 2.16 and 2.17. For epsilon larger than 9×10^{-3} we are unable to find solutions, either they have disappeared entirely or they occur only for large surface tension.

For epsilon less than zero we find similar results to the last Section, solutions occur at values of λ considerably less than a half. We present results for two values of ε in Figures 2.18 and 2.19.

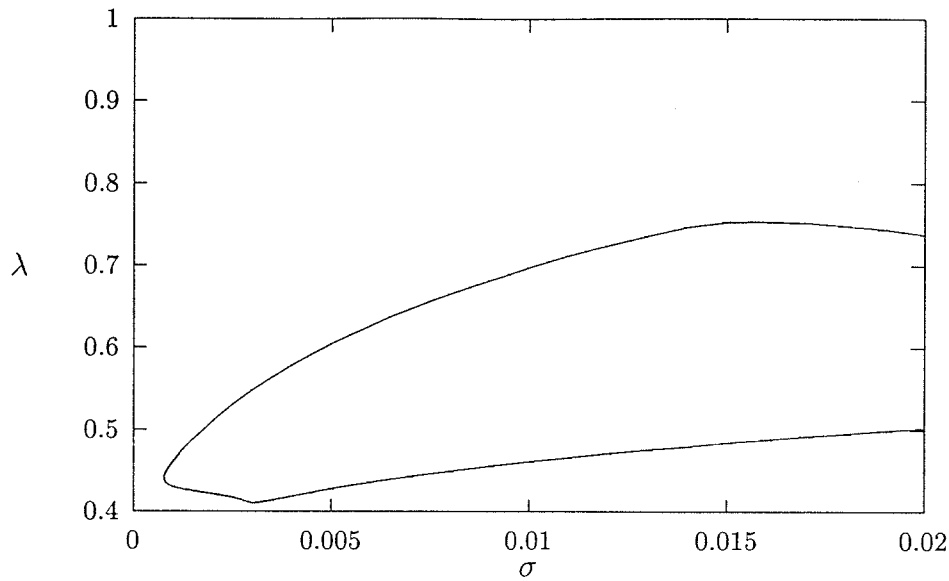

Figure 2.15: Width as a function of σ with $\varepsilon = -0.075$.

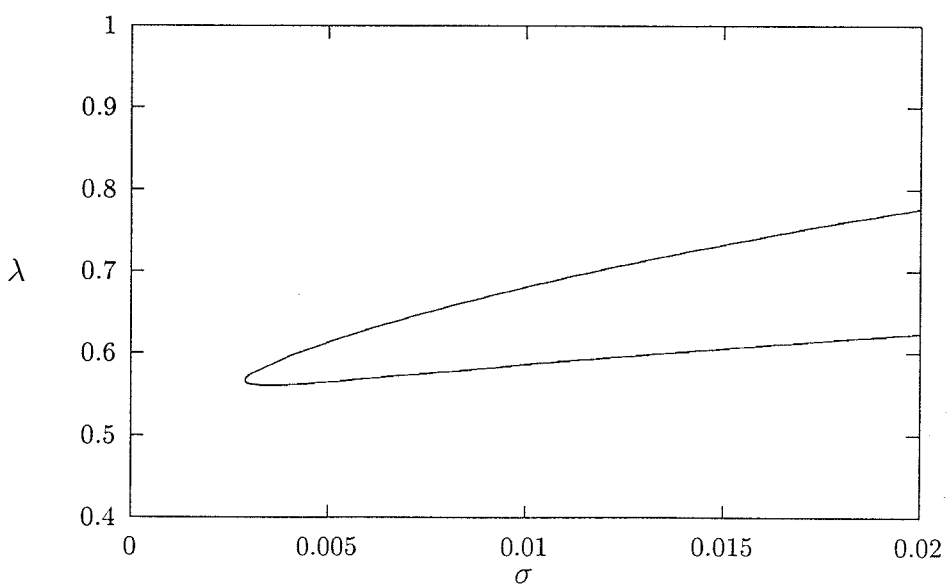

Figure 2.16: Width as a function of σ with $\varepsilon = 0.005$.

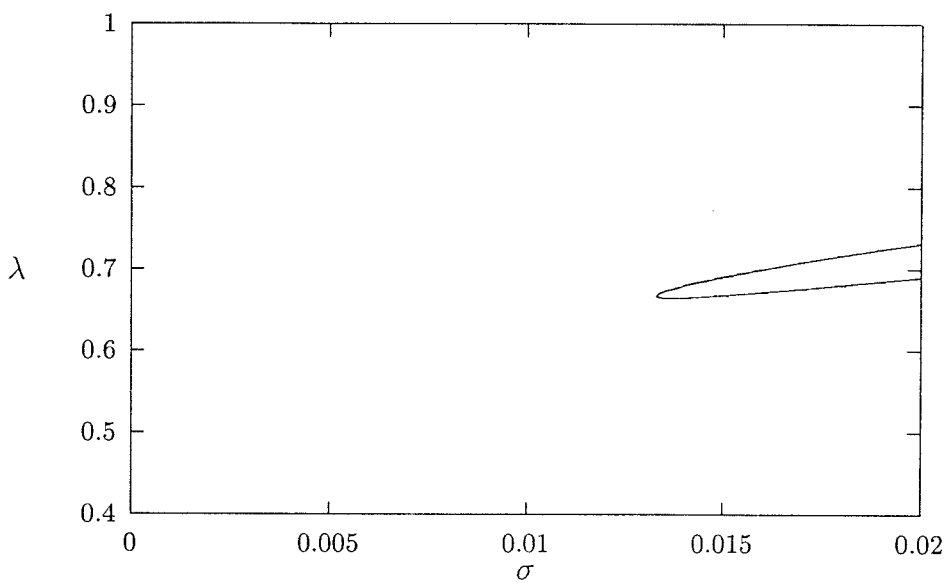

Figure 2.17: Width as a function of σ with $\varepsilon = 0.009$.

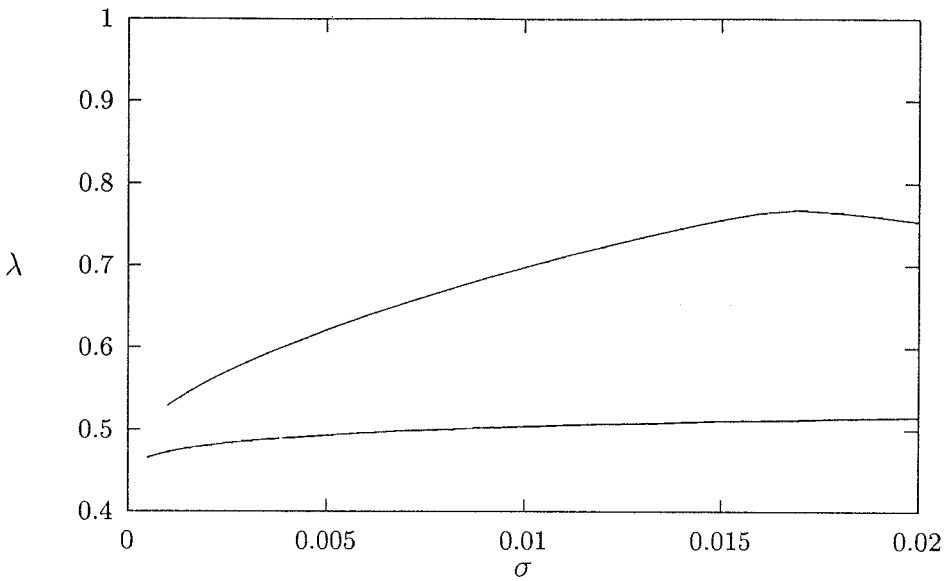

Figure 2.18: Width as a function of σ with $\varepsilon = -0.01$.

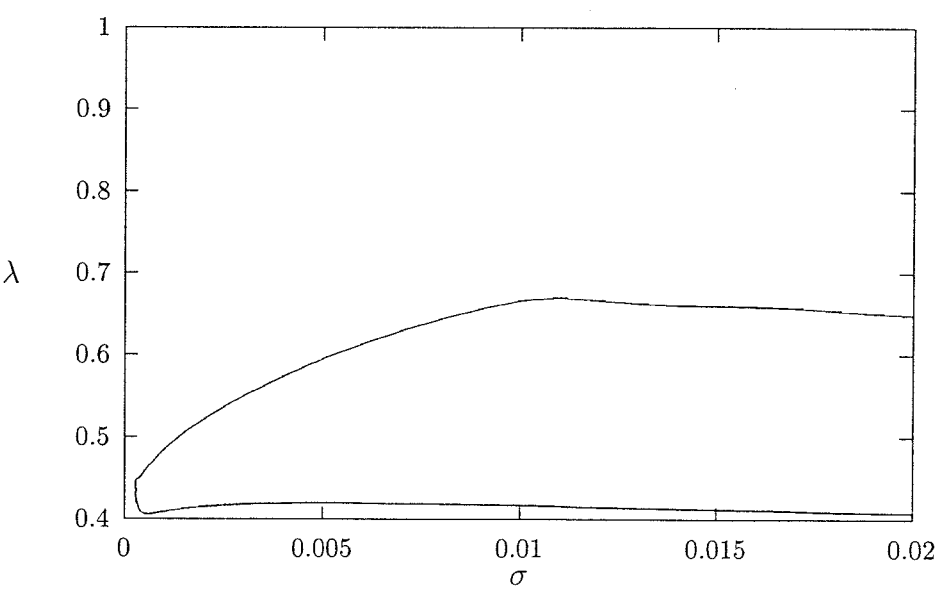

Figure 2.19: Width as a function of σ with $\varepsilon = -0.04$.

Chapter 3 Analytic Selection Mechanism for Small Gap Variations

3.1 Introduction

In this chapter we consider the fingering problem from an analytic point of view. Since the discovery by McLean and Saffman [4] that surface tension selects a discrete set of solutions from the continuous one parameter family of Saffman-Taylor fingers there has been extensive investigation of the analytic basis for the selection mechanism. A regular expansion in surface tension was attempted by McLean and Saffman [3], [4] but yielded no selection mechanism in contrast to their numerical results. The resolution of the contradiction was found by several groups simultaneously [13], [14], [15], and later by Tanveer [16]. The resolution involved exponential terms in surface tension neglected in a regular asymptotic expansion. Since then several authors have considered similar fingering problems with altered boundary conditions and in different geometries. Dorsey and Martin [17] considered the effect of anisotropic surface tension on the fingering problem in a channel and found that all widths are possible not just those greater than a half. Finger selection in sector geometry was investigated analytically by Combescot [18] for small sector opening angles. Solution branches were found to merge for finite surface tension. The fingering problem in a radially symmetric porous cylinder was considered numerically by Levine and Tu [19] and again solution branches were found to merge for finite surface tension.

We consider the effect of a small variation in the distance between the plates in the direction perpendicular to the motion of the finger. We quickly specialise to a particular variation corresponding to a cosine shaped bulge or contraction in the plates. In the case where the plates are closer along the centreline than at the edges we find solutions with widths less than a half. By contrast, when the plates bulge

apart along the centreline we find that the solution branches merge in pairs for finite surface tension.

There are two natural steps in the solution of the problem. First we consider the problem in the absence of surface tension and find that the solution is a regular perturbation to the Saffman-Taylor solution. The width, λ, of the finger is still a free parameter. We express the result in terms of an integral and do an explicit calculation for one particular choice of perturbation to the gap. We then add surface tension in a similar way to Tanveer [16]. It is possible to find a regular expansion for the small surface tension correction in powers of the surface tension, however, this expansion neglects the presence of exponential terms in surface tension and again yields no selection mechanism. Only for certain values of λ can the exponential terms be guaranteed to be small in the physical domain. These exponential terms become order one in the domain outside the finger and it is there that we must seek them.

We find a second order differential equation satisfied by the analytic continuation of the small surface tension correction to the interface in the region outside the physical domain. In general it is found that the effect of gap variation is small, however, the effect becomes significant as λ tends to a half. We analyse the equation in this limit and it is found that only the asymptotic behaviour of the zero surface tension correction is required. The linearised equation can be treated using WKBJ theory and is found to have three turning points in contrast to the constant gap case with two turning points. The ability to construct a uniformly small solution is dependant on the location of these turning points and this gives rise to the selection mechanism. The selection mechanism for the full nonlinear equation is similar but in the absence of a simplifying theory we resort to numerical integration along special contours to determine the selected widths.

3.2 Formulation of Problem

The statement of the problem is identical to the Chapter 2. Our problem is to find a dimensionless pressure ϕ satisfying

$$\nabla.(h^3(y)\nabla\phi) = 0, \tag{3.1}$$

in the fluid filled domain and a finger shape Γ such that the following boundary conditions are satisfied on the finger and the fixed walls:

$$\begin{aligned} c\phi|_\Gamma &= -\sigma\kappa, & (3.2)\\ c\frac{\partial\phi}{\partial n}|_\Gamma &= \mathbf{n}.\mathbf{e}_x/h^2(y), & (3.3)\\ \frac{\partial\phi}{\partial y}|_{y=\pm1} &= 0, & (3.4)\\ \phi|_{x\to\infty} &\sim x, & (3.5) \end{aligned}$$

where

$$\begin{aligned} c &= \frac{\int_{-\lambda}^{\lambda} h(y)dy}{\int_{-1}^{1} h^3(y)dy}, & (3.6)\\ \sigma &= \frac{Tb^2}{12\mu Ua^2}. & (3.7) \end{aligned}$$

For analytical work it is convenient to map the problem to the unit semicircle in the upper half complex plane. We seek a conformal map, $z(\zeta)$, that maps the fluid filled domain to the unit semicircle with the unit arc corresponding to the finger boundary and the real diameter corresponding to the straight walls (see Figures 3.1 and 3.2.) We will be working with the complex variables $z = x + iy$, and $\zeta = \xi + i\eta$ or alternatively $\zeta = r\exp i\theta$. We will seek ϕ in the form $\phi = \phi(\zeta, \bar{\zeta})$. Under the change of variables $\zeta = \zeta(z), \bar{\zeta} = \bar{\zeta}(\bar{z})$, the equation for ϕ becomes

$$4\phi_{\zeta\bar{\zeta}} + 3i\frac{h'}{h}(\bar{z}_{\bar{\zeta}}\frac{\partial}{\partial\zeta} - z_\zeta\frac{\partial}{\partial\bar{\zeta}})\phi = 0. \tag{3.8}$$

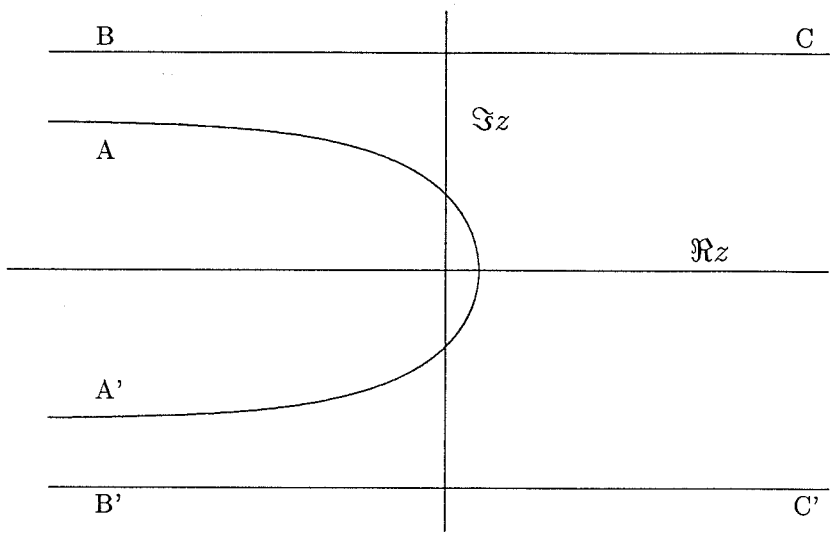

Figure 3.1: The finger in the z plane.

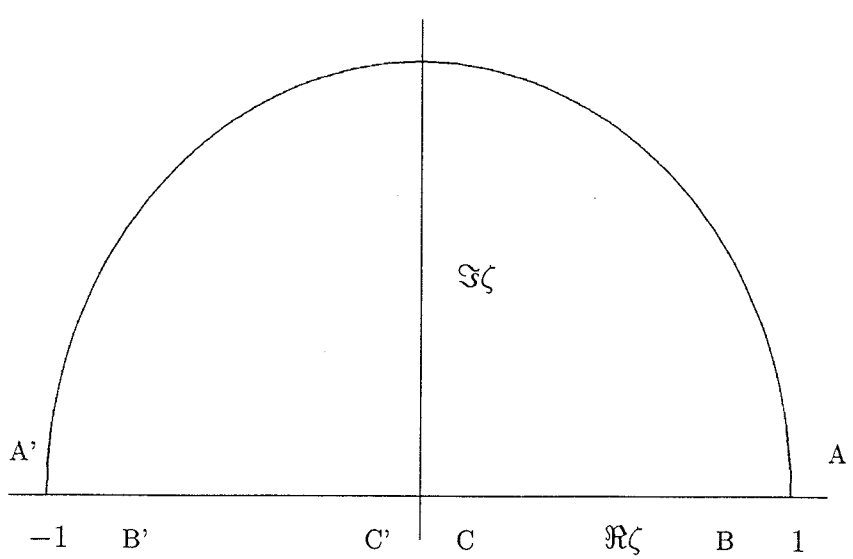

Figure 3.2: Fluid filled domain in ζ plane.

The boundary conditions on the unknown finger become the following boundary conditions on the upper arc of the unit semicircle:

$$c\phi = -\sigma\left(\frac{1+\mathrm{Re}(\zeta z_{\zeta\zeta}/z_\zeta)}{|z_\zeta|}\right), \tag{3.9}$$

$$c\frac{\partial\phi}{\partial r} = \frac{\mathrm{Re}(\zeta z_\zeta)}{h^2(\mathrm{Im}\, z(\zeta))}. \tag{3.10}$$

The boundary condition on the diameter of the unit semi-circle is

$$\frac{\partial\phi}{\partial\eta} = 0. \tag{3.11}$$

The solution to the problem when $\sigma = 0$, $h(y) = 1$ is the Saffman-Taylor solution given by

$$z_{st}(\zeta) = -\frac{2}{\pi}\ln\zeta + \frac{2}{\pi}(1-\lambda)\ln(\zeta^2-1) - i(1-2\lambda), \tag{3.12}$$

$$\phi_0(\zeta,\bar{\zeta}) = -\frac{1}{\pi}(\ln -i\zeta + \ln i\bar{\zeta}). \tag{3.13}$$

3.3 Problem for Zero Surface Tension

We first formulate the problem for small gap width and zero surface tension and then consider the effect of non-zero surface tension. We introduce the small parameter ε as follows:

$$h(y) = 1 + \varepsilon h_1(y). \tag{3.14}$$

While we formulate the problem for general $h_1(y)$, we do specific calculations for the specific choice of

$$h_1(y) = \cos\pi(y+1). \tag{3.15}$$

We look for a solution that is close to the Saffman-Taylor solution and to do this we assume

$$z(\zeta) = z_{st}(\zeta) + \varepsilon f_\varepsilon(\zeta) + O(\varepsilon^2), \tag{3.16}$$

$$\phi(\zeta,\bar{\zeta}) = \phi_0(\zeta,\bar{\zeta}) + \varepsilon\phi_\varepsilon(\zeta,\bar{\zeta}) + O(\varepsilon^2), \tag{3.17}$$

and it follows from (3.6) that

$$c = \lambda + \varepsilon c_1(\lambda) + O(\varepsilon^2),$$

where

$$c_1(\lambda) = \int_{-\lambda}^{\lambda} h_1(y)dy. \tag{3.18}$$

The leading order problem is

$$\phi_{0\zeta\bar{\zeta}} = 0, \tag{3.19}$$

with boundary conditions

$$\lambda\frac{\partial\phi_0}{\partial r} = \mathrm{Re}(\zeta z_{st\zeta}), \tag{3.20}$$

$$\phi_0 = 0, \tag{3.21}$$

on the arc of the unit semicircle and

$$\frac{\partial\phi_0}{\partial\eta} = 0, \quad -1 < \zeta < 1. \tag{3.22}$$

The solution to this problem is the Saffman-Taylor solution above. We note that equation (3.19) is Laplace's equation expressed in terms of ζ and $\bar{\zeta}$.

The order ε problem for ϕ_ε and f_ε is

$$\phi_{\varepsilon\zeta\bar{\zeta}} = -\frac{3}{4}ih_1'(\frac{z_{st}-\bar{z}_{st}}{2i})(\bar{z}_{st\bar{\zeta}}\frac{\partial}{\partial\zeta} - z_{st\zeta}\frac{\partial}{\partial\bar{\zeta}})\phi_0. \tag{3.23}$$

with boundary conditions

$$\lambda\frac{\partial\phi_\varepsilon}{\partial r} = -c_1\frac{\partial\phi_0}{\partial r} + \mathrm{Re}(\zeta f_{\varepsilon\zeta}) - 2h_1(\frac{z_{st}-\bar{z}_{st}}{2i})\,\mathrm{Re}(\zeta z_{st\zeta}), \tag{3.24}$$

$$\phi_\varepsilon = 0, \tag{3.25}$$

on the arc, and

$$\frac{\partial \phi_\varepsilon}{\partial \eta} = 0, \quad -1 < \zeta < 1. \tag{3.26}$$

Note equation (3.23) is a Poisson equation for ϕ_ε. Now ϕ_ε is entirely determined by equation (3.23) and boundary conditions (3.25) and (3.26). Once we have determined $\phi_\varepsilon(\zeta, \bar{\zeta})$, equation (3.24) serves to determine $f_{\varepsilon\zeta}$.

3.3.1 Solution of the Order ε Equation

We can solve the Poisson equation (3.23) if we can find a particular solution $\phi_{\varepsilon P}$. Once we have $\phi_{\varepsilon P}$ then

$$\phi_\varepsilon = \phi_{\varepsilon H} + \phi_{\varepsilon P}, \tag{3.27}$$

where

$$\nabla^2 \phi_{\varepsilon H} = 0, \tag{3.28}$$

$$\phi_{\varepsilon H} = -\phi_{\varepsilon P}, \qquad \zeta = e^{i\theta},\ 0 < \theta < \pi, \tag{3.29}$$

$$\frac{\partial \phi_{\varepsilon H}}{\partial \eta} = -\frac{\partial \phi_{\varepsilon P}}{\partial \eta}, \qquad -1 < \zeta < 1. \tag{3.30}$$

We now construct a particular solution $\phi_{\varepsilon P}(\zeta, \bar{\zeta})$ to (3.23). We can simplify (3.23) with some simple observations. First we note

$$\frac{\partial}{\partial \zeta} h_1\left(\frac{z_{st}(\zeta) - \bar{z}_{st}(\bar{\zeta})}{2i}\right) = \frac{1}{2i} h_1'\left(\frac{z_{st}(\zeta) - \bar{z}_{st}(\bar{\zeta})}{2i}\right) \frac{dz_{st}}{d\zeta}, \tag{3.31}$$

$$\frac{\partial}{\partial \bar{\zeta}} h_1\left(\frac{z_{st}(\zeta) - \bar{z}_{st}(\bar{\zeta})}{2i}\right) = -\frac{1}{2i} h_1'\left(\frac{z_{st}(\zeta) - \bar{z}_{st}(\bar{\zeta})}{2i}\right) \frac{d\bar{z}_{st}}{d\bar{\zeta}}. \tag{3.32}$$

Second, since ϕ_0 is harmonic,

$$\phi_0 = \operatorname{Re} w_0 = \frac{1}{2}(w_0(\zeta) + \bar{w}_0(\bar{\zeta})), \tag{3.33}$$

$$w_0 = -\frac{2}{\pi} \ln(-i\zeta). \tag{3.34}$$

With the second of these simplifications equation (3.23) becomes

$$\phi_{\varepsilon\zeta\bar{\zeta}} = \frac{-3i}{8}[h_1'(\frac{z_{st}(\zeta)-\bar{z}_{st}(\bar{\zeta})}{2i})\frac{d\bar{z}}{d\bar{\zeta}}\frac{dw_0}{d\zeta} - h_1'(\frac{z_{st}(\zeta)-\bar{z}_{st}(\bar{\zeta})}{2i})\frac{dz}{d\zeta}\frac{d\bar{w}_0}{d\bar{\zeta}}]. \tag{3.35}$$

A particular solution to this is the sum of two particular solutions, one for each member on the right hand side. We concentrate on a particular solution for the first member and using the first simplification above we find

$$\phi_{\varepsilon\zeta\bar{\zeta}} = \frac{-3i}{8}h_1'(\frac{z_{st}(\zeta)-\bar{z}_{st}(\bar{\zeta})}{2i})\frac{d\bar{z}}{d\bar{\zeta}}\frac{dw_0}{d\zeta}, \tag{3.36}$$

$$= -\frac{3}{4}\frac{\partial}{\partial\bar{\zeta}}h_1(\frac{z_{st}(\zeta)-\bar{z}_{st}(\bar{\zeta})}{2i})\frac{dw_0}{d\zeta}. \tag{3.37}$$

We can now integrate with respect to $\bar{\zeta}$ to get

$$\phi_{\varepsilon\zeta} = -\frac{3}{4}h_1(\frac{z_{st}(\zeta)-\bar{z}_{st}(\bar{\zeta})}{2i})\frac{dw_0}{d\zeta}, \tag{3.38}$$

integrating again with respect to ζ we find

$$\phi_{\varepsilon} = -\frac{3}{4}\int^{\zeta} h_1(\frac{z_{st}(\zeta)-\bar{z}_{st}(\bar{\zeta})}{2i})\frac{dw_0}{d\zeta}d\zeta. \tag{3.39}$$

We can repeat this for the second member to get the final result

$$\phi_{\varepsilon P}(\zeta,\bar{\zeta}) = -\frac{3}{4}\left[\int^{\zeta} h_1(\frac{z_{st}(\zeta)-\bar{z}_{st}(\bar{\zeta})}{2i})\frac{dw_0}{d\zeta}d\zeta \right. \tag{3.40}$$

$$\left. + \int^{\bar{\zeta}} h_1(\frac{z_{st}(\zeta)-\bar{z}_{st}(\bar{\zeta})}{2i})\frac{d\bar{w}_0}{d\bar{\zeta}}d\bar{\zeta}\right]. \tag{3.41}$$

If we can calculate this $\phi_{\varepsilon P}$ then we can use it to solve for $\phi_{\varepsilon H}$. In particular if $\phi_{\varepsilon P}$ satisfies $\partial\phi_{\varepsilon P}/\partial\eta = 0$ on the real diameter then, since $\bar{\zeta} = 1/\zeta$ on the unit circle,

$$\phi_{\varepsilon H} = \mathrm{Re}\,\frac{-1}{2\pi i}\int_{\frown}\frac{d\zeta'}{\zeta'}K(\zeta,\zeta')\phi_{\varepsilon P}(\zeta',\frac{1}{\zeta'}), \tag{3.42}$$

where $K(\zeta,\zeta')$ is the Poisson Kernel for harmonic functions with zero Neumann deriv-

ative on the diameter of the unit semi-circle

$$K(\zeta,\zeta') = \frac{\zeta'+\zeta}{\zeta'-\zeta} + \frac{1+\zeta\zeta'}{1-\zeta\zeta'}, \tag{3.43}$$

and the path of integration counter-clockwise along the arc of the upper unit semi-circle.

For the case $h_1(y) = \cos\pi(y+1)$ we calculate

$$h_1(\frac{z_{st}(\zeta) - \bar{z}_{st}(\bar{\zeta})}{2i})$$

in Appendix B and we calculate $\phi_{\varepsilon P}$ explicitly in Appendix C. We find, in this case, that $\partial\phi_{\varepsilon P}/\partial\eta = 0$ on the real diameter.

3.3.2 Calculation of the Order ε Conformal Map

Having determined a particular solution $\phi_{\varepsilon P}$ we now move on to the determination of $f_{\varepsilon\zeta}(\zeta)$. We use remaining boundary condition (3.24) which can be simplified using the Saffman-Taylor solution to

$$\begin{aligned} \mathrm{Re}(\zeta f_{\varepsilon\zeta}) &= -\frac{2}{\pi}c_1(\lambda) + \lambda\frac{\partial\phi_\varepsilon}{\partial r} - \frac{4}{\pi}\lambda h_1(\frac{z_{st}-\bar{z}_{st}}{2i}), & (3.44)\\ &= -\frac{2}{\pi}c_1(\lambda) + \lambda(\frac{\partial\phi_{\varepsilon H}}{\partial r} + \frac{\partial\phi_{\varepsilon P}}{\partial r}) - \frac{4}{\pi}\lambda h_1(\frac{z_{st}-\bar{z}_{st}}{2i}), & (3.45)\end{aligned}$$

on the arc of the unit semi-circle. Now $\phi_{\varepsilon H}$ is harmonic and thus $\phi_{\varepsilon H} = \mathrm{Re}\, w_\varepsilon$ where $w_\varepsilon(\zeta)$ is an analytic function inside the unit semi-circle with $\mathrm{Im}\, w_\varepsilon = 0$ on the real diameter. Thus

$$\frac{\partial\phi_{\varepsilon H}}{\partial r} = \mathrm{Re}(\zeta w_{\varepsilon\zeta}). \tag{3.46}$$

In general ϕ_ε is a function of ζ and $\bar{\zeta}$ however on the arc of the unit semi-circle we know $\bar{\zeta} = 1/\zeta$ and thus

$$\begin{aligned} \phi_\varepsilon(\zeta,\bar{\zeta}) &= \phi_\varepsilon(\zeta,1/\zeta), & (3.47)\\ \frac{\partial\phi_\varepsilon(\zeta,\bar{\zeta})}{\partial r} &= \frac{\partial\phi_\varepsilon(\zeta,1/\zeta)}{\partial r}, & (3.48)\end{aligned}$$

so clearly both are functions of ζ alone on the boundary. We can now employ the Poisson integral formula for the semi-circle to find $f_{\varepsilon\zeta}$. We proceed by integrating (3.45) times the Poisson kernel along the arc of the unit semi-circle, that is,

$$\begin{aligned}\frac{1}{2\pi i}\int_{\curvearrowleft}\frac{d\zeta'}{\zeta'}K(\zeta,\zeta')\,\mathrm{Re}(\zeta' f_{\varepsilon\zeta}(\zeta')) &= \frac{-1}{2\pi i}\int_{\curvearrowleft}\frac{d\zeta'}{\zeta'}K(\zeta,\zeta')\frac{2}{\pi}c_1(\lambda) \\ &+\frac{1}{2\pi i}\int_{\curvearrowleft}\frac{d\zeta'}{\zeta'}K(\zeta,\zeta')\lambda\zeta' w_{\varepsilon\zeta}(\zeta') \\ &+\frac{1}{2\pi i}\int_{\curvearrowleft}\frac{d\zeta'}{\zeta'}K(\zeta,\zeta')\lambda\frac{\partial\phi_{\varepsilon P}}{\partial r}(\zeta',\frac{1}{\zeta'}) \\ &-\frac{1}{2\pi i}\int_{\curvearrowleft}\frac{d\zeta'}{\zeta'}K(\zeta,\zeta')\frac{4}{\pi}\lambda h_1(\zeta',1/\zeta').\end{aligned} \tag{3.49}$$

Since both f_ε and w_ε are analytic inside the unit semi-circle with vanishing imaginary part on the real diameter we may evaluate two of the integrations to find

$$\begin{aligned}\zeta f_{\varepsilon\zeta}(\zeta) &= -\frac{2}{\pi}c_1(\lambda)+\lambda\zeta w_{\varepsilon\zeta}(\zeta)+\frac{\lambda}{2\pi i}\int_{\curvearrowleft}\frac{d\zeta'}{\zeta'}K(\zeta,\zeta')\frac{\partial\phi_{\varepsilon P}}{\partial r}(\zeta',1/\zeta') \\ &-\frac{\lambda}{2\pi i}\int_{\curvearrowleft}\frac{d\zeta'}{\zeta'}K(\zeta,\zeta')\frac{4}{\pi}h_1(\zeta',1/\zeta').\end{aligned} \tag{3.50}$$

We can compute w_ε given $\phi_{\varepsilon P}$ since $\phi_{\varepsilon H}=\mathrm{Re}\,w_\varepsilon=-\phi_{\varepsilon P}$ on the unit semi-circle. Thus

$$w_\varepsilon(\zeta)=-\frac{1}{2\pi i}\int_{\curvearrowleft}\frac{d\zeta'}{\zeta'}K(\zeta,\zeta')\phi_{\varepsilon P}(\zeta',1/\zeta'). \tag{3.51}$$

Substituting this into equation (3.50) we obtain an expression for the correction to the map for ζ inside the unit semi-circle in terms of $\phi_{\varepsilon P}$ and $\partial\phi_{\varepsilon P}/\partial r$ on the unit semi-circle

$$\begin{aligned}f_{\varepsilon\zeta}(\zeta) &= -\frac{2}{\pi\zeta}c_1(\lambda)-\frac{\lambda}{2\pi i}\frac{d}{d\zeta}\int_{\curvearrowleft}\frac{d\zeta'}{\zeta'}K(\zeta,\zeta')\phi_{\varepsilon P}(\zeta',1/\zeta') \\ &+\frac{1}{\zeta}\frac{\lambda}{2\pi i}\int_{\curvearrowleft}\frac{d\zeta'}{\zeta'}K(\zeta,\zeta')\frac{\partial\phi_{\varepsilon P}}{\partial r}(\zeta',1/\zeta') \\ &-\frac{1}{\zeta}\frac{4}{\pi}\frac{\lambda}{2\pi i}\int_{\curvearrowleft}\frac{d\zeta'}{\zeta'}K(\zeta,\zeta')h_1(\zeta',1/\zeta').\end{aligned} \tag{3.52}$$

For convenience we write this as

$$f_{\varepsilon\zeta}(\zeta) = -\frac{2}{\pi\zeta}c_1(\lambda) - \lambda\frac{d}{d\zeta}I_1(\zeta) + \frac{\lambda}{\zeta}I_2(\zeta) - \frac{\lambda}{\zeta}\frac{4}{\pi}I_3(\zeta). \tag{3.53}$$

The analytic continuation of this expression outside the unit circle is

$$\begin{aligned} f_{\varepsilon\zeta}(\zeta) &= -\frac{2}{\pi\zeta}c_1(\lambda) - \lambda\frac{d}{d\zeta}[I_1(\zeta) + 2\phi_{\varepsilon P}(\zeta, 1/\zeta)] \\ &\quad + \frac{\lambda}{\zeta}[I_2(\zeta) + 2\frac{\partial\phi_{\varepsilon P}}{\partial r}(\zeta, 1/\zeta)] - \frac{\lambda}{\zeta}\frac{4}{\pi}[I_3(\zeta) + 2h_1(\zeta, 1/\zeta)]. \end{aligned} \tag{3.54}$$

The asymptotic behavior of $f_{\varepsilon\zeta}(\zeta)$ as $\zeta \to \infty$ is needed in order to compute the small surface tension correction correctly and we present this asymptotic behaviour in Appendix C, again for the particular choice $h_1(y) = \cos\pi(y+1)$.

In this Section we have developed an integral expression (3.53) for the order ε correction to the derivative of the zero surface tension map. This expression is in terms of $\phi_{\varepsilon P}$ and $\partial\phi_{\varepsilon P}/\partial r$ and the height perturbation on the arc of the unit semi-circle. There is no restriction on this procedure and we are able to find a solution for any value of λ indicating that gap variation is a regular perturbation to the Saffman-Taylor finger for zero surface tension. Later we will need the analytic continuation of this expression into the upper half-plane outside the unit semi-circle, and we present this expression in (3.54).

3.4 Effect of Non-Zero Surface Tension

We now consider the effect of non-zero surface tension. In order to satisfy the pressure boundary condition for σ non-zero we will add corrections $f_\sigma(\zeta)$ and ϕ_σ to the zero surface tension solution $\widehat{z}(\zeta)$ and $\widehat{\phi}$ respectively, where we have introduced the hats to denote the zero surface tension solution. Both $f_\sigma(\zeta)$ and ϕ_σ are $O(\sigma)$ for ζ on and inside the unit semi-circle. More precisely we set

$$z(\zeta) = \widehat{z}(\zeta) + f_\sigma(\zeta), \tag{3.55}$$

$$\phi(\zeta,\bar{\zeta}) = \widehat{\phi}(\zeta,\bar{\zeta}) + \phi_\sigma(\zeta,\bar{\zeta}), \tag{3.56}$$

where

$$\widehat{z}(\zeta) = z_{st}(\zeta) + \varepsilon f_\varepsilon(\zeta) + O(\varepsilon^2), \tag{3.57}$$

$$\widehat{\phi}(\zeta,\bar{\zeta}) = \phi_0(\zeta,\bar{\zeta}) + \varepsilon\phi_\varepsilon(\zeta,\bar{\zeta}) + O(\varepsilon^2). \tag{3.58}$$

We find the dimensionless pressure equation (3.8) takes the form

$$\widehat{\phi}_{\zeta\bar{\zeta}} + \phi_{\sigma\zeta\bar{\zeta}} = -\frac{3}{4}i\frac{h'}{h}(\overline{z}_{\bar{\zeta}}\frac{\partial}{\partial\zeta} - z_\zeta\frac{\partial}{\partial\bar{\zeta}})(\widehat{\phi} + \phi_\sigma), \tag{3.59}$$

with boundary conditions

$$c\frac{\partial\widehat{\phi}}{\partial r} + c\frac{\partial\phi_\sigma}{\partial r} = \frac{\mathrm{Re}(\zeta\widehat{z}_\zeta)}{h^2} + \frac{\mathrm{Re}(\zeta f_{\sigma\zeta})}{h^2}, \tag{3.60}$$

$$c(\widehat{\phi} + \phi_\sigma) = -\sigma\left(\frac{1 + \mathrm{Re}(\zeta z_{\zeta\zeta}/z_\zeta)}{|z_\zeta|}\right). \tag{3.61}$$

We can make the error $O(\varepsilon^2, \varepsilon\sigma)$ if we choose

$$\phi_{\sigma\zeta\bar{\zeta}} = 0, \tag{3.62}$$

with boundary conditions

$$\lambda\frac{\partial\phi_\sigma}{\partial r} = \mathrm{Re}(\zeta f_{\sigma\zeta}), \tag{3.63}$$

$$\lambda\phi_\sigma = -\sigma\left(\frac{1 + \mathrm{Re}(\zeta z_{\zeta\zeta}/z_\zeta)}{|z_\zeta|}\right). \tag{3.64}$$

Since ϕ_σ is harmonic it is the real part of an analytic function and we can write

$$\phi_\sigma = \mathrm{Re}\, w_\sigma. \tag{3.65}$$

Thus equation (3.63) can be written as

$$\lambda \operatorname{Re}(\zeta w_{\sigma\zeta}) = \operatorname{Re}(\zeta f_{\sigma\zeta}). \tag{3.66}$$

Further, since both w_σ and f_σ are analytic inside the unit semi-circle with $\operatorname{Im} w_\sigma = \operatorname{Im} f_\sigma = 0$ on the real diameter, we can use the Poisson integral formula to conclude

$$\lambda w_\sigma = f_\sigma. \tag{3.67}$$

Thus equation (3.64) can be written

$$\operatorname{Re} f_\sigma = -\sigma \left(\frac{1 + \operatorname{Re}(\zeta z_{\zeta\zeta}/z_\zeta)}{|z_\zeta|} \right). \tag{3.68}$$

This equation relates various derivatives of f_σ on the unit semi-circle since

$$z = \widehat{z} + f_\sigma.$$

3.4.1 Regular Expansion in Surface Tension

We can use equation (3.68) to get the first two terms in a regular double expansion of $f(\zeta)$ in σ and ε and indicate how this regular expansion fails to capture the selection mechanism which is due to transcendentally small terms in σ. To do this we set

$$f_\sigma(\zeta) = \sigma f_1(\zeta). \tag{3.69}$$

Once f_1 is found we will have the linear terms in the regular double expansion of f , that is

$$f(\zeta) = f_{st}(\zeta) + \varepsilon f_\varepsilon(\zeta) + \sigma f_1(\zeta) + O(\sigma^2, \sigma\varepsilon, \varepsilon^2). \tag{3.70}$$

On substituting $f_\sigma(\zeta) = \sigma f_1(\zeta)$ into (3.68) and retaining terms linear in σ we find

$$\operatorname{Re} f_1(\zeta) = \frac{-1}{|z_{st\zeta}(\zeta)|} \tag{3.71}$$

on the arc of the unit semicircle. We can now use the Poisson integral formula to get

$$f_1(\zeta) = \frac{1}{2\pi i}\int_{\frown} K(\zeta,\zeta')\frac{-1}{|z_{st\zeta}(\zeta')|}\frac{d\zeta'}{\zeta'}. \tag{3.72}$$

While this first order correction is a uniform approximation to $f_\sigma(\zeta)$, it is not a uniform approximation to its derivatives near $\zeta = \pm 1$. When $h_1(y) = 0$ it has been shown by Tanveer [16] that one can construct a matched asymptotic expansion valid near $\zeta = \pm 1$ and furthermore that this matching procedure can be done for any λ yielding no selection mechanism. The details of this matching in the $h_1 \neq 0$ case are difficult and we make no attempt to reproduce the result in this case. We assume that the matching can be done. The selection mechanism is due to transcendentally small terms which are generated elsewhere in the complex plane.

3.5 Linearised Equation

The absence of a selection mechanism in the regular expansion is due to transcendentally small terms in σ which result from derivatives of f_σ which were neglected as unimportant in the regular expansion in the previous section.

Our approach is to assume that the regular expansion only has transcendentally small corrections in the physical domain. With this assumption we derive an equation for the analytic continuation of f_σ outside the unit semi-circle. We show, for λ close to one half, that the solution of this equation is incompatible with the assumption that the regular expansion only contains transcendentally small corrections in the physical domain. Only for certain values of λ can the analytic continuation be made compatible with the regular expansion.

To retain the derivative terms in the simplest possible way we linearise equation (3.68) in f_σ and get the following relationship involving f_σ and its derivatives;

$$\frac{1}{\sigma}|\widehat{z}_\zeta|\,\mathrm{Re}\, f_\sigma + \mathrm{Re}\left(\frac{\zeta}{\widehat{z}_\zeta}(\widehat{z}_{\zeta\zeta} + f_{\sigma\zeta\zeta} - \frac{\widehat{z}_{\zeta\zeta}}{\widehat{z}_\zeta}f_{\sigma\zeta})\right) = -1. \tag{3.73}$$

This is to hold on the arc of the upper unit semi-circle along with $\mathrm{Im}(f_\sigma) = 0$ on the

real diameter. We wish to use the Poisson integral formula to analytically continue (3.73), however, one can show that the second term on the left hand side has simple poles at $\zeta = \pm 1$. In order to remove the singularity from this expression we resort to a trick. It is easy to show that

$$\frac{-2\zeta^2}{\zeta^2 - 1} \tag{3.74}$$

has simple poles of the same strength and real part of minus one on the unit semicircle. Thus (3.73) is equivalent to

$$\frac{1}{\sigma}|\widehat{z}_\zeta| \operatorname{Re} f_\sigma = -\operatorname{Re}\left(\frac{2}{\zeta^2 - 1} + \frac{\zeta}{\widehat{z}_\zeta}\widehat{z}_{\zeta\zeta} + \frac{\zeta}{\widehat{z}_\zeta} f_{\sigma\zeta\zeta} - \frac{\zeta \widehat{z}_{\zeta\zeta}}{\widehat{z}_\zeta^2} f_{\sigma\zeta}\right). \tag{3.75}$$

We can now use the Poisson integral formula to obtain an equation for f_σ valid inside the unit circle. We multiply (3.75) by

$$\frac{1}{2\pi i} K(\zeta, \zeta') \tag{3.76}$$

and integrate counter-clockwise along the arc of the unit semicircle. The right hand side of (3.75) is analytic inside the unit semicircle and has vanishing imaginary part on the real diameter. Thus the result of the integration is

$$-\frac{2}{\zeta^2 - 1} - \frac{\zeta}{\widehat{z}_\zeta}\widehat{z}_{\zeta\zeta} - \frac{\zeta}{\widehat{z}_\zeta} f_{\sigma\zeta\zeta} + \frac{\zeta \widehat{z}_{\zeta\zeta}}{\widehat{z}_\zeta^2} f_{\sigma\zeta}. \tag{3.77}$$

Now we will work on the left hand side. Since $\bar{\zeta} = 1/\zeta$ we can write

$$|\widehat{z}_\zeta| = \sqrt{\widehat{z}_\zeta \overline{\widehat{z}_\zeta}} = \sqrt{\widehat{z}_\zeta(\zeta)\widehat{z}_\zeta(1/\zeta)}. \tag{3.78}$$

Further, $\operatorname{Re} f(\zeta) = (f(\zeta) + f(1/\zeta))/2$ since $\operatorname{Im} f = 0$ on the real diameter. Thus for ζ inside the unit circle the result of the integration can be expressed as

$$\frac{1}{2\pi i}\int_\frown \frac{d\zeta'}{\zeta'} K(\zeta, \zeta') \frac{f_\sigma(\zeta') + f_\sigma(1/\zeta')}{2} \sqrt{\widehat{z}_\zeta(\zeta')\widehat{z}_\zeta(1/\zeta')} = I(f_\sigma, \zeta). \tag{3.79}$$

The analytic continuation of expression (3.79) outside the unit semicircle is

$$I(f_\sigma,\zeta)+f_\sigma(\zeta)\sqrt{\widehat{z}_\zeta(\zeta)\widehat{z}_\zeta(1/\zeta)}+f_\sigma(1/\zeta)\sqrt{\widehat{z}_\zeta(\zeta)\widehat{z}_\zeta(1/\zeta)}. \tag{3.80}$$

In this way we get an equation for $f_\sigma(\zeta)$ valid for ζ outside the unit semicircle;

$$\begin{aligned}&\sigma\frac{\zeta}{\widehat{z}_\zeta}f_{\sigma\zeta\zeta}-\sigma\frac{\zeta\widehat{z}_{\zeta\zeta}}{\widehat{z}_\zeta^2}f_{\sigma\zeta}+f_\sigma(\zeta)\sqrt{\widehat{z}_\zeta(\zeta')\widehat{z}_\zeta(1/\zeta')}\\ =\;&-f_\sigma(1/\zeta)\sqrt{\widehat{z}_\zeta(\zeta)\widehat{z}_\zeta(1/\zeta)}-\sigma\left(\frac{2}{\zeta^2-1}+\frac{\zeta}{\widehat{z}_\zeta}\widehat{z}_{\zeta\zeta}\right)-I(f_\sigma,\zeta).\end{aligned} \tag{3.81}$$

For ζ outside the unit semicircle $1/\zeta$ is inside the unit semicircle and we replace $f_\sigma(1/\zeta)$ by the first term in its regular expansion, i.e., $\sigma f_1(1/\zeta)$ since we are assuming that in the physical domain $f_1(\zeta)$ only contains exponentially small corrections. In this way we get an inhomogeneous differential equation for f_σ valid outside the unit semicircle as follows:

$$f_{\sigma\zeta\zeta}+P(\zeta)f_{\sigma\zeta}+\frac{1}{\sigma}Q(\zeta)f_\sigma=R(\zeta). \tag{3.82}$$

where

$$P(\zeta) = -\frac{\widehat{z}_{\zeta\zeta}}{\widehat{z}_\zeta}, \tag{3.83}$$

$$Q(\zeta) = \frac{\widehat{z}_\zeta}{\zeta}\sqrt{\widehat{z}_\zeta(\zeta)\widehat{z}_\zeta(1/\zeta)}, \tag{3.84}$$

$$R(\zeta) = -\frac{2}{\zeta^2-1}\frac{\widehat{z}_\zeta}{\zeta}-\widehat{z}_{\zeta\zeta}-\frac{\widehat{z}_\zeta}{\zeta}\sqrt{\widehat{z}_\zeta(\zeta)\widehat{z}_\zeta(1/\zeta)}f_1(1/\zeta)-I(f_1,\zeta). \tag{3.85}$$

In the above

$$\widehat{z}_\zeta = z_{st\zeta}+\varepsilon f_{\varepsilon\zeta}+O(\varepsilon^2), \tag{3.86}$$

$$z_{st\zeta} = \frac{2}{\pi}\frac{(1-p\zeta)(1+p\zeta)}{\zeta(\zeta^2-1)}, \tag{3.87}$$

$$p = \sqrt{2\lambda-1}. \tag{3.88}$$

The parameter $p=\sqrt{2\lambda-1}$ will play a crucial role in the selection mechanism and

enters the problem through $z_{st\zeta}$ which appears in the coefficient functions of the differential equation.

For small σ we can gain insight into the solution to (3.82) using WKBJ theory. The two WKBJ approximations to the homogeneous solutions are

$$f_{\sigma\pm} \sim A_{\pm} Q(\zeta)^{-1/4} \exp[\pm \frac{1}{\sqrt{\sigma}} S(\zeta) - \frac{1}{2} \int^{\zeta} P(\zeta) d\zeta], \tag{3.89}$$

where

$$S(\zeta) = i \int^{\zeta} \sqrt{Q(\zeta)} d\zeta. \tag{3.90}$$

This approximation is valid away from the so-called turning points of the equation where $Q(\zeta) = 0$. The complex plane is divided into regions by the lines of $\mathrm{Re}\, S = 0$ emanating from the turning points. These lines are sometimes known as Stokes lines (though almost as frequently referred to as Anti-Stokes lines.) These lines intersect only at the turning points or at infinity and on them the solution is oscillatory. The regions of the complex plane separated by the Stokes lines are known as Stokes regions. The complex plane is also divided into regions by the Anti-Stokes lines given by $\mathrm{Im}\, S = 0$. These regions are likewise known as Anti-Stokes regions. In any given Stokes region one of the solutions, $f_{\sigma\pm}$, is dominant and the other subdominant depending on the sign of $\mathrm{Re}\, S(\zeta)$. Note that if one of these WKBJ approximations is dominant in one Stokes region it becomes subdominant on crossing a Stokes line into an adjacent region.

In general a homogeneous solution, $f_{\sigma h}$, of (3.82) is a linear combination of $f_{\sigma+}$ and $f_{\sigma-}$, that is

$$f_{\sigma h}(\zeta) = A_{+} f_{\sigma+}(\zeta) + A_{-} f_{\sigma-}(\zeta). \tag{3.91}$$

The values of $A_{\pm}$ are constant in any given Anti-Stokes region but can vary from region to region. A globally valid homogeneous solution can be constructed by matching to a solution in the neighbourhood of a turning point [23]. The solutions in the neighbourhood of a turning point can usually be expressed in terms of modified Bessel functions [22]. Once globally valid homogeneous solutions have been constructed,

a solution to the inhomogeneous problem can be written down using the method of variation of parameters. For a general inhomogeneous second order differential equation the solution can only be made to decay in two Stokes regions by suitable choice of the limits of integration in the variation of parameters formula, equivalent to fixing the constants multiplying the two homogeneous solutions. For our problem it is the requirement that the solution decay in a third Stokes region that yields the selection mechanism.

The turning points of the differential equation (3.82) are crucial and are determined by the zeros of $Q(\zeta)$ and thus by the zeros of $\widehat{z}(\zeta)$ and $\widehat{z}(1/\zeta)$. When $\varepsilon = 0$ it is clear that there are four turning points at $\zeta = \pm p, \pm 1/p$. Since $0 < \lambda < 1$ we know $|p| < 1$ and thus two of the zeros are outside the unit circle and two inside. The Stokes lines for $\varepsilon = 0$ are fully discussed by Tanveer [16] and we present a sketch of some of the relevant Stokes and anti-Stokes lines in Figure (3.3). We note that three Stokes regions emanating from two turning points impinge on the physical domain. Tanveer discusses the selection mechanism for $\varepsilon = 0$ in some detail.

An examination of $Q(\zeta)$ for $|p| = O(1)$ shows that the effect of the term $\varepsilon f_\varepsilon(\zeta)$ on the position of the turning points and the position of the Stokes lines is $O(\varepsilon)$ and we expect the effect of the gap perturbation on the selected value of p to likewise be $O(\varepsilon)$.

As $p \to 0$, at least for the constant gap case, the turning points occur at large $|\zeta|$ and we can no longer assume that the $\varepsilon f_\varepsilon(\zeta)$ term is uniformly small. It is possible that additional turning points are formed or that the existing ones are moved by a large amount. We will analyse equation (3.75) in detail for small p (corresponding to λ near $1/2$) in the following sections.

3.5.1 Linearised Equation for Small Positive p

From an examination of zeros of $Q(\zeta)$ we suspect that the turning points outside the unit circle coalesce at infinity as $p \to 0$. With this in mind we introduce a new

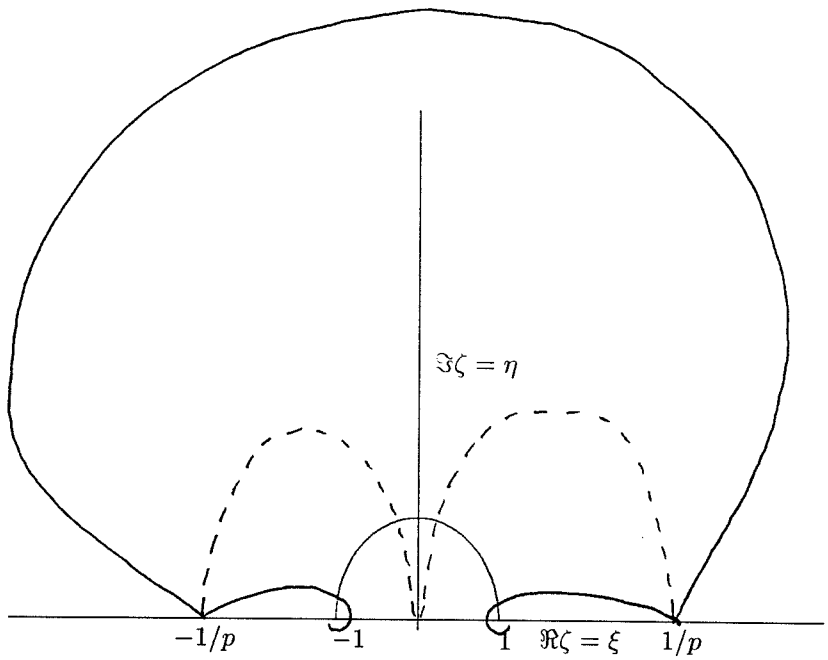

Figure 3.3: Relevant Stokes lines for $\varepsilon = 0$. Stokes lines solid, anti-Stokes lines dashed.

complex variable ω given by

$$\omega = \frac{1}{|p|\zeta}. \tag{3.92}$$

This change of variables has the effect of mapping infinity to the origin and the upper half plane to the lower half plane. It also has the effect of keeping the turning points distinct as $p \to 0$ as we will see. In the new ω variable we are interested in the behaviour in the lower half plane. The finger boundary has been mapped to infinity in the lower half plane. We assume that f_σ must match to σf_1 for large $|\omega|$ in the lower half plane and thus our selection mechanism will be given by the requirement that our solution should have no exponentially large terms as $|\omega| \to \infty$ for $-\pi < \arg\omega < 0$.

We can work out the asymptotic behaviour of $\widehat{z}_\zeta(\zeta)$ for the particular choice

$$h_1(y) = \cos\pi(y+1). \tag{3.93}$$

Since we want the behaviour near the turning points, we must be careful to take the

limit with ω fixed and order one as $p \to 0$ and not just the large ζ asymptotics. We keep the leading order behaviour in $|p|$. Calculation (see Appendix C) yields

$$z_{st\zeta} \sim \frac{2}{\pi}|p|^3\omega(\omega^2-1), \qquad p \to 0, \tag{3.94}$$

$$f_{\varepsilon\zeta} \sim \frac{2}{\pi}\frac{3}{4}i\ln|p|, \qquad p \to 0. \tag{3.95}$$

Thus

$$\widehat{z}_\zeta = \frac{2}{\pi}|p|^3\left(\omega(\omega^2-1)-\gamma\right), \tag{3.96}$$

where

$$\gamma = -\frac{3}{4}\frac{\varepsilon\ln|p|}{|p|^3}, \tag{3.97}$$

$$p = \sqrt{2\lambda-1}. \tag{3.98}$$

We re-scale our dependant variable as follows

$$F_\sigma = f_\sigma/|p|^2. \tag{3.99}$$

Keeping only the leading order terms in $|p|$, equation (3.82) becomes

$$\frac{d^2F_\sigma}{d\omega^2} + P(\omega)\frac{dF_\sigma}{d\omega} + \delta Q(\omega)F_\sigma = R(\omega), \tag{3.100}$$

where

$$P(\omega) = \frac{2}{\omega} + \frac{(1-3\omega^2)}{\omega(\omega^2-1)-i\gamma}, \tag{3.101}$$

$$Q(\omega) = i\frac{1}{\omega^2}[(\omega^2-1)-\frac{i\gamma}{\omega}]^{3/2}, \tag{3.102}$$

$$R(\omega) = [2\omega^4+i\gamma\omega]/\omega^4, \tag{3.103}$$

$$\delta = \left(\frac{2}{\pi}\right)^2|p|^3/\sigma. \tag{3.104}$$

We can examine this equation using the WKBJ approximation when δ is large. The effect of $\gamma \neq 0$ now becomes clear. By examining $Q(\omega)$ we find three turning points

instead of two and this can be expected to have a non-trivial effect on the solution. As before the selection mechanism is determined by the elimination of unwanted exponentially growing terms as $\omega \to \infty$. The first term in the asymptotic expansion (in δ) of the solution away from the turning points would seem to be

$$F_\sigma = \frac{1}{\delta}\frac{R(\omega)}{Q(\omega)} + O(\delta^{-2}), \tag{3.105}$$

however, we can only guarantee that the actual solution has this expansion in two Stokes regions. We cannot eliminate the possibility of the presence of exponentially small terms which are solutions of the homogeneous equation which in general become exponentially large in adjacent Stokes regions of the complex plane. It is the requirement that the solution be of the form (3.105) in more than two Stokes regions which gives us the selection mechanism. Only for certain values of the parameters δ and γ can this requirement be satisfied as we will see.

In order to determine the selection mechanism we need the turning points and Stokes lines of (3.100). In this case the turning points are given by the zeros of $Q(\omega)$ which are given by the zeros of the cubic

$$\omega(\omega^2 - 1) - i\gamma. \tag{3.106}$$

This cubic has three roots, one on the imaginary axis which we will call ω_0 and two symmetric roots of the form $\pm x + iy$ which we will call $\omega_\pm$. As γ tends to zero these roots tend to 0, ± 1. For $\gamma > 0$, ω_0 has negative imaginary part and $\omega_\pm$ have positive imaginary part, the opposite is true for $\gamma < 0$. The topology of the Stokes regions is dependant on the value of γ. We will see that for γ greater than some critical γ_0 there is a topology change in the Stokes regions and a consequent loss of solutions.

For $\gamma < \gamma_0$ (where γ_0 is to be determined) the situation is similar to $\gamma = 0$. There are three Stokes regions at infinity in the lower half plane. One Stokes line comes in from $\infty \exp(-i5\pi/6)$ to ω_- another leaves ω_- and loops down to the negative imaginary axis crossing the axis at $y_0 < \omega_0$. This Stokes line continues symmetrically

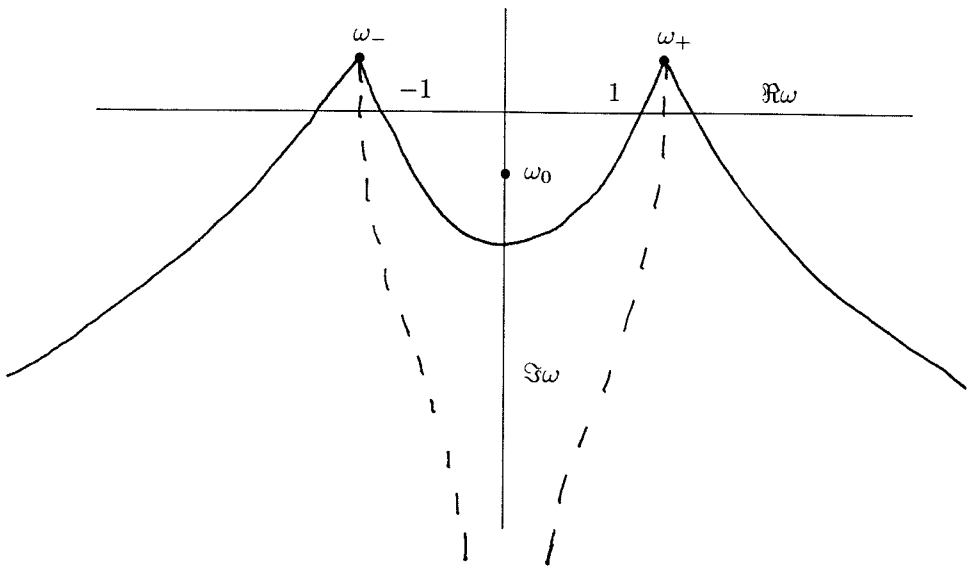

Figure 3.4: Stokes lines for $\gamma < \gamma_0$. Stokes lines solid, anti-Stokes lines dashed.

on to ω_+. A final Stokes line leaves ω_+ and asymptotes to $\propto \exp(-i\pi/6)$. We sketch the relevant Stokes lines in Figure (3.4). The turning point at ω_0 is hidden by the Stokes line joining ω_+ to ω_-. Since there are two turning points with three Stokes regions that extend to infinity there is the possibility that large contributions from each turning point could be made to cancel yielding a consistent solution that will match with the regular expansion for large $|\omega|$ in the lower half plane.

When $\gamma > \gamma_0$ there are five Stokes regions at infinity as depicted in Figure (3.5) and the turning point at ω_0 is no longer hidden. There are three Stokes regions extending from the single turning point at ω_0 to infinity and there is no longer any freedom to remove exponentially growing terms in all three regions and thus we expect to find no consistent solutions in this case.

The transition between the two topologies occurs when ω_0 is on the Stokes line

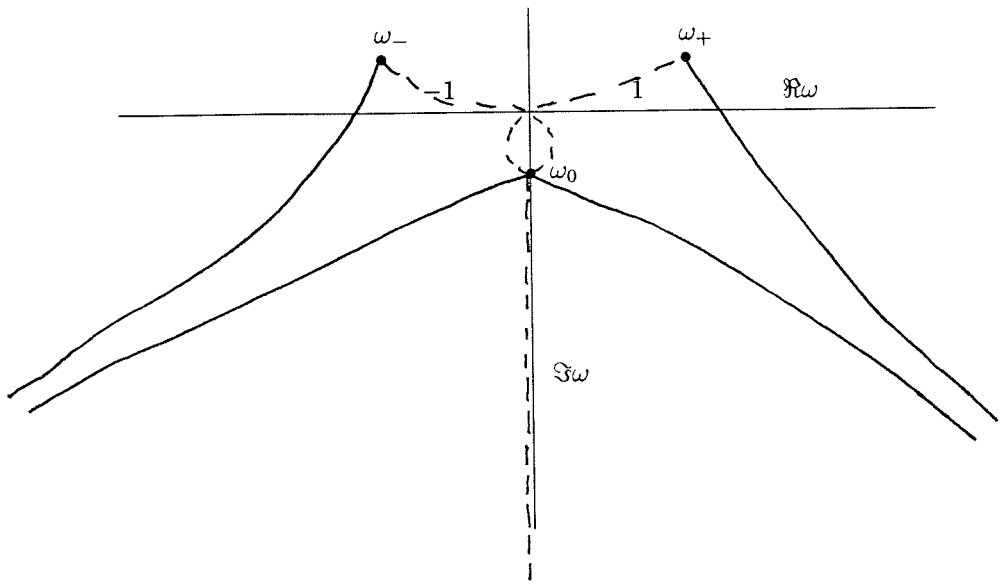

Figure 3.5: Stokes lines for $\gamma > \gamma_0$. Stokes lines solid, anti-Stokes lines dashed.

from ω_- to ω_+. This occurs when γ is such that

$$\mathrm{Re}\left(i\int_{\omega 0}^{\omega_+}\sqrt{Q(\omega)}d\omega\right) = 0. \tag{3.107}$$

Numerical calculation of this integral yields $\gamma_0 = 0.2826$. Thus we expect no solutions for $\gamma > \gamma_0$ in the limit of large δ. This value is consistent with the numerical results for the selection mechanism for smaller values of δ.

3.5.2 Linearised Equation for Small Imaginary p

When λ is less than a half it is clear that p is purely imaginary. In this case we write

$$p = i|p|. \tag{3.108}$$

With the same substitutions as before we find

$$z_{st\zeta} \sim \frac{2}{\pi}|p|^3\omega(\omega^2+1), \qquad p \to 0 \tag{3.109}$$

$$f_{\varepsilon\zeta} \sim \frac{2}{\pi}\frac{3}{4}i\ln|p|, \qquad p \to 0 \tag{3.110}$$

which differs in a sign from the p positive case. We now get a slightly different equation for F_σ as follows;

$$\frac{d^2F_\sigma}{d\omega^2} + P(\omega)\frac{dF_\sigma}{d\omega} + \delta Q(\omega)F_\sigma = R(\omega), \tag{3.111}$$

where

$$P(\omega) = \frac{2}{\omega} + \frac{(1+3\omega^2)}{\omega(\omega^2+1)-i\gamma}, \tag{3.112}$$

$$Q(\omega) = i\frac{1}{\omega^2}[(\omega^2+1) - \frac{i\gamma}{\omega}]^{3/2}, \tag{3.113}$$

$$R(\omega) = [2\omega^4 + i\gamma\omega]/\omega^4, \tag{3.114}$$

$$\delta = \left(\frac{2}{\pi}\right)^2 |p|^3/\sigma, \tag{3.115}$$

$$\gamma = -\frac{3}{4}\frac{\varepsilon\ln|p|}{|p|^3}. \tag{3.116}$$

Note that there are some sign changes in the coefficients of the differential equation. The turning points of equation (3.111) are given by the zeros of the cubic

$$\omega(\omega^2+1) - i\gamma. \tag{3.117}$$

For $|\gamma| > 2/\sqrt{27}$ this cubic has three roots as before; one imaginary root ω_0 and two roots $\omega_\pm$ of the form $x \pm iy$. For $|\gamma| < 2/\sqrt{27}$ the cubic has three purely imaginary roots. As before it is possible to eliminate the transcendentally small terms only if there are three Stokes regions in the lower half plane emanating from two turning points. This situation only occurs for $\gamma < -2/\sqrt{27}$. Thus we predict that solutions are possible with $\lambda < 1/2$ if $\gamma < -2/\sqrt{27}$. As before further analysis is difficult and

we rely on a numerical procedure to determine the allowed values of δ as a function of γ.

3.5.3 Numerical Determination of Selection Mechanism for Small p

We can determine the selection mechanism by numerical integration of (3.100) and (3.111) along a special path in the complex plane with suitable initial conditions. We use a method due to Martin and Dorsey [17]. This method relies on the observation that the solution we want satisfies $\operatorname{Im} F_\sigma = 0$ when ω is on the imaginary axis. If we can remove growing terms from F_σ in the left half of the lower plane and $\operatorname{Im} F_\sigma = 0$ on the imaginary axis then the solution in the right half of the plane is given by $\bar{F}(-\bar{\zeta})$ and is guaranteed to be free of exponentially large terms. This corresponds to the analytic continuation of the surface tension correction being symmetric about the channel centreline. For fixed γ we have one equation, $\operatorname{Im} F_\sigma = 0$, and one unknown, δ.

We start with a solution that is free of exponentially small terms on the Stokes line which asymptotes to $r\exp(-i5\pi/6)$ and integrate along a curve that initially follows the Stokes line but then curves to the imaginary axis hitting it at some negative value of $\operatorname{Im}\omega$. We ensure that the solution is free of solutions to the homogeneous equation on the Stokes line by imposing the initial condition

$$F_\sigma \sim -\frac{2i}{\delta\omega} - \operatorname{sgn}(p^2)\frac{3i}{\delta\omega^3} + \frac{6}{\delta^2\omega^4} + \frac{4\gamma}{\delta\omega^4} + O(1/\omega^5), \tag{3.118}$$

$$\frac{dF_\sigma}{d\omega} \sim \frac{2i}{\delta\omega^2} + \operatorname{sgn}(p^2)\frac{9i}{\delta\omega^4} - \frac{24}{\delta^2\omega^5} - \frac{16\gamma}{\delta\omega^5} + O(1/\omega^6), \tag{3.119}$$

which corresponds to the regular expansion in powers of $1/\omega$ of the particular solution. Since the homogeneous solutions are oscillatory and O(1) on the Stokes line this suffices to eliminate them from the solution.

For λ greater than a half we proceed as follows; using Newton's method with $\gamma = 0$ we identify the values of δ such that $\operatorname{Im} F_\sigma = 0$ on the imaginary axis. We

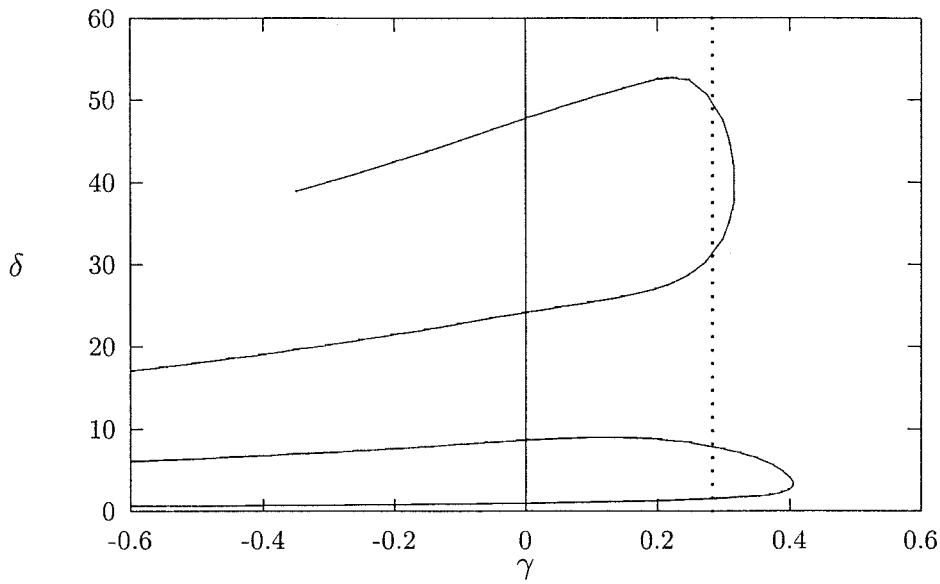

Figure 3.6: δ versus γ for $\lambda > 1/2$ (-), (..) WKBJ cutoff.

then continue each of these values of δ in γ, again using Newton's method, to get the selected values of δ and γ. We find that for $\gamma > 0$ the solution curves in the δ, γ plane join up in pairs and thus there is some value of γ beyond which no solutions exist. For $\gamma < 0$ there does not appear to be any branch merger and the solutions remain distinct. The resulting existence curve is plotted in Figure 3.6.

For λ less than a half we identified two branches of solutions by fixing γ at some reasonable value less than zero and noting $\operatorname{Im} F_\sigma$ as δ was varied from zero upwards. These two solutions were then followed in γ using Newton's method and the resulting curves are plotted in Figure 3.7. It was not possible to follow the solution paths accurately for δ much larger than sixty. The problem becomes increasingly stiff for large δ. The question of branch merger in this case remains open.

With results both for λ greater than and less than a half it is now possible to present composite pictures for the behaviour of the existence curves in the λ, σ plane. From the definition of γ,

$$\gamma = -\frac{3}{4}\frac{\varepsilon \ln |p|}{|p|^3}, \tag{3.120}$$

it is clear that $\gamma > 0$ corresponds to $\varepsilon > 0$ and vice versa. It is also clear from Figures 3.6 and 3.7 that when $\varepsilon > 0$ solutions only exist for $\lambda > 1/2$. Given $\varepsilon > 0$ it is possible

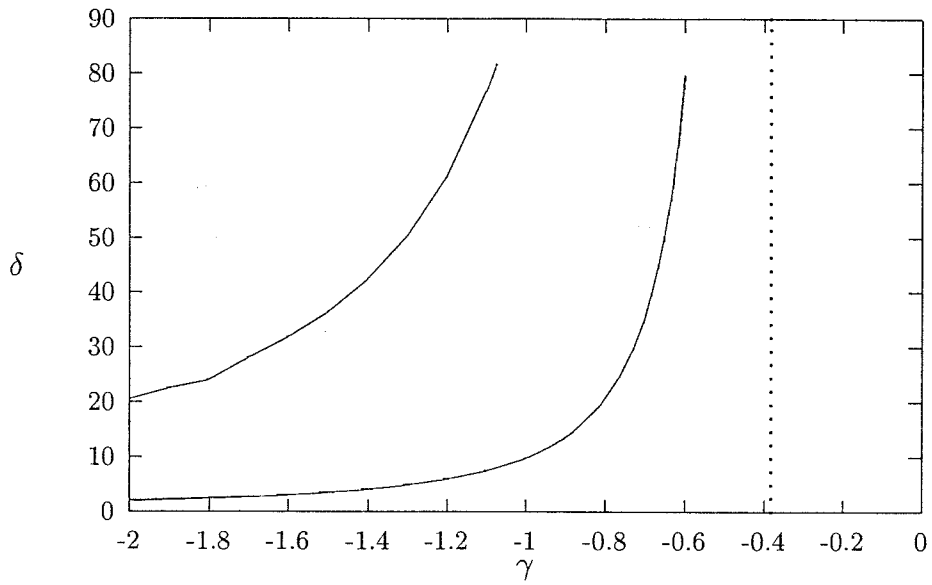

Figure 3.7: δ versus γ for $\lambda < 1/2$ (-), (..) WKBJ cutoff.

to invert the definitions of γ and δ to find λ and σ and we do this for three positive values of ε in Figures 3.8-3.10.

When ε is less than zero it is clear from Figures 3.6 and 3.7 that solutions exist for $\lambda > 1/2$ and $\lambda < 1/2$. We plot these curves for three different values of $\varepsilon < 0$ in Figures 3.11-3.13. Each portion of the curves is distinct and they do not join at $\lambda = 1/2$. The limit $\lambda \to 1/2$ corresponds to $\gamma \to -\infty$. Unfortunately in this limit the turning points also coalesce at infinity in the complex plane and our small p asymptotic expansion breaks down. In this case we suspect that a re-scaling of the independent variable is necessary and there is no fundamental problem. Such a re-scaling has not been attempted here.

The curves show reasonable qualitative agreement with the full numerical computations from chapter 2, however we do not expect the agreement to be as good as for the full non-linear equation which we will study in the next section.

3.6 Non-Linear Equation

We now derive a more accurate non-linear equation. The selection mechanism is the same, that is the elimination of unwanted exponentially large terms, however we lose

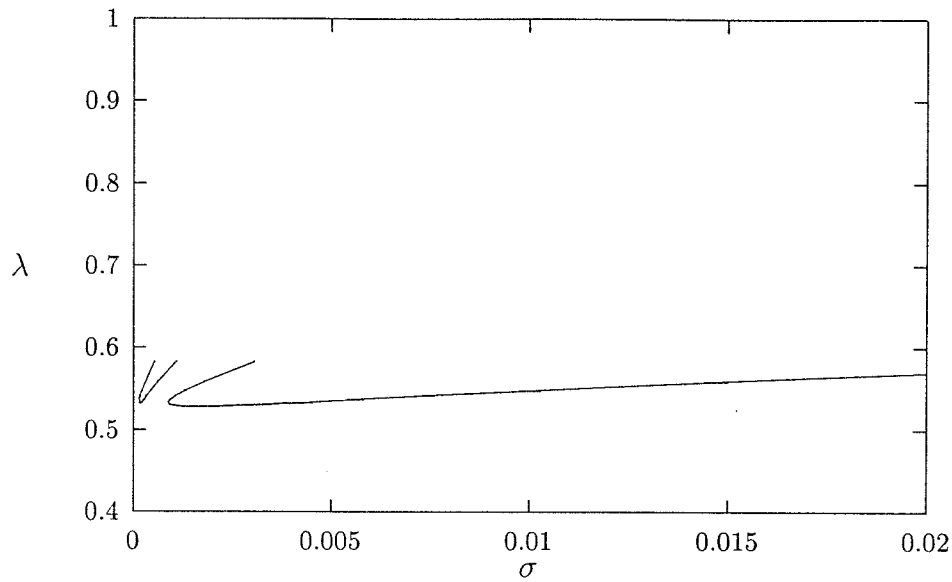

Figure 3.8: Width as a function of σ with $\varepsilon = 0.005$.

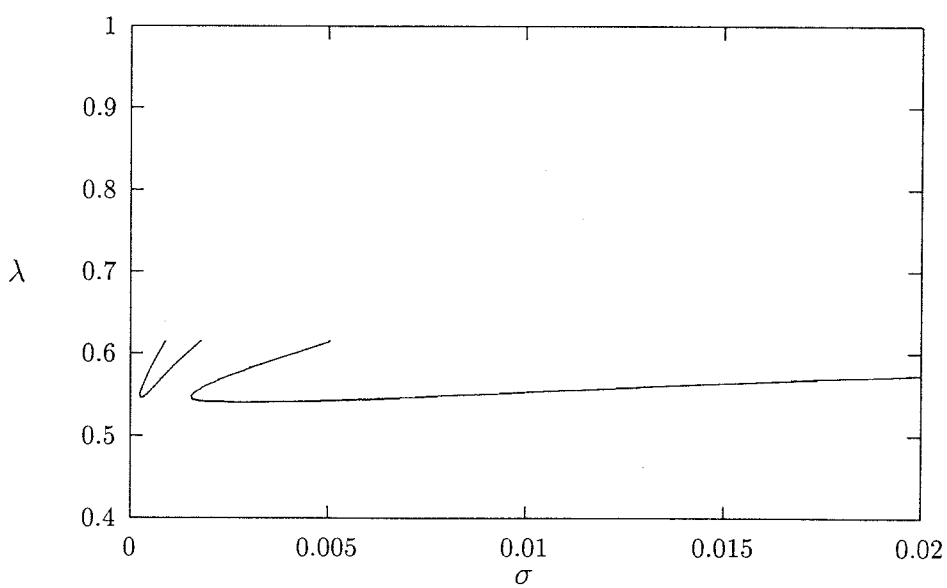

Figure 3.9: Width as a function of σ with $\varepsilon = 0.01$.

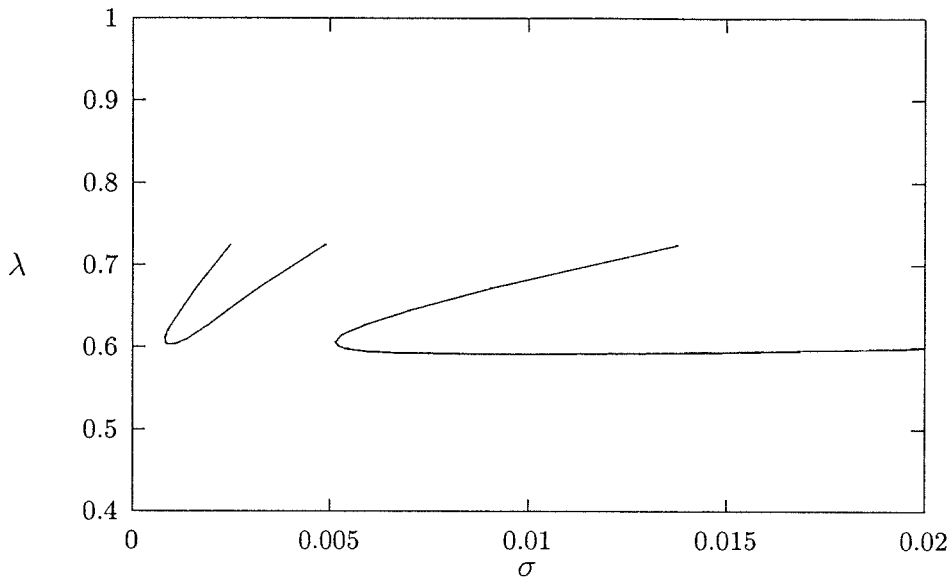

Figure 3.10: Width as a function of σ with $\varepsilon = 0.05$.

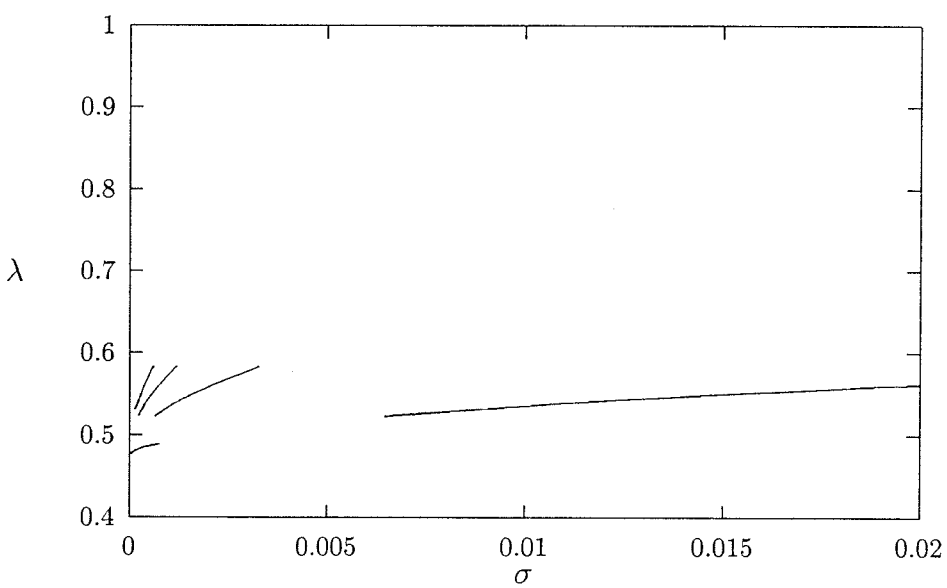

Figure 3.11: Width as a function of σ with $\varepsilon = -0.005$.

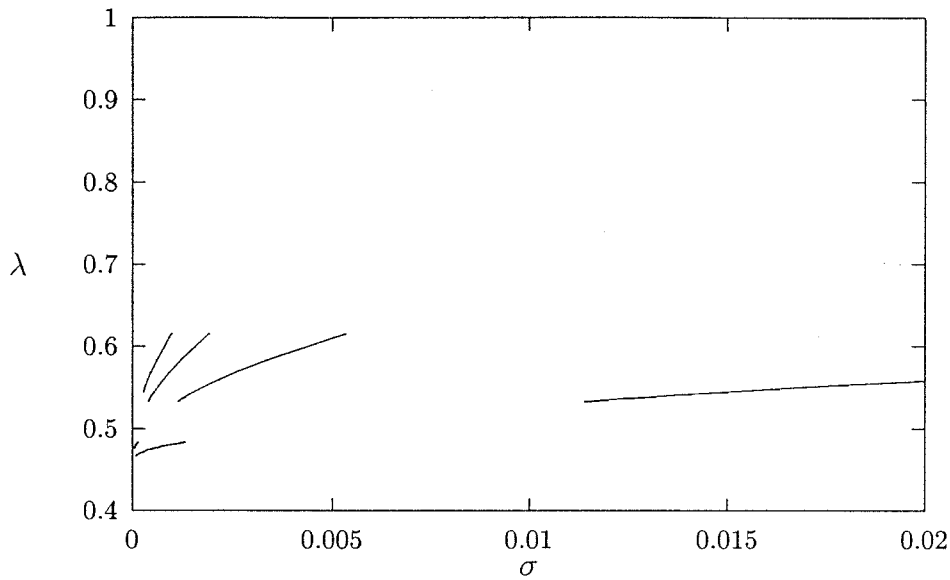

Figure 3.12: Width as a function of σ with $\varepsilon = -0.01$.

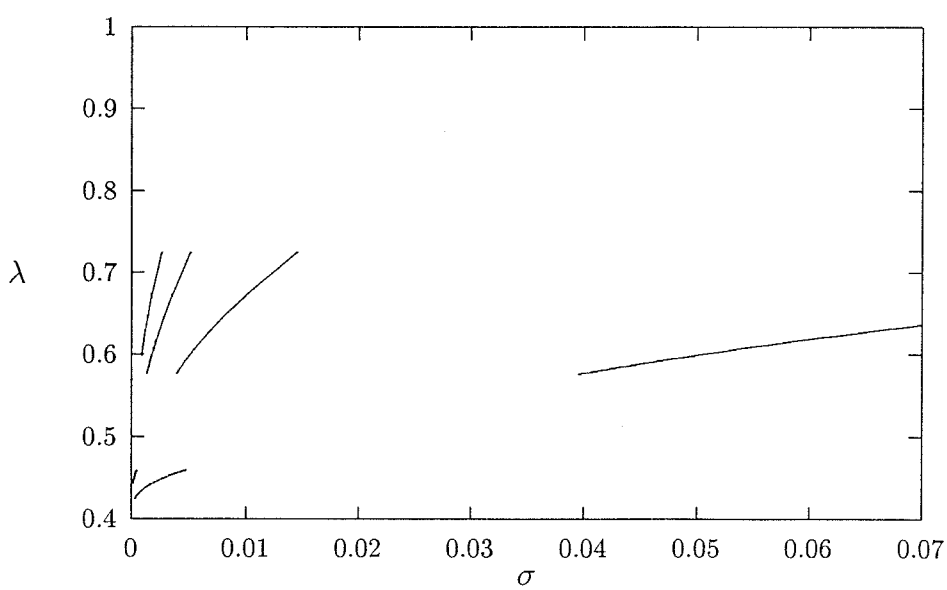

Figure 3.13: Width as a function of σ with $\varepsilon = -0.05$.

the ability to analyse the equation using WKBJ theory and so we resort to numerical integration. Our starting point is the same as before that is equation (3.68) which we rewrite as

$$|z_\zeta| \operatorname{Re} f_\sigma + \sigma \operatorname{Re}\left(1 + \zeta \frac{d}{d\zeta} \ln z_\zeta\right) = 0. \tag{3.121}$$

We know $d/d\zeta \ln z_\zeta$ has simple poles at $\zeta = \pm 1$ however, as in the linear case these can be removed by adding $2\zeta^2/(\zeta^2 - 1)$ and subtracting a term with the same real part, i.e., 1. In this way we get

$$|z_\zeta| \operatorname{Re} f_\sigma + \sigma \operatorname{Re}\left(\frac{2\zeta^2}{\zeta^2 - 1} + \zeta \frac{d}{d\zeta} \ln z_\zeta\right) = 0. \tag{3.122}$$

We can now use the Poisson integral formula to get

$$\frac{2\zeta^2}{\zeta^2 - 1} + \zeta \frac{z_{\zeta\zeta}}{z_\zeta} + \frac{1}{\sigma 2\pi i} \int_\curvearrowleft |z_\zeta| \operatorname{Re} f_\sigma K(\zeta, \zeta') \frac{d\zeta'}{\zeta'} = 0. \tag{3.123}$$

We now proceed as before, analytically continuing this expression outside the unit semicircle and replacing f_σ on and inside the unit semicircle by its regular expansion $\sigma f_1(\zeta)$. In this way we get the following inhomogeneous equation for f_σ

$$f_{\sigma\zeta\zeta} + P(f_\sigma, \zeta) f_{\sigma\zeta} + Q(f_\sigma, \zeta) f_\sigma = R(f_\sigma, \zeta), \tag{3.124}$$

where

$$P(f_\sigma, \zeta) = \frac{2}{\zeta^2 - 1} + \frac{1}{\sigma} \frac{|z_\zeta|}{\zeta} f_\sigma(\zeta) + \frac{|z_\zeta|}{\zeta} f_1(1/\zeta) + \frac{1}{\zeta} I(\zeta), \tag{3.125}$$

$$Q(f_\sigma, \zeta) = \frac{1}{\sigma} \frac{|z_\zeta| \widehat{z}_\zeta}{\zeta}, \tag{3.126}$$

$$R(f_\sigma, \zeta) = -\widehat{z}_{\zeta\zeta} - \frac{2}{\zeta^2 - 1} \widehat{z}_\zeta - \frac{|z_\zeta| \widehat{z}_\zeta}{\zeta} f_1(1/\zeta) - \frac{\widehat{z}_\zeta}{\zeta} I(\zeta), \tag{3.127}$$

$$I(\zeta) = \frac{1}{2\pi i} \int_\curvearrowleft |z_\zeta| \operatorname{Re} f_{1\sigma}(\zeta') K(\zeta, \zeta') \frac{d\zeta'}{\zeta'}, \tag{3.128}$$

$$|z_\zeta| = \sqrt{[\widehat{z}_\zeta(\zeta) + f_{\sigma\zeta}(\zeta)][\widehat{z}_\zeta(1/\zeta) + f_{\sigma\zeta}(1/\zeta)]}. \tag{3.129}$$

To solve this equation would require detailed knowledge of $f_{\varepsilon\zeta}(\zeta)$ when $|\zeta| = O(1)$ which we do not have. We have knowledge of the asymptotic behaviour of $f_{\varepsilon\zeta}(\zeta)$ which we can use to analyse this equation in the limit of small $|p|$.

3.6.1 Non-linear Equation for Small p

For small p we proceed as in the linear case. We set

$$\zeta = \frac{1}{|p|\omega} \tag{3.130}$$

and keep terms to leading order in $|p|$. We re-scale f_σ by setting $f_\sigma = |p|^2 F_\sigma$. We find the following non-linear differential equation for F_σ

$$\frac{d^2F_\sigma}{d\omega^2} + \left[\frac{1}{\omega} - \frac{i\delta}{\omega}MF_\sigma\right]\frac{dF_\sigma}{d\omega} + \frac{i\delta}{\omega^3}M\left[\omega(\omega^2 - \mathrm{sgn}(p^2)) - i\gamma\right]F_\sigma = 2 + \frac{i\gamma}{\omega^3}, \tag{3.131}$$

where

$$M = \sqrt{(\omega^2 - \mathrm{sgn}(p^2)) - \frac{i\gamma}{\omega} - \omega\frac{dF_\sigma}{d\omega}} \tag{3.132}$$

$$\delta = \left(\frac{2}{\pi}\right)\frac{|p|^3}{\sigma}, \tag{3.133}$$

$$\gamma = -\frac{3}{4}\frac{\varepsilon \ln|p|}{|p|^3}. \tag{3.134}$$

This is a nonlinear second order inhomogeneous differential equation. Unlike the linearised equation, we are unable to perform a large δ asymptotic analysis. One of our few analytic resources remaining is an asymptotic expansion of the solution for large $|\omega|$. It is possible to produce the first few terms of such an expansion and it appears to be a regular expansion in negative powers of ω given by (3.137.) However if we linearise about this solution, that is we set $F_\sigma = -2i/\delta\omega + .. + h(\omega)$ and linearise in h we find that h satisfies the following homogeneous equation for large ω;

$$\frac{d^2h}{d\omega^2} + \frac{1}{\omega}\frac{dh}{d\omega} + i\delta\omega h = 0. \tag{3.135}$$

The controlling factor of the two homogenous solutions for h is

$$h \sim \exp \pm 2e^{-i\pi/4}\delta^{1/2}\omega^{3/2}/3, \tag{3.136}$$

and so it is clear that the asymptotic expansion of the solution to the full nonlinear equation may contain exponentially small terms which can again become unbounded on crossing the Stokes lines.

Our numerical approach is the same as in the linear case. We start on the Stokes line that asymptotes to $\infty \exp(-i5\pi/6)$ with an initial condition that excludes transcendentally small terms and then integrate along a path that swings towards the imaginary axis. The initial condition is

$$F_\sigma \sim -\frac{2i}{\delta\omega} - \mathrm{sgn}(p^2)\frac{3i}{\delta\omega^3} + \frac{8}{\delta^2\omega^4} + \frac{4\gamma}{\delta\omega^4} + O(1/\omega^5), \tag{3.137}$$

$$\frac{dF_\sigma}{d\omega} \sim \frac{2i}{\delta\omega^2} + \mathrm{sgn}(p^2)\frac{9i}{\delta\omega^4} - \frac{32}{\delta^2\omega^5} - \frac{16\gamma}{\delta\omega^5} + O(1/\omega^6). \tag{3.138}$$

The selection criterion is again $\mathrm{Im}\, F_\sigma = 0$ on the imaginary axis. For λ both greater than and less than a half we find that the δ versus γ curves are qualitatively similar to the curves for the linearised equation and we present them in Figures 3.14 and 3.15.

As before the curves in the δ, γ plane can be inverted to give curves in the λ, σ plane for fixed ε. These curves give good agreement with the full numerical results from Chapter 2 for small ε. We present a comparison for several values of ε in Figures 3.16-3.20. The analytical results seem to accurately capture the branch merger for $\varepsilon > 0$. They also predict the values of λ well for $\varepsilon < 0$. The only unresolved issue is the question of branch merger for $\varepsilon < 0$ and very small surface tension. The numerical determination of the selection mechanism based on the analytic formulation fails in this case as does the full numerical computation from Chapter 2. We feel that a WKBJ analysis is possible but has not been performed.

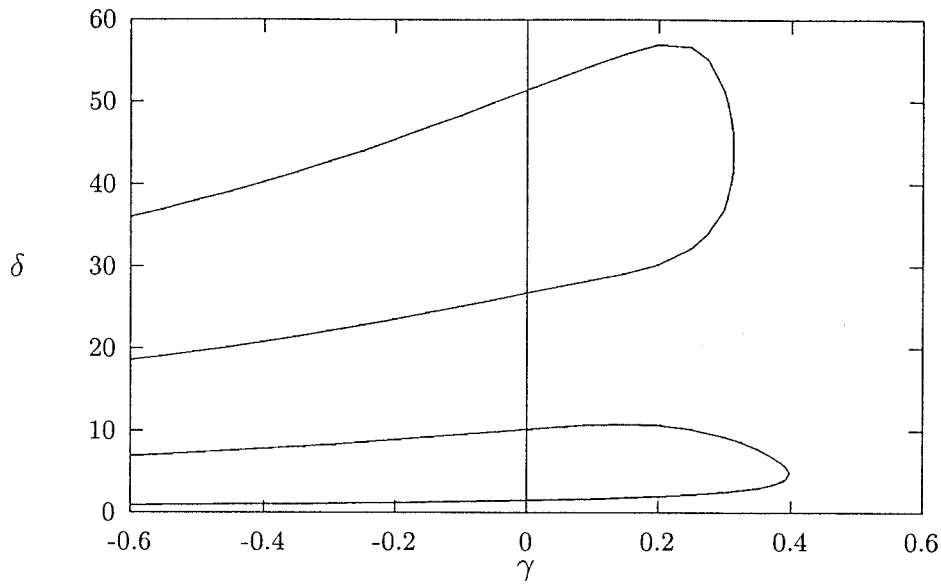

Figure 3.14: δ versus γ for $\lambda > 1/2$.

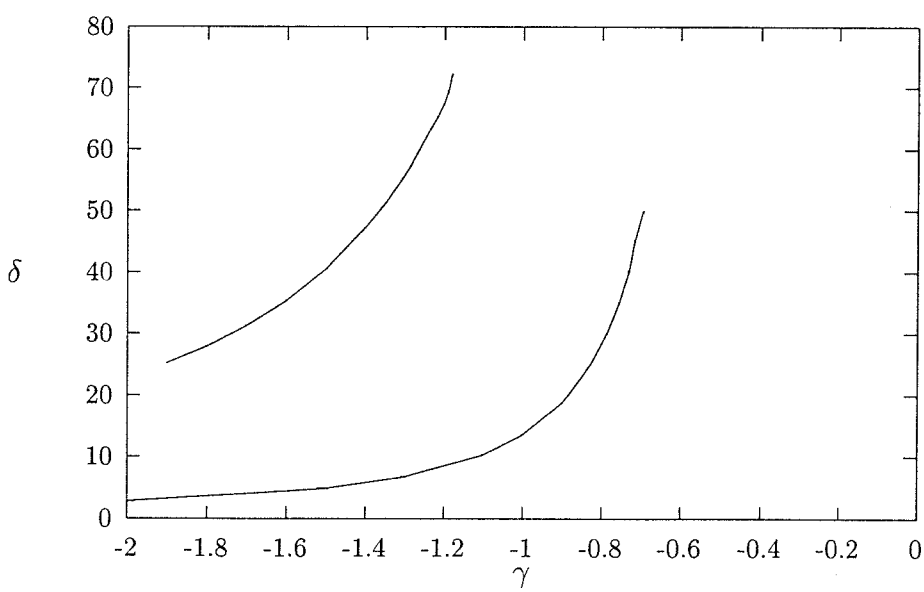

Figure 3.15: δ versus γ for $\lambda < 1/2$.

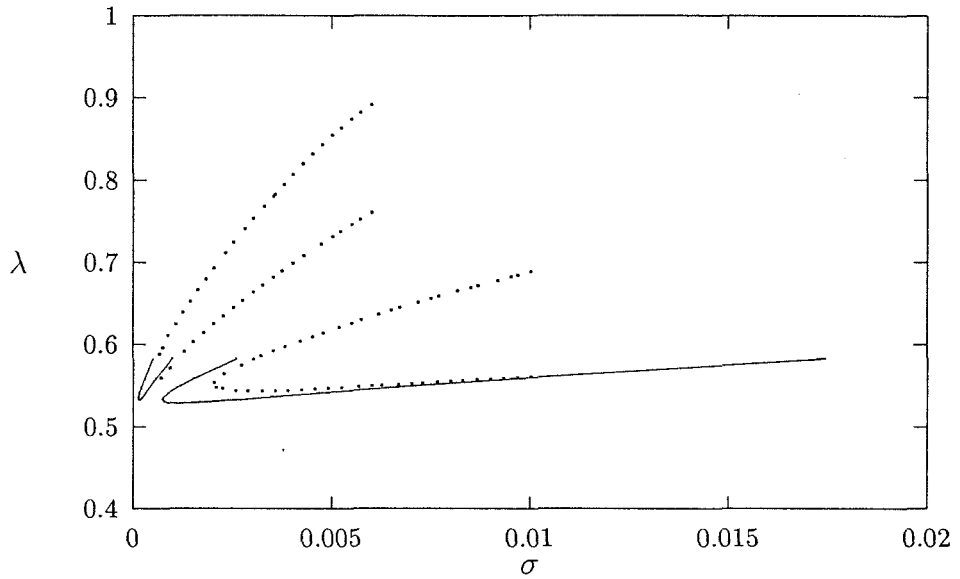

Figure 3.16: Width as a function of σ with $\varepsilon = 0.005$. (-) asymptotic, (..) full numerical computation from Chapter 2.

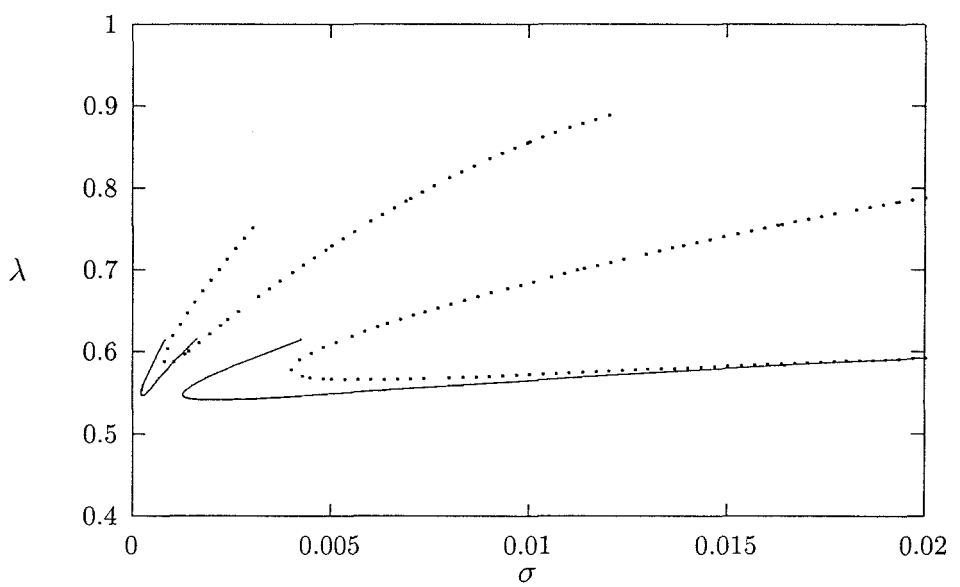

Figure 3.17: Width as a function of σ with $\varepsilon = 0.01$. (-) asymptotic, (..) full numerical computation from Chapter 2.

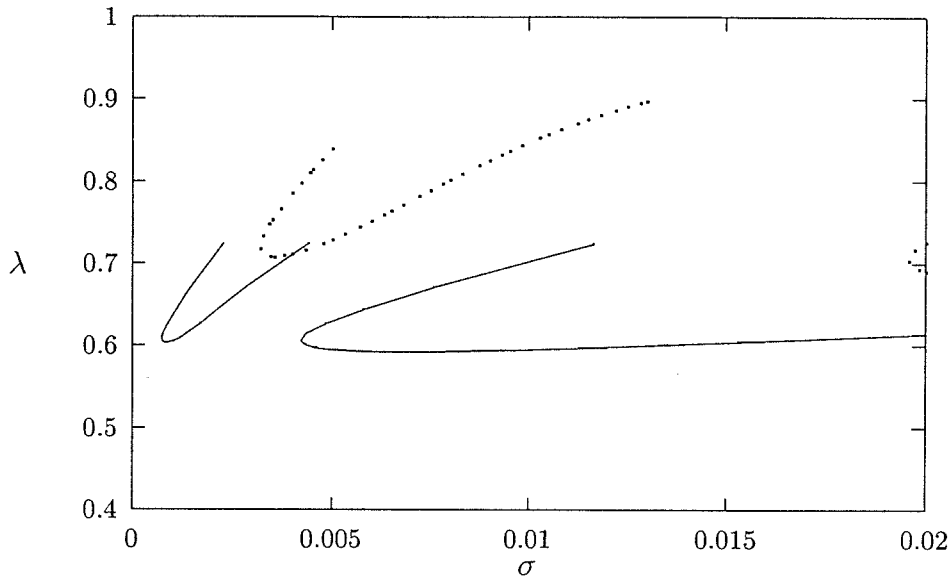

Figure 3.18: Width as a function of σ with $\varepsilon = 0.05$. (-) asymptotic, (..) full numerical computation from Chapter 2.

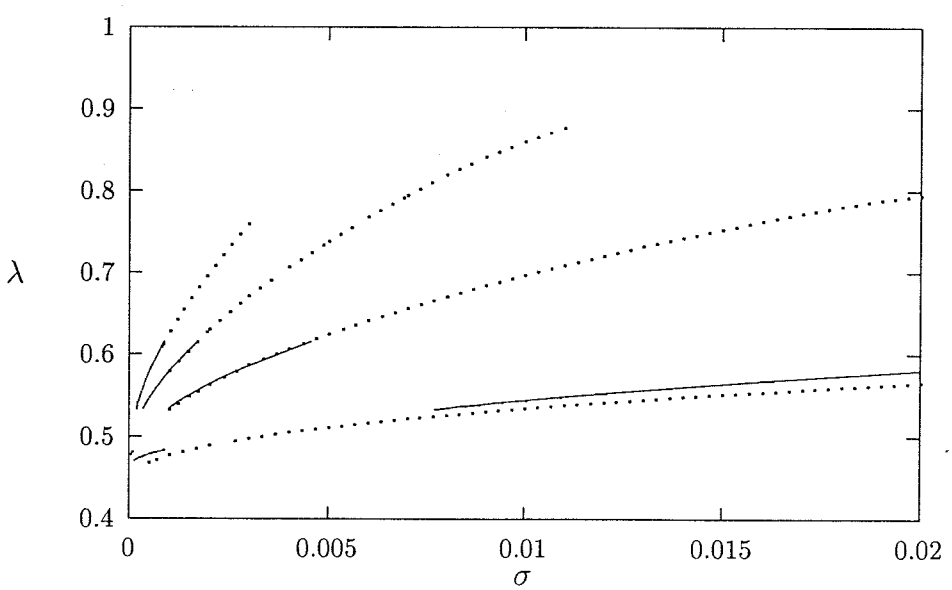

Figure 3.19: Width as a function of σ with $\varepsilon = -0.01$. (-) asymptotic, (..) full numerical computation from Chapter 2.

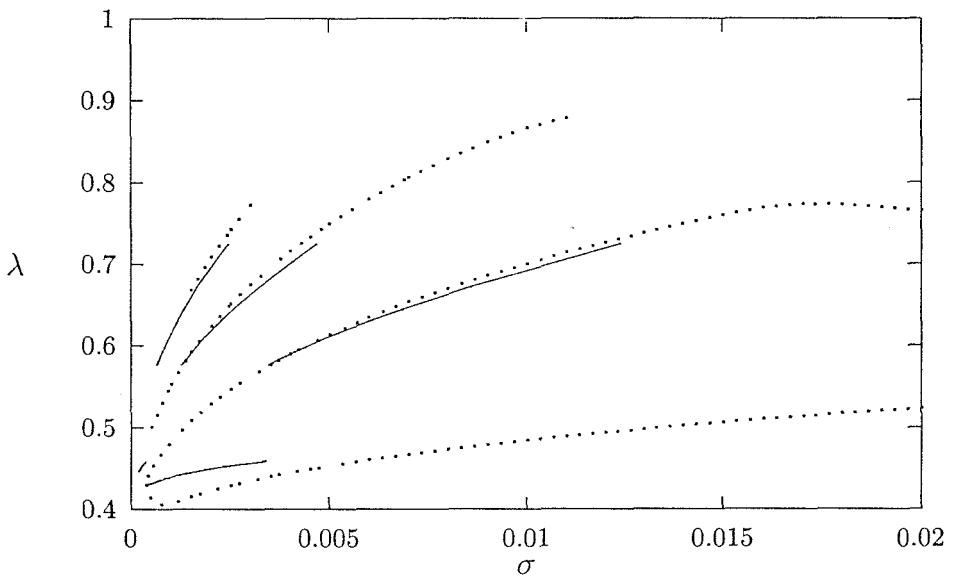

Figure 3.20: Width as a function of σ with $\varepsilon = -0.05$. (-) asymptotic, (..) full numerical computation from Chapter 2.

Chapter 4 Steady Flows with Finite Interfaces

4.1 Introduction

While fingers are one class of steady flow in a Hele-Shaw cell, there are also steady solutions corresponding to interfaces that span the cell. For a Hele-Shaw cell of constant gap there is a solution corresponding to a flat interface moving at constant speed. There are many other solutions found by McLean [3], [4] that bifurcate from this solution. The flat interface is unstable to small perturbations [1] except for larger values of surface tension. For a cell of non-constant gap the flat interface is no longer a steady solution and the question naturally arises as to what the corresponding solution is in this case. It is not clear what the appropriate boundary conditions are at the cell edges. There is a viscous boundary layer of thickness on the order of the distance between the plates in which the fluid flow is three dimensional and the lubrication theory approximation used here breaks down. The slope of the interface is undoubtedly a complex function of the speed of the interface and fluid properties, among other things.

The channel may also be considered as one period of a periodic flow in a Hele-Shaw cell of infinite extent in the lateral y direction (see Figure 4.1.) If we consider one period stretching from $y = -a$ to a, and if the distance between the plates is a function of period $2a$, symmetric about the line $y = 0$, then we expect solutions with periodic interfaces satisfying zero derivative conditions on the wall $y = \pm a$.

We present solutions corresponding to finite interfaces in a Hele-Shaw cell with varying gap which satisfy the condition that the interface meets the walls at a right angle. For most values of surface tension the solutions are close to the flat interface solution if the gap perturbation is small. At certain values of surface tension we find

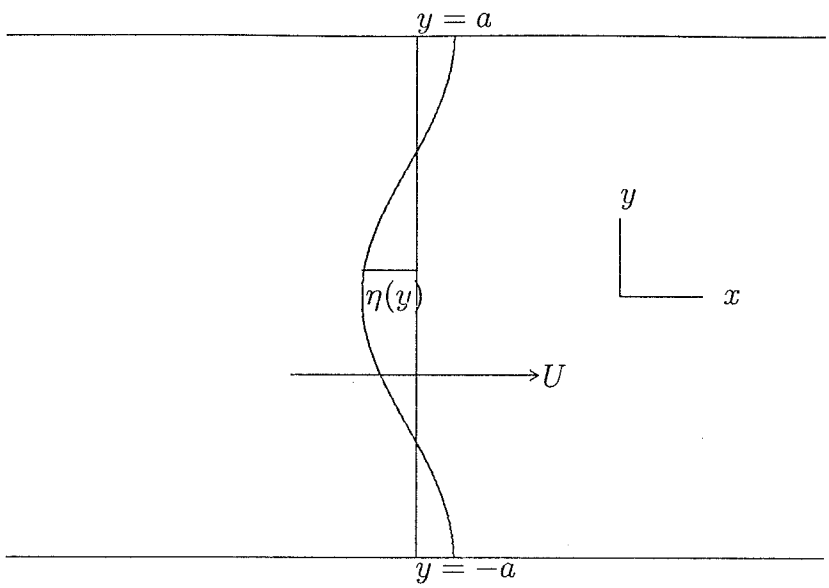

Figure 4.1: Finite interface moving at speed U.

a bifurcation to finite amplitude solutions. The structure of these bifurcations, first found by McLean [3] for constant gap, is heavily dependent on the height perturbation. In some cases a pitchfork bifurcation is perturbed into two independent branches of solution. In other cases the pitchfork is left structurally intact.

4.2 Analytic Results For Small Gap Width

In this section we calculate, using asymptotic methods, the effect of small change in gap width on the flow. We use a formulation that is convenient for analytical work, that is we let the unknown steady interface be given by $x = Ut + \eta(y)$. Thus we seek the pressure $p(x, y)$ satisfying

$$\nabla \cdot \left(h^3(y)\nabla p\right) = 0. \tag{4.1}$$

The boundary conditions are the kinematic condition

$$\frac{D}{Dt}\left(x - Ut - \eta(y)\right) = 0, \tag{4.2}$$

the dynamic condition on the interface

$$p|_\eta = T\left(\kappa - 2/h(y)\right), \tag{4.3}$$

and the flux conditions

$$\frac{\partial p}{\partial y} = 0, \qquad y = \pm a, \tag{4.4}$$

$$p \sim cx, \qquad x \to \infty, \tag{4.5}$$

with

$$c = \frac{U}{12\mu}\int_{-a}^{a} h(y)dy \left[\int_{-a}^{a} h^3(y)dy\right]^{-1}. \tag{4.6}$$

The curvature, κ, is given in terms of $\eta(y)$ by

$$\kappa = \frac{\eta''}{(1+\eta'^2)^{3/2}}. \tag{4.7}$$

We make the dependent and independent variables dimensionless in the same way as Chapter 2 to get the following free boundary problem for the pressure, $\phi(x,y)$, and the interface $\eta(y)$:

$$\boldsymbol{\nabla}\cdot\left(h^3(y)\boldsymbol{\nabla}\phi\right) = 0, \tag{4.8}$$

with boundary conditions

$$\phi|_\eta = \sigma\left(\frac{-\eta''}{(1+\eta'^2)^{3/2}} + \frac{2b/a}{h(y)}\right), \tag{4.9}$$

$$\left.\frac{\partial\phi}{\partial x}\right|_\eta = \frac{\partial\eta}{\partial y}\left.\frac{\partial\phi}{\partial y}\right|_\eta - 1/h^2(y), \tag{4.10}$$

$$\frac{\partial\phi}{\partial y} = 0, \qquad y = \pm 1, \tag{4.11}$$

$$\phi|_{x\to\infty} \sim cx, \qquad x \to \infty. \tag{4.12}$$

In the above

$$c = \frac{1}{\int_{-1}^{1} h^3(y)dy}. \tag{4.13}$$

When $h(y) = 1$ there is a trivial solution to these equations corresponding to a flat interface moving with unit speed. This solution is given by

$$\phi = x + 2\sigma a/b, \tag{4.14}$$

$$\eta = 0. \tag{4.15}$$

In fact McLean [4] showed that any solution of

$$\sigma\eta'' + (1+\eta'^2)^{3/2}\eta = 0, \tag{4.16}$$

gives an exact solution of the equations with

$$\phi = x + 2\sigma a/b, \tag{4.17}$$

provided $h(y) = 1$. The problem suggests no boundary conditions for η and there are infinitely many solutions of equation (4.16) for any value of $\sigma > 0$. In order to make progress we need boundary conditions and as mentioned before we choose to impose the conditions

$$\eta'(1) = \eta'(-1) = 0. \tag{4.18}$$

In this case the only solution is the flat interface $\eta = 0$ unless $\sigma = (2/n\pi)^2$ in which case there a pitchfork bifurcation to finite amplitude solutions. The reason for this will become clear in the subsequent discussion.

When h varies across the cell the flat interface is no longer a solution but we suspect that if $h(y)$ is close to a constant that the solution will be close to the flat interface. We set

$$h = 1 + \varepsilon h^{(1)}(y), \tag{4.19}$$

where $|\varepsilon| \ll 1$. In the following sections we will attempt to find solutions which are asymptotic expansions in the small parameter epsilon.

4.2.1 Regular Asymptotic Expansion

We attempt a regular asymptotic expansion in ε for the unknown functions ϕ and η, that is we try

$$\phi = \phi^{(0)} + \varepsilon\phi^{(1)} + o(\varepsilon), \tag{4.20}$$

$$\eta = \eta^{(0)} + \varepsilon\eta^{(1)} + o(\varepsilon). \tag{4.21}$$

The solution to the zero order problem is the trivial solution given in the last Section

$$\phi^{(0)} = x + 2\sigma a/b, \tag{4.22}$$

$$\eta^{(0)} = 0. \tag{4.23}$$

At order epsilon we find

$$\nabla^2\phi^{(1)} = 0, \tag{4.24}$$

with boundary conditions

$$\phi^{(1)}\Big|_{x=0} + \eta^{(1)} = \sigma(-\eta^{(1)\prime\prime} - 2a/bh^{(1)}), \tag{4.25a}$$

$$\left.\frac{\partial\phi^{(1)}}{\partial x}\right|_{x=0} = -2h^{(1)}, \tag{4.25b}$$

$$\frac{\partial\phi^{(1)}}{\partial y} = 0, \qquad y = \pm 1, \tag{4.25c}$$

$$\phi|_{x\to\infty} \sim 0, \qquad x \to \infty, \tag{4.25d}$$

$$\frac{d\eta}{dy} = 0, \qquad y = \pm 1. \tag{4.25e}$$

We notice that the equation for $\phi^{(1)}$ can be solved using boundary conditions (4.25b)-(4.25d). Once $\phi^{(1)}$ is determined, equation (4.25a) is an inhomogeneous ordinary differential equation for the interface $\eta^{(1)}$. The pressure, $\phi^{(1)}$, can be found by an

eigenfunction expansion

$$\phi^{(1)} = \sum_{n=1}^{\infty} a_n^{(1)} \exp(-n\pi x/2) \cos n\pi(y+1)/2. \tag{4.26}$$

Note that each of the eigenfunctions in this sum has zero normal derivative on the walls $y = \pm 1$. Since the set of functions $\cos n\pi(y+1)/2$, is complete in the space of piecewise continuous functions on $(-1, 1)$ we can express $h^{(1)}(y)$ as

$$h^{(1)} = \sum_{n=1}^{\infty} h_n^{(1)} \cos n\pi(y+1)/2. \tag{4.27}$$

On substitution into the kinematic condition (4.25b) we find

$$a_n = h_n^{(1)} \frac{4}{n\pi}. \tag{4.28}$$

The dynamic boundary (4.25a) gives us the differential equation for $\eta^{(1)}$,

$$\sigma\eta^{(1)\prime\prime} + \eta^{(1)} = -2\sigma\frac{a}{b}h^{(1)} - \sum_{n=1}^{\infty} a_n \cos n\pi(y+1)/2, \tag{4.29}$$

with boundary conditions $\eta'(1) = \eta'(-1) = 0$. The homogeneous equation has no non-trivial solutions when $\sigma \neq (2/n\pi)^2$ and thus if we can find a particular solution satisfying the boundary conditions it is the solution. Such a particular solution can be found using an eigenfunction expansion for $\eta^{(1)}$ of the form

$$\eta^{(1)} = \sum_{n=1}^{\infty} \eta_n^{(1)} \cos n\pi(y+1)/2. \tag{4.30}$$

Substituting into the differential equation (4.29) and using the expression for a_n we find

$$\eta_n^{(1)} = -\frac{h_n^{(1)}\left(4/n\pi + 2\sigma\frac{a}{b}\right)}{(1 - \sigma(n\pi/2)^2)}. \tag{4.31}$$

Since

$$\eta_n^{(1)} \sim c h_n^{(1)}/n^2, \tag{4.32}$$

we conclude that if $h(y)$ is twice continuously differentiable then $\eta(y)$ is twice continuously differentiable and satisfies

$$\left.\frac{d\eta^{(1)}}{dy}\right|_{y=-1} = \left.\frac{d\eta^{(1)}}{dy}\right|_{y=1} = 0. \tag{4.33}$$

It is clear from the expression (4.31) that the assumption that $\eta(y)$ is order epsilon breaks down when $\sigma = (2/n\pi)^2 + O(\varepsilon)$. This difficulty is associated with a resonance phenomenon and in the neighbourhood of any one of these values of σ a different scaling is required in order to construct a valid approximation to the solution.

4.2.2 Asymptotic Expansion Near Resonance

In the previous section we constructed a simple asymptotic expansion in integer powers of epsilon for the interface and pressure which is valid except when σ is near $(2/n\pi)^2$. We now construct an expansion which is valid when $\sigma = (2/n\pi)^2 + O(\varepsilon^{2/3})$. This region overlaps with the region in which the regular expansion is valid and thus we will have asymptotic solutions valid for all values of σ. We will see that the failure of the regular expansion is due to the neglect of non-linear terms in the curvature which cannot be uniformly neglected near resonance. We find a new scaling which reflects the importance of the non-linear terms and we will see that the effect of the perturbation to the gap is to destroy a pitchfork bifurcation first discovered by McLean [3].

We proceed as before with

$$h(y) = 1 + \varepsilon h^{(1)}, \tag{4.34}$$

however we now set

$$\phi = \phi^{(0)} + \alpha(\varepsilon)\phi^{(1)} + o(\alpha), \tag{4.35}$$

$$\eta = \eta^{(0)} + \beta(\varepsilon)\eta^{(1)} + o(\beta), \tag{4.36}$$

where α and β are $o(1)$ and attempt to find a suitable scaling to find a bounded solution. As before the zero order solution is

$$\phi^{(0)} = x + 2\sigma a/b, \tag{4.37}$$

$$\eta^{(0)} = 0. \tag{4.38}$$

We find on expanding the pressure equation (4.8) that

$$\nabla^2\phi^{(1)} = 0 + O(\varepsilon), \tag{4.39}$$

and that the kinematic condition (4.2) is

$$\alpha\frac{\partial\phi^{(1)}}{\partial x} = -2\varepsilon h^{(1)} + O(\alpha\varepsilon, \alpha\beta). \tag{4.40}$$

The consistent balance for α is $\alpha = \varepsilon$ with $\beta = o(1)$. Without yet committing ourselves to a scaling for β we can solve (4.39) for $\phi^{(1)}$ as a function of $h^{(1)}$. As before we find from (4.40) that

$$\phi^{(1)=}\sum_{n=1}^{\infty}\frac{4}{n\pi}h_n^{(1)}\exp -n\pi x/2\cos n\pi(y+1)/2, \tag{4.41}$$

where, as before, $h_n^{(1)}$ are the Fourier coefficients of $h^{(1)}$. Substituting into the dynamic condition (4.25a) we get the following ode for $\eta^{(1)}$:

$$\beta\eta^{(1)\prime\prime} - \frac{3}{2}\beta^3(\eta^{(1)\prime})^2\eta^{(1)\prime\prime} + \frac{\beta}{\sigma}\eta^{(1)} = \varepsilon R(y)/\sigma + o(\varepsilon, \beta^3), \tag{4.42}$$

where

$$R(y) = \sum_{n=1}^{\infty}A_n\cos n\pi(y+1)/2, \tag{4.43}$$

$$A_n = -\left(\frac{4}{n\pi} + 2\sigma\frac{a}{b}\right)h_n^{(1)}. \tag{4.44}$$

The reason for the resonance is now clear. For $\sigma \neq (2/n\pi)^2$ the dominant balance is given by $\beta = \varepsilon$ and the solution is the one derived in the previous section. Near the resonant values of σ the nonlinear terms in the equation balance the right hand side and prevent the solution from becoming unbounded. The scaling which balances the non-linear terms with the forcing is $\beta = \varepsilon^{1/3}$.

To investigate the behaviour of the solution near resonance we are thus lead to an expansion for η of the form

$$\phi = \varepsilon\phi^{(1)} + o(\varepsilon) \tag{4.45}$$

$$\eta = \varepsilon^{1/3}\eta^{(1)} + \varepsilon\eta^{(2)} + o(\varepsilon), \tag{4.46}$$

$$\sigma = (2/n\pi)^2 + \sigma_1\varepsilon^{2/3} + o(\varepsilon^{2/3}). \tag{4.47}$$

It is necessary to carry the expansion for η out to two terms to get a solvability condition for $\eta^{(1)}$. Before proceeding further we introduce some simplifying notation

$$\omega = \sqrt{1/\sigma}, \tag{4.48}$$

$$\omega_0 = n\pi/2. \tag{4.49}$$

The expansion for ω is

$$\omega = \omega_0 + \varepsilon^{2/3}\omega_1 + o(\varepsilon^{2/3}), \tag{4.50}$$

with

$$\sigma_1 = -2\omega_1/\omega_0^3. \tag{4.51}$$

At order $\varepsilon^{1/3}$ the equation is

$$\eta^{(1)''} + \omega_0^2\eta^{(1)} = 0, \tag{4.52}$$

with $\eta^{(1)\prime}(1) = \eta^{(1)\prime}(-1) = 0$. The solution is

$$\eta^{(1)} = B\cos\omega_0(y+1), \tag{4.53}$$

where B is arbitrary. In order to fix B we must proceed to the next order.

At order ε the problem is

$$\eta^{(2)''} + \omega_0^2 \eta^{(2)} = -2\omega_0\omega_1\eta^{(1)} + \frac{2}{3}\eta^{(1)''}\eta^{(1)'} + \omega_0^2 R(y), \tag{4.54}$$

again with boundary conditions $\eta^{(2)'}(1) = \eta^{(2)'}(-1) = 0$. In order that this equation have a solution, the right hand side must be orthogonal to the solution of the homogeneous equation. This is equivalent to the eigenfunction expansion of the right-hand side not containing any term proportional to $\cos\omega_0(y+1)$. After some algebra we find that this condition, expressed in terms of σ_1, is

$$B^3 - \frac{8}{3}\sigma_1 B - \frac{A_n}{\omega_0^2} = 0. \tag{4.55}$$

This cubic in B can be considered as an amplitude equation for $B(\sigma_1)$, since A_n and ω_0 are known. The cubic equation (4.55) has real coefficients and either has one or three real roots depending on the value of σ_1. We find that it has three real roots if and only if

$$\sigma_1 > 2\left(\frac{9}{16}\right)^{2/3} |A_n|^{2/3}\,\omega_0^{-4/3}. \tag{4.56}$$

We can solve the cubic equation (4.55) exactly, since it is has no quadratic term, and we present the results for $A_n/\omega^2 = 1, 0$, and -1 respectively in Figures 4.2-4.4. We present a comparison with a full numerical calculation in the next section.

We notice from the plots of B against σ_1 that the local behaviour of solutions near resonant values of the surface tension depends strongly on the value of A_n which is proportional to the Fourier coefficient of the gap perturbation with that wave-number. If $A_n = 0$ we have a pitchfork bifurcation to finite amplitude solutions. If $A_n \neq 0$ then we have two separate branches of solutions and their structure depends on the sign of A_n.

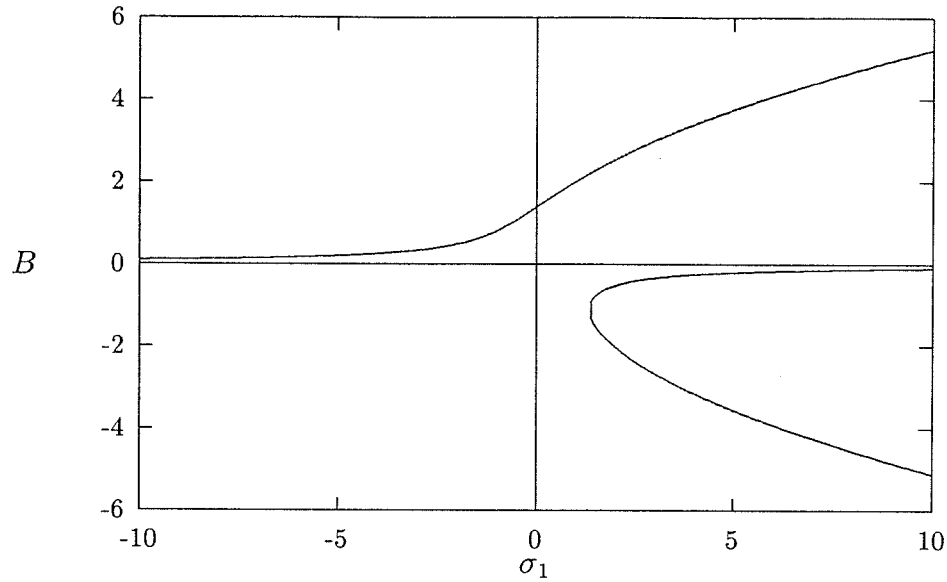

Figure 4.2: B as a function of σ_1 with $A_n/\omega_0^2 = 1$.

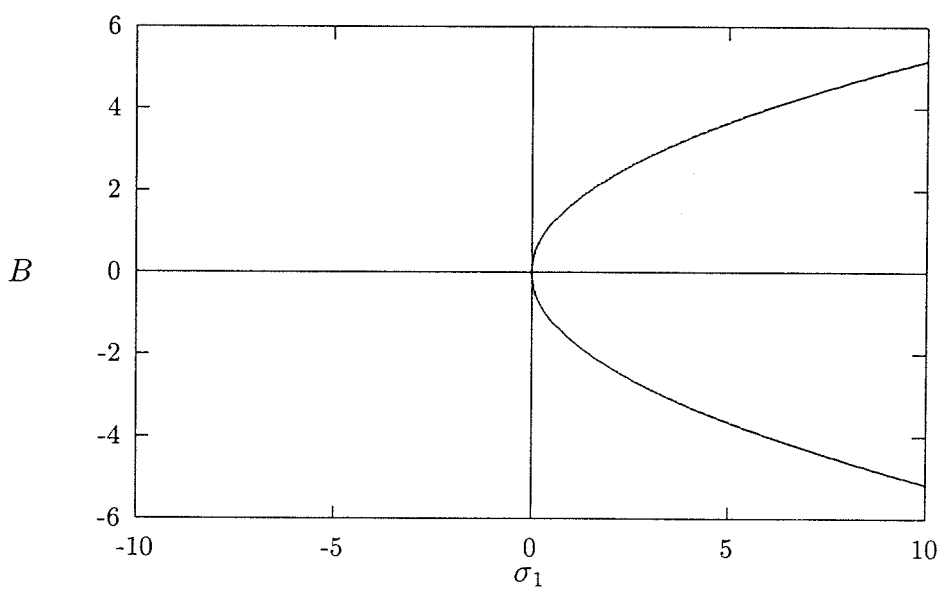

Figure 4.3: B as a function of σ_1 with $A_n/\omega_0^2 = 0$.

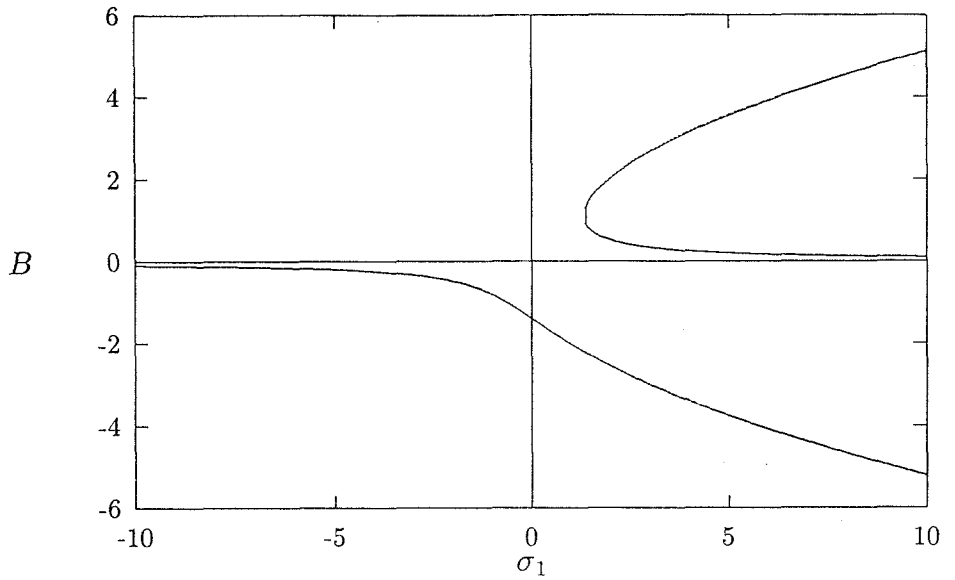

Figure 4.4: B as a function of σ_1 with $A_n/\omega_0^2 = -1$.

4.3 Numerical Results

A numerical scheme was constructed to compute a solution to the full equations. The method is very similar to the method we used for the fingers. We seek a conformal map that maps the unit strip in the ζ plane to the fluid filled domain. As before the unknowns of the problem are the coefficients of the conformal map. The conformal map has a simple form

$$z(\zeta) = \zeta + \sum_{n=1}^{N} u_n \exp -n\pi(\zeta + i)/2. \tag{4.57}$$

The details of the solution of the pressure equation and the Newton iteration are almost identical to the finger problem and we do not repeat them here.

In order to verify the results of the previous section we computed solutions with

$$h(y) = 1 + 0.01 \cos \pi(y + 1). \tag{4.58}$$

We plot the coefficient of the dominant u_j as a function of surface tension in Figure 4.5. The two bifurcations represented are those at $\sigma = (2/\pi)^2$ and $\sigma = (1/\pi)^2$

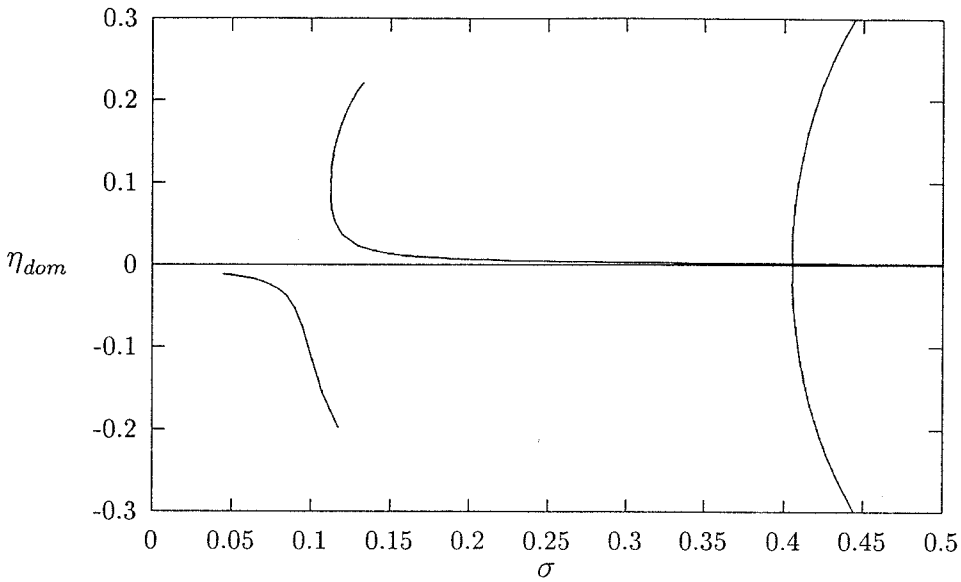

Figure 4.5: Dominant coefficient of the conformal map as a function of surface tension.

respectively. The dominant coefficient at the first bifurcation is u_1 and elsewhere is u_2 in agreement with the perturbation analysis. In Figure 4.6 we compare the results from the asymptotic analysis with the full numerical calculation. The solid line is u_2 and the dotted line is the coefficient of the dominant term in the asymptotic expansion near resonance with $\varepsilon = 0.01$. There is surprisingly good agreement between the two curves. In both Figures $N = 16$ was used for smaller amplitude solutions and $N = 32$ for the larger amplitudes.

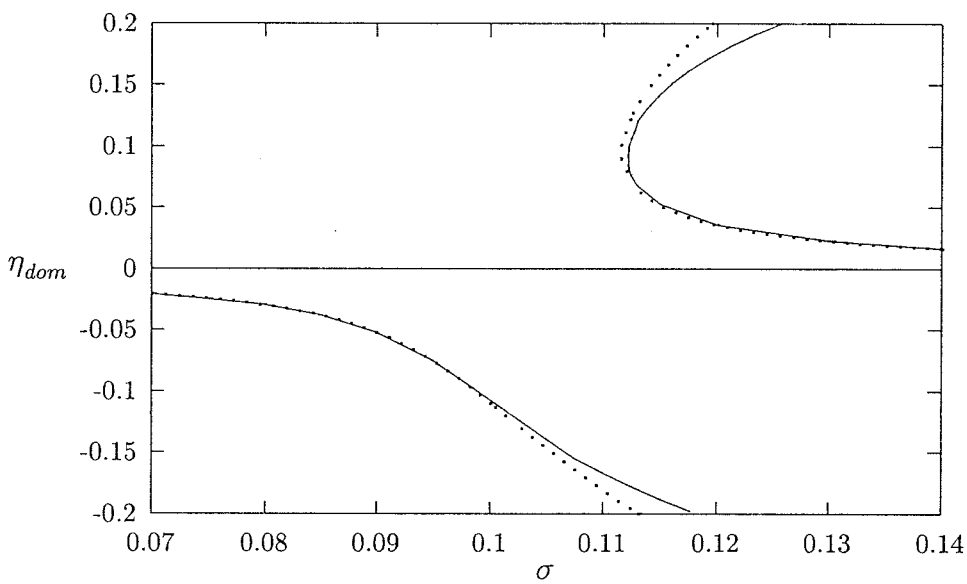

Figure 4.6: Comparison between numerical solution (-) and asymptotic solution (..) near resonance.

Appendix A Asymptotics of Conformal Map

A.1 Asymptotic Behaviour of $z(\zeta)$

In Chapter 2 we introduced the conformal map $(\xi, \eta) \to (x, y)$ given by the analytic function $z = z(\zeta)$, where z is in fact the composition of several maps,

$$z(\zeta) = z_{st} \circ \zeta_4 \circ \zeta_3 \circ \zeta_2 \circ \zeta_1(\zeta). \tag{A.1}$$

These maps are given by the formulae

$$\begin{aligned}
\zeta_1(\zeta) &= \zeta + \sum_{l=0}^{L} u_l \exp(-l\pi\zeta), && \text{(A.2)}\\
\zeta_2(\zeta_1) &= i\sinh(\pi\zeta_1/2), && \text{(A.3)}\\
\zeta_3(\zeta_2) &= \frac{2\theta}{\pi}\left[\frac{(\zeta_2+1)^{2\theta/\pi} + (\zeta_2-1)^{2\theta/\pi}}{(\zeta_2+1)^{2\theta/\pi} - (\zeta_2-1)^{2\theta/\pi}}\right], && \text{(A.4)}\\
\zeta_4(\zeta_3) &= \frac{2}{\pi}\ln\left(-i\pi\zeta_3/2\theta + \sqrt{1-(\pi\zeta_3/2\theta)^2}\right), && \text{(A.5)}\\
z_{st}(\zeta_4) &= \zeta_4 + \frac{1}{k}\ln\frac{1}{2}\left(1+\exp(-\pi\zeta_4)\right). && \text{(A.6)}
\end{aligned}$$

In the above, given the width of the finger, λ, we require k to satisfy (2.36) and once that value of k is determined θ is given by

$$\theta = k(1-\lambda),$$

as described in Chapter 2.

We are concerned with the behaviour of the composite map, z, as $\zeta \to i$ as this will give us the asymptotic shape of the tails as $x \to -\infty$ in the physical domain. It

is possible to show the following results:

$$\zeta_1 \sim i + C_1(\zeta - i) + O(\zeta - i)^2, \qquad \zeta \to i, \tag{A.7}$$

$$\zeta_2 \sim -1 - (\pi/2)^2(\zeta_1 - i)^2/2 + O(\zeta_1 - i)^4, \qquad \zeta_1 \to i, \tag{A.8}$$

$$\zeta_3 \sim -2\theta/\pi + (2\theta/\pi)(-2)^{1-2\theta/\pi}(\zeta_2 + 1)^{2\theta/\pi} + O(\zeta_2 + 1)^{4\theta/\pi}, \ \zeta_2 \to -1, \tag{A.9}$$

$$\zeta_4 \sim i - (2i/\sqrt{\theta\pi})\sqrt{\zeta_3 + 2\theta/\pi} + O(\zeta_3 + \frac{2\theta}{\pi}), \qquad \zeta_3 \to -\frac{2\theta}{\pi}, \tag{A.10}$$

$$z_{st} \sim i + \frac{1}{k}\ln\frac{\pi}{2}(\zeta_4 - i) + O(\zeta_4 - i), \qquad \zeta_4 \to i. \tag{A.11}$$

In the above

$$C_1 = 1 - \pi\sum_{l=0}^{L} l(-1)^l u_l, \tag{A.12}$$

and we have used $\zeta_1(i) = i$, i.e.,

$$\sum_{l=0}^{L}(-1)^l u_l = 0. \tag{A.13}$$

By composing these expansions we find

$$\zeta_4 \sim i + D_1(\zeta - i)^{2\theta/\pi}, \qquad \zeta \to i, \tag{A.14}$$

$$D_1 = \left(\frac{\pi}{4}\right)^{2\theta/\pi - 1} C_1^{2\theta/\pi}. \tag{A.15}$$

Thus

$$z(\zeta) \sim i + \frac{1}{k}\ln\frac{\pi}{2}D_1(\zeta - i)^{2\theta/\pi} + O(\zeta - i)^{2\theta/\pi}, \qquad \zeta \to i. \tag{A.16}$$

Unfortunately, as we will see in the next section, this two term expansion of $z(\zeta)$ is insufficient to get the two term asymptotic expansion of the shape of the interface $Y(x)$. In order to get $Y(x)$ a three term expansion is necessary. The algebra is difficult to perform. We find that if we impose the condition that

$$\zeta_1 = i + C_1(\zeta - i) + O(\zeta - i)^3, \tag{A.17}$$

that is there are no quadratic terms, then

$$z(\zeta) \sim i+\frac{1}{k}\ln\frac{\pi}{2}D_1(\zeta-i)^{2\theta/\pi}+D_1(1-\pi/2k)(\zeta-i)^{2\theta/\pi}+o(\zeta-i)^{2\theta/\pi}, \qquad \zeta \to i. \quad \text{(A.18)}$$

We also find that if the quadratic terms are present in ζ_1 they only affect the coefficient of $(\zeta - i)^{2\theta/\pi}$, something which is difficult to show analytically but can be verified numerically. This restriction is equivalent to

$$\frac{d^2\zeta_1}{d\zeta^2}|_{\zeta=i} = 0, \qquad \text{(A.19)}$$

or

$$\sum_{l=0}^{L}(-1)^l l^2 u_l = 0. \qquad \text{(A.20)}$$

As we will see in the next section this restriction is equivalent to choosing one finger from among all the fingers which differ only by translation in the x direction.

A.1.1 Asymptotic Shape of Interface

We recall that the shape of the interface is given by the image under $z(\zeta)$ of the line $\zeta = i\eta$, $-1 < \eta < 1$. To get the asymptotic shape of the interface defined by (A.18) we let

$$\zeta = i + \rho e^{-i\pi/2}. \qquad \text{(A.21)}$$

We substitute this into (A.18) and take real and imaginary parts. Eliminating ρ we find

$$Y(x) \sim (1-\frac{\theta}{k}) + \frac{2}{\pi}\sin\theta(1-\frac{\pi}{2k})\exp(kx), \qquad x \to -\infty. \qquad \text{(A.22)}$$

Again if we had not imposed (A.19) then the coefficient of $\exp(kx)$ would be different, something which could also be accomplished by the translation $x \to x + x_0$. Thus (A.19) is equivalent to removing the translation invariance.

From (A.22) it is clear that the constant A referred to in Chapter 2 has the value

$$A = \frac{2}{\pi}(1-\frac{\pi}{2k})\sin\theta. \qquad \text{(A.23)}$$

A.1.2 Asymptotic Solution of Equation

In order to implement our numerical scheme accurately we need an asymptotic solution of the partial differential equation (2.55) in the corner ($\xi \to 0$, $\eta \to 1$). One way to do this is to determine the effect of the inverse map $\zeta = \zeta(z)$ on the asymptotic solution of the equation as determined in Chapter 2, that is

$$\phi \sim C + Dg(y;k)\exp(kx), \qquad x \to -\infty. \tag{A.24}$$

We express the solution in terms of local polar coordinates in the corner $\zeta = i$. To that end we introduce polar coordinates (ρ, ψ) as follows:

$$\zeta = i + \rho \exp -i\psi. \tag{A.25}$$

On substitution into the expression (A.18) for the conformal map we find, on taking real and imaginary parts,

$$x \sim \frac{1}{k}\ln\left(\frac{\pi}{2}D_1\rho^{2\theta/\pi}\right) + O(\rho^{2\theta/\pi}), \tag{A.26}$$

$$y \sim (1-(2\theta/\pi)\psi) + (1-\pi/2k)D_1\rho^{2\theta/\pi}\sin 2\theta\psi/\pi. \tag{A.27}$$

Substituting into the expression for the pressure (A.24) we get

$$\phi \sim D\frac{\pi}{2}D_1\rho^{2\theta/\pi}g(1-2\theta\psi/\pi;k). \tag{A.28}$$

Since, from Chapter 2,

$$D = \frac{k}{h^2(\lambda)g'(\lambda;k)}A, \tag{A.29}$$

we get the final result

$$\phi(\rho,\psi) \sim \frac{k\sin\theta}{h^2(\lambda)g'(\lambda;k)}(1-\frac{\pi}{2k})D_1\rho^{2\theta/\pi}g(1-2\theta\psi/\pi;k) + O(\rho^{4\theta/\pi}),\ \rho \to 0. \tag{A.30}$$

In solving for ϕ numerically we performed one last map $\xi \to q$ given by

$$q = 1 - e^{-\xi}. \tag{A.31}$$

Under this transformation

$$q \sim \xi,\ \xi \to 0, \tag{A.32}$$

and thus (A.30) is unchanged. We conclude that the ϕ_{asym} that we seek is given by

$$\begin{aligned}
\phi_{asym}(\rho, \psi) &= D_2 \rho^{2\theta/\pi} g(1 - 2\theta\psi/\pi; k) + O(\rho^{4\theta/\pi}), && \text{(A.33)} \\
D_2 &= \frac{k \sin\theta}{h^2(\lambda) g'(\lambda; k)} (1 - \frac{\pi}{2k}) D_1 && \text{(A.34)} \\
\rho &= \sqrt{q^2 + \eta^2}, && \text{(A.35)} \\
\psi &= -\arctan q/\eta, && \text{(A.36)}
\end{aligned}$$

where q and η are Cartesian coordinates on the square $0 < q < 1$, $0 < \eta < 1$.

Appendix B Calculation of Gap Perturbation

In this Appendix we derive an expression for $h_1(y) = \cos\pi(y+1)$ in terms of ζ and $\bar{\zeta}$. In particular we want an explicit expression for

$$h_1(\frac{z_{st}(\zeta) - \bar{z}_{st}(\bar{\zeta})}{2i}). \tag{B.1}$$

We start with the expression for $z_{st}(\zeta)$;

$$z_{st}(\zeta) = -\frac{2}{\pi}\ln\zeta + \frac{2}{\pi}(1-\lambda)(\ln(\zeta-1)+\ln(\zeta+1)) - 2i(1-\lambda) + i, \tag{B.2}$$

$$\bar{z}_{st}(\bar{\zeta}) = -\frac{2}{\pi}\ln\bar{\zeta} + \frac{2}{\pi}(1-\lambda)(\ln(\bar{\zeta}-1)+\ln(\bar{\zeta}+1)) + 2i(1-\lambda) - i. \tag{B.3}$$

Thus

$$\begin{aligned} z_{st}(\zeta) - \bar{z}_{st}(\bar{\zeta}) &= -\frac{2}{\pi}(\ln\zeta - \ln\bar{\zeta}) - 4i(1-\lambda) + 2i \\ &\quad + \frac{2}{\pi}(1-\lambda)(\ln(\zeta-1) - \ln(\bar{\zeta}-1) + \ln(\zeta+1) - \ln(\bar{\zeta}+1)). \end{aligned} \tag{B.4}$$

Now

$$h_1(\frac{z_{st}(\zeta) - \bar{z}_{st}(\bar{\zeta})}{2i}) = \cos\pi(\frac{z_{st}(\zeta) - \bar{z}_{st}(\bar{\zeta})}{2i} + 1) \tag{B.5}$$

$$= -\frac{1}{2}(\exp\frac{\pi}{2}(z_{st} - \bar{z}_{st}) + \exp\frac{-\pi}{2}(z_{st} - \bar{z}_{st})). \tag{B.6}$$

From the expression for $z_{st} - \bar{z}_{st}$ we have

$$\exp\frac{\pi}{2}(z_{st} - \bar{z}_{st}) = (\frac{\bar{\zeta}}{\zeta})(\frac{\zeta-1}{\bar{\zeta}-1})^{1-\lambda}(\frac{\zeta+1}{\bar{\zeta}+1})^{1-\lambda}e^{i\pi(2\lambda-1)}. \tag{B.7}$$

Thus the final expression for h_1 is

$$h_1(\frac{z_{st}(\zeta)-\bar{z}_{st}(\bar{\zeta})}{2i}) = \frac{1}{2}[(\frac{\bar{\zeta}}{\zeta})(\frac{\zeta-1}{\bar{\zeta}-1})^{1-\lambda}(\frac{\zeta+1}{\bar{\zeta}+1})^{1-\lambda}e^{i\pi 2\lambda} + (\frac{\zeta}{\bar{\zeta}})(\frac{\bar{\zeta}-1}{\zeta-1})^{1-\lambda}(\frac{\bar{\zeta}+1}{\zeta+1})^{1-\lambda}e^{-i\pi 2\lambda}]. \tag{B.8}$$

We introduce some notation to simplify things.

$$h_1(\frac{z_{st}(\zeta)-\bar{z}_{st}(\bar{\zeta})}{2i}) = h_1(\zeta,\bar{\zeta}) = \frac{1}{2}[\frac{g(\zeta)}{\bar{g}(\bar{\zeta})}+\frac{\bar{g}(\bar{\zeta})}{g(\zeta)}], \tag{B.9}$$

where

$$g(\zeta) = \frac{1}{\zeta}(\zeta-1)^{1-\lambda}(\zeta+1)^{1-\lambda}e^{i\pi\lambda}. \tag{B.10}$$

Appendix C Explicit Calculation of a Particular Solution

In the case of one specific choice of h_1 it is possible to make some simplifications in the calculation of $\phi_{\varepsilon P}$. We will examine

$$h_1(y) = \cos \pi(y+1). \tag{C.1}$$

We saw already that

$$\begin{aligned} \phi_{\varepsilon P}(\zeta,\bar{\zeta}) &= -\frac{3}{4}[\int^{\zeta} h_1(\frac{z_{st}(\zeta)-\bar{z}_{st}(\bar{\zeta})}{2i})\frac{dw_0}{d\zeta}d\zeta \\ &\quad + \int^{\bar{\zeta}} h_1(\frac{z_{st}(\zeta)-\bar{z}_{st}(\bar{\zeta})}{2i})\frac{d\bar{w}_0}{d\bar{\zeta}}d\bar{\zeta}] \end{aligned} \tag{C.2}$$

We know from Appendix B that

$$h_1(\frac{z_{st}(\zeta)-\bar{z}_{st}(\bar{\zeta})}{2i}) = h_1(\zeta,\bar{\zeta}) = \frac{1}{2}[\frac{g(\zeta)}{\bar{g}(\bar{\zeta})} + \frac{\bar{g}(\bar{\zeta})}{g(\zeta)}], \tag{C.3}$$

where

$$g(\zeta) = \frac{1}{\zeta}(\zeta-1)^{1-\lambda}(\zeta+1)^{1-\lambda}e^{i\pi\lambda}. \tag{C.4}$$

We know

$$w_0 = -\frac{2}{\pi}\ln -i\zeta. \tag{C.5}$$

Thus equation (C.2) becomes

$$\begin{aligned} \phi_{\varepsilon P}(\zeta,\bar{\zeta}) &= \frac{3}{4\pi}\left[\frac{1}{\bar{g}(\bar{\zeta})}\int_{a_1}^{\zeta} g(\zeta)\frac{d\zeta}{\zeta} + \bar{g}(\bar{\zeta})\int_{a_2}^{\zeta}\frac{1}{g(\zeta)}\frac{d\zeta}{\zeta}\right. \\ &\quad \left. + g(\zeta)\int_{a_3}^{\bar{\zeta}}\frac{1}{\bar{g}(\bar{\zeta})}\frac{d\bar{\zeta}}{\bar{\zeta}} + \frac{1}{g(\zeta)}\int_{a_4}^{\bar{\zeta}}\bar{g}(\bar{\zeta})\frac{d\bar{\zeta}}{\bar{\zeta}}\right]. \end{aligned} \tag{C.6}$$

$$= \frac{3}{4\pi}\left[P_1(\zeta,\bar{\zeta}) + P_2(\zeta,\bar{\zeta}) + P_3(\zeta,\bar{\zeta}) + P_4(\zeta,\bar{\zeta})\right]. \qquad \text{(C.7)}$$

Careful choice of the limits of integration allows us to make $\phi_{\varepsilon P}$ such that $\partial\phi_{\varepsilon P}/\partial\eta = 0$ on the real diameter.

In order to determine the correct limits of integration $(a_1..a_4)$ we need some elementary properties of $g(\zeta)$ namely that $g(\zeta)$ is real valued for $-1 < \zeta < 1$ and that it is purely imaginary on the imaginary axis. We thus take $a_2 = a_3 = 0$. This choice will ensure that P_2 and P_3 are bounded on the unit semi-circle and real valued on the real axis. The choice of a_1 and a_4 is slightly more involved. After some algebra one can show

$$\int_i^{-1} g(\zeta)\frac{d\zeta}{\zeta} = \alpha - i\beta, \qquad \text{(C.8)}$$

$$\int_i^{1} g(\zeta)\frac{d\zeta}{\zeta} = -\alpha - i\beta, \qquad \text{(C.9)}$$

where

$$\alpha = \int_0^{\pi/2} (2\cos\theta)^{1-\lambda}\cos\lambda\theta d\theta, \qquad \text{(C.10)}$$

$$\beta = \int_0^{\pi/2} (2\cos\theta)^{1-\lambda}\sin\lambda\theta d\theta. \qquad \text{(C.11)}$$

Further

$$\int_{iy}^{i} g(\zeta)d\zeta = i\gamma, \qquad \text{(C.12)}$$

where

$$\gamma = \int_y^{\lambda} \frac{(1+\rho^2)^{1-\lambda}}{\rho^2} d\rho. \qquad \text{(C.13)}$$

Thus if we choose y such that $\gamma = \beta$ and choose $a_1 = iy$, $a_2 = -iy$, then we are guaranteed that P_1 and P_4 are real on the real axis. Even after this choice it is clear that P_1 and P_4 are unbounded at $\zeta = \pm 1$. We thus subtract off the singular parts. We claim that the following function is a particular solution that is bounded on the

unit semi-circle, and satisfies $\partial\phi_{\varepsilon P}/\partial y = 0$ on the real diameter.

$$\begin{aligned}\phi_{\varepsilon P}(\zeta,\bar{\zeta}) &= \frac{3}{4\pi}\left[\frac{1}{\bar{g}(\bar{\zeta})}\int_{iy}^{\zeta} g(\zeta)\frac{d\zeta}{\zeta} + \bar{g}(\bar{\zeta})\int_0^{\zeta}\frac{1}{g(\zeta)}\frac{d\zeta}{\zeta} + \right. \qquad \text{(C.14)}\\ &\quad g(\zeta)\int_0^{\bar{\zeta}}\frac{1}{\bar{g}(\bar{\zeta})}\frac{d\bar{\zeta}}{\bar{\zeta}} + \frac{1}{g(\zeta)}\int_{-iy}^{\bar{\zeta}}\bar{g}(\bar{\zeta})\frac{d\bar{\zeta}}{\bar{\zeta}}\\ &\quad \left. + \frac{\alpha}{\zeta g(\zeta)} + \frac{\alpha}{\bar{\zeta}\bar{g}(\bar{\zeta})}\right].\\ &= \frac{3}{4\pi}\left[P_1(\zeta,\bar{\zeta}) + P_2(\zeta,\bar{\zeta}) + P_3(\zeta,\bar{\zeta}) + P_4(\zeta,\bar{\zeta})\right. \qquad \text{(C.15)}\\ &\quad \left. + \frac{\alpha}{\zeta g(\zeta)} + \frac{\alpha}{\bar{\zeta}\bar{g}(\bar{\zeta})}\right].\end{aligned}$$

From the point of view of evaluating these functions it is useful to note that each P_i is of the form

$$P_i(\zeta,\bar{\zeta}) = Q_i(\zeta)\bar{R}_i(\bar{\zeta}) \qquad \text{(C.16)}$$

We need both $\phi_{\varepsilon P}$ and $\partial\phi_{\varepsilon P}/\partial r$ evaluated on the unit circle i.e. when $\bar{\zeta} = 1/\zeta$. We note that

$$\frac{\partial\phi_{\varepsilon P}}{\partial r}|_{r=1} = \zeta\frac{\partial\phi_{\varepsilon P}}{\partial\zeta} + \frac{1}{\zeta}\frac{\partial\phi_{\varepsilon P}}{\partial\bar{\zeta}}. \qquad \text{(C.17)}$$

Thus, on the unit circle,

$$\begin{aligned}\phi_{\varepsilon P}(\zeta,\frac{1}{\zeta}) &= \frac{3}{4\pi}[Q_1(\zeta)\bar{R}_1(\frac{1}{\zeta}) + Q_2(\zeta)\bar{R}_2(\frac{1}{\zeta}) + Q_3(\zeta)\bar{R}_3(\frac{1}{\zeta}) + Q_4(\zeta)\bar{R}_4(\frac{1}{\zeta})\\ &\quad + \frac{\alpha}{\zeta g(\zeta)} + \frac{\alpha\zeta}{\bar{g}(1/\zeta)}], \qquad \text{(C.18)}\end{aligned}$$

and

$$\begin{aligned}\frac{\partial\phi_{\varepsilon P}}{\partial r}(\zeta,\frac{1}{\zeta}) &= \frac{3}{4\pi}\zeta[Q_1'(\zeta)\bar{R}_1(\frac{1}{\zeta}) + Q_2'(\zeta)\bar{R}_2(\frac{1}{\zeta}) + Q_3'(\zeta)\bar{R}_3(\frac{1}{\zeta}) + Q_4'(\zeta)\bar{R}_4(\frac{1}{\zeta})]\\ &\quad \frac{3}{4\pi}\frac{1}{\zeta}[Q_1(\zeta)\bar{R}_1'(\frac{1}{\zeta}) + Q_2(\zeta)\bar{R}_2'(\frac{1}{\zeta}) + Q_3(\zeta)\bar{R}_3'(\frac{1}{\zeta}) + Q_4(\zeta)\bar{R}_4'(\frac{1}{\zeta})]\\ &\quad + \frac{d}{d\zeta}(\frac{\alpha}{\zeta g(\zeta)}) + \frac{d}{d\bar{\zeta}}(\frac{\alpha}{\bar{\zeta}\bar{g}(\bar{\zeta})})|_{\bar{\zeta}=1/\zeta}. \qquad \text{(C.19)}\end{aligned}$$

In the above

$$Q_1(\zeta) = \int_{iy}^{\zeta} g(\zeta)\frac{d\zeta}{\zeta}, \qquad \bar{R}_1(\bar{\zeta}) = \frac{1}{\bar{g}(\bar{\zeta})}, \tag{C.20}$$

$$Q_2(\zeta) = \int_{0}^{\zeta} \frac{1}{g(\zeta)}\frac{d\zeta}{\zeta}, \qquad \bar{R}_2(\bar{\zeta}) = \bar{g}(\bar{\zeta}), \tag{C.21}$$

$$Q_3(\zeta) = g(\zeta), \qquad \bar{R}_3(\bar{\zeta}) = \int_{0}^{\bar{\zeta}} \frac{1}{\bar{g}(\bar{\zeta})}\frac{d\bar{\zeta}}{\bar{\zeta}}, \tag{C.22}$$

$$Q_4(\zeta) = \frac{1}{g(\zeta)}, \qquad \bar{R}_4(\bar{\zeta}) = \int_{-iy}^{\bar{\zeta}} \bar{g}(\bar{\zeta})\frac{d\bar{\zeta}}{\bar{\zeta}}. \tag{C.23}$$

C.1 Asymptotic Behaviour of Particular Solution

We are now in a position to work out the asymptotics of ϕ_ε and $\partial\phi_\varepsilon/\partial r$. We make the substitution

$$\zeta = \frac{1}{|p|\omega}, \tag{C.24}$$

and look for the asymptotic behaviour as $|p| \to 0$ with ω fixed and order one. In each case we keep the dominant term in $|p|$. The asymptotic behaviour of Q_1 and Q_2 is subtle and we gratefully acknowledge the contribution of Dr. J. A. Pelesko in finding the asymptotic behaviour. We omit the details for the sake of brevity. We find

$$Q_1(\zeta) \sim -i\ln|p|\omega, \qquad \overline{R}_1(1/\zeta) \sim -|p|\omega, \tag{C.25}$$

$$Q_2(\zeta) \sim i\ln|p|\omega, \qquad \overline{R}_2(1/\zeta) \sim \frac{-1}{|p|\omega}, \tag{C.26}$$

$$Q_3(\zeta) \sim i\omega^{p^2}, \qquad \overline{R}_3(1/\zeta) \sim -|p|\omega, \tag{C.27}$$

$$Q_4(\zeta) \sim -i\omega^{-p^2}, \qquad \overline{R}_4(1/\zeta) \sim \frac{1}{|p|\omega}. \tag{C.28}$$

For the derivatives of these functions we find

$$Q_1'(\zeta) = Q_3(\zeta)/\zeta, \qquad \overline{R}_1'(1/\zeta) \sim -1, \tag{C.29}$$

$$Q_2'(\zeta) = Q_4(\zeta)/\zeta, \qquad \overline{R}_2'(1/\zeta) \sim \frac{1}{|p|^2\omega^2}, \tag{C.30}$$

$$Q_3'(\zeta) \sim -ip^2|p|^{-1}\omega^{p^2}, \qquad \overline{R}_3'(1/\zeta) = \overline{R}_1(1/\zeta)/\zeta, \tag{C.31}$$

$$Q_4'(\zeta) \sim ip^2|p|\omega^{1-p^2}, \qquad \overline{R}_4'(1/\zeta) = \overline{R}_2(1/\zeta)/\zeta. \tag{C.32}$$

C.2 Asymptotic Behaviour of Conformal Map

We are now in a position to compute the asymptotic behaviour of $f_{\varepsilon\zeta}(\zeta)$. As above we introduce

$$\zeta = \frac{1}{|p|\omega}, \tag{C.33}$$

and seek the behaviour as $|p| \to 0$ with ω fixed and order one. From (3.54) we recall

$$\begin{aligned} f_{\varepsilon\zeta}(\zeta) &= -\frac{2}{\pi\zeta}c_1(\lambda) - \lambda\frac{d}{d\zeta}[I_1(\zeta) + 2\phi_{\varepsilon P}(\zeta, 1/\zeta)] \\ &\quad + \frac{\lambda}{\zeta}[I_2(\zeta) + 2\frac{\partial\phi_{\varepsilon P}}{\partial r}(\zeta, 1/\zeta)] - \frac{\lambda}{\zeta}\frac{4}{\pi}[I_3(\zeta) + 2h_1(\zeta, 1/\zeta)]. \end{aligned} \tag{C.34}$$

Each of the terms I_1, I_2, I_3, has a Laurent expansion about infinity and behaves like a constant at infinity. It is easy to show

$$h_1(\zeta, 1/\zeta) \sim \frac{-i}{|p|\omega^{p^2+1}}. \tag{C.35}$$

It is clear that the dominant contribution to $f_{\varepsilon\zeta}$ comes from

$$f_{\varepsilon\zeta}(\zeta) \sim 2\lambda\frac{d}{d\zeta}\phi_{\varepsilon P}(\zeta, 1/\zeta) + \frac{2\lambda}{\zeta}\frac{\partial\phi_{\varepsilon P}}{\partial r}(\zeta, 1/\zeta), \qquad \zeta \to \infty. \tag{C.36}$$

On substitution of the results above we find

$$f_{\varepsilon\zeta} \sim i\frac{3}{4}\frac{2}{\pi}\ln|p|\omega. \tag{C.37}$$

For ω fixed and order one the dominant contribution is

$$f_{\varepsilon\zeta} \sim i\frac{3}{4}\frac{2}{\pi}\ln|p|. \tag{C.38}$$

Bibliography

[1] P. G. Saffman, and G. I. Taylor, The Penetration of a Fluid into a Porous Medium or Hele-Shaw Cell Containing a More Viscous Liquid, *Proc. R. Soc.*, Vol. 245, 1958, pp. 312-329.

[2] P. G. Saffman, Viscous Fingering in Hele-Shaw Cells, *J. Fluid. Mech.*, Vol. 173, 1986, pp. 73-94.

[3] J. W. McLean, Ph.D. Thesis, California Institute of Technology, 1980.

[4] J. W. McLean, and P. G. Saffman, The Effect of Surface Tension on the Shape of Fingers in a Hele-Shaw Cell, *J. Fluid Mech.*, Vol. 102, 1981, pp. 455-469.

[5] S. Tanveer, Analytic Theory for the Linear Stability of the Saffman-Taylor Finger, *Phys. Fluids,* Vol. 30 (8), August 1987, pp. 2318-2329.

[6] D. A. Kessler and H. Levine, Stability of Finger Patterns in Hele-Shaw Cells, *Phys. Rev* A, Vol. 32 (3) , September 1985, pp. 1930-1933.

[7] D. Bensimon, Stability of Viscous Fingering, *Phys. Rev* A, Vol. 33 (2) , February 1986, pp. 1302-1309.

[8] M. Ben Amar, Viscous Fingering in a Wedge, *Phys. Rev. A,* Vol. 44 (6), 1991, pp. 3673-3685.

[9] Y. Couder, N. Gérard, and M. Rabaud, Narrow Fingers in the Saffman-Taylor Instability, *Phys. Rev. A,* Vol. 34 (6), December 1986, pp. 5175-5178.

[10] G. Zocchi, B. E. Shaw, A. Libchaber, and L. Kadanoff, Finger Narrowing Under Local Perturbations in the Saffman-Taylor Problem, *Phys. Rev. A,* Vol. 36 (4), August 1987, pp1894-1900.

[11] P. Tabeling, G. Zocchi, and A. Libchaber, An Experimental Study of the Saffman-Taylor Instability, *J. Fluid Mech.,* Vol. 177, 1987, pp. 67-82.

[12] C. W. Park, and G. M. Homsy, Two-Phase Displacement in Hele–Shaw Cells: Theory, *J. Fluid Mech.,* Vol 139, 1984, pp. 291-308.

[13] B. I. Shraiman, Velocity Selection and the Saffman-Taylor Problem, *Phys. Rev. Lett.*, Vol. 56 (19), May 1986, pp. 2028-2031.

[14] D. C. Hong and J. S. Langer, Analytic Theory of the Selection Mechanism in the Saffman-Taylor Problem, *Phys. Rev. Lett.*, Vol. 56 (19), May 1986, pp. 2032-2035.

[15] R. Combescot, T. Dombre, V. Hakim and Y. Pomeau, Shape Selection of the Saffman-Taylor Fingers, *Phys. Rev. Lett.*, Vol. 56 (19), May 1986, pp. 2036-2039.

[16] S. Tanveer, Analytic Theory for the Selection of a Symmetric Saffman-Taylor Finger in a Hele-Saw Cell, *Phys. Fluids*, Vol. 30 (6), 1987, pp. 1589-1605.

[17] A. T. Dorsey and O. Martin, Saffman-Taylor Fingers with Anisotropic Surface Tension, Phys. Rev. A, Vol. 35 (9), 1987, pp. 3989-3992.

[18] R. Combescot, Saffman-Taylor Fingers in the Sector Geometry, *Phys. Rev. A,* Vol. 45 (2), January 1992, pp. 873-884.

[19] H. Levine and Y. Tu, Mean-Field Diffusion Limited Aggregation and the Saffman-Taylor Problem in Three Dimensions, *Phys. Rev. A,* Vol. 45 (2), January 1992, pp. 1044-1052.

[20] L. Romero, Ph.D. Thesis, California Institute of Technology, 1982.

[21] J. Vanden-Broeck, Fingers in a Hele-Shaw Cell With Surface Tension, *Phys. Fluids*, Vol. 26(8), August 1983, pp. 2033-2034.

[22] F. W. J. Olver, General Connection Formulae for Liouville-Green Approximations in the Complex Plane, *Phil. Trans. Roy. Soc. Lond. Ser. A*, Vol. 289, 1978, pp. 501-548.

[23] J. Heading, Global Phase Integral Methods, *J. Mech. Appl. Math.*, Vol. XXX, Pt. 3, 1977, pp.281-302.